uOttawa

L'Université canadienne
Canada's university

FACULTÉ DES ÉTUDES SUPÉRIEURES ET POSTOCTORALES

uOttawa

L'Université canadienne
Canada's university

FACULTY OF GRADUATE AND POSDOCTORAL STUDIES

Zijun Liu

AUTEUR DE LA THÈSE / AUTHOR OF THESIS

M.A.Sc. (Chemical Engineering)

GRADE / DEGREE

Department of Chemical Engineering

FACULTÉ, ÉCOLE, DÉPARTEMENT / FACULTY, SCHOOL, DEPARTMENT

Preparation of Biodegradable Polymeric Scaffolds with Porosity Gradients and Interconnected Structures Using a Sub Critical CO2 Foaming Process

TITRE DE LA THÈSE / TITLE OF THESIS

Dr. Cao

DIRECTEUR (DIRECTRICE) DE LA THÈSE / THESIS SUPERVISOR

CO-DIRECTEUR (CO-DIRECTRICE) DE LA THÈSE / THESIS CO-SUPERVISOR

EXAMINATEURS (EXAMINATRICES) DE LA THÈSE / THESIS EXAMINERS

Dr. J. Thibault

Dr. A. Macchi

Dr. J. Zhang

Gary W. Slater

Le Doyen de la Faculté des études supérieures et postdoctorales / Dean of the Faculty of Graduate and Postdoctoral Studies

PREPARATION OF BIODEGRADABLE POLYMERIC SCAFFOLDS WITH POROSITY GRADIENTS AND INTERCONNECTED STRUCTURES USING A SUB CRITICAL CO_2 FOAMING PROCESS

Zijun Liu

Thesis submitted to the
Faculty of Graduate and Postdoctoral Studies
In partial fulfillment of the requirements
For the MASc degree in Chemical Engineering

Chemical Engineering Department
Faculty of Engineering
University of Ottawa

Your file Votre référence
ISBN: 978-0-494-50903-6
Our file Notre référence
ISBN: 978-0-494-50903-6

Abstract

The use of CO_2 at sub-critical states and formation of porous structures with porosity gradients and interconnectivities from biodegradable polymers and their blends were investigated. Porous structures with well-defined pore sizes ranging from very large (i.e. d>100μm) to very small pores (i.e. d<10μm) were prepared by foaming multilayered films of poly (dl-lactic-co-glycolic acid) (PLGA 50/50), poly ε-caprolactone (PCL), poly (dl-lactic-co-caprolactone) (PLCL) and their blends.

In order to improve the interconnectivity, a ternary system comprised of poly (lactic-co-glycolic acid) (PLGA 50/50)/ poly (ethylene glycol) (PEG)/ethanol (C_2H_5OH)/CO_2 was foamed by CO_2 under sub-critical conditions. By varying the PEG concentration in the mixture, and subsequently foaming the samples by either pressure quench or temperature quench, an interconnected porous structure was generated. Investigations demonstrated that the (PLGA 50/50)/PEG blend in ratios of 95/5, 90/10, 75/25 , 50/50 and 33/67 wt% can be foamed into a wide range of pore sizes from 10 to 500 μm and opening sizes from 5 to 250 μm. The generated scaffolds geometry in the investigated systems ranged from partially open to completely open, well interconnected, homogeneous or heterogeneous big pore structures. The scaffolds could find potential applications in tissue engineering.

Résumé

L'utilisation du CO2 aux états sous-critiques et la formation des structures poreuses avec des gradients et des interconnectivities de porosité a base de polymères biodégradables et de leurs mélanges ont été étudiées. Des structures poreuses avec des pores de largeur bien défini entre très grand (c.-à-d. d>100μm) à très petits (c.-à-d. d<10μm) ont été préparés en écumant des films multicouche de poly (acide DL-lactique-Co-glycolique) (PLGA 50/50), poly ε-caprolactone (PCL), poly (DL-lactique-Co-caprolactone) (PLCL) et leurs mélanges.

Afin d'améliorer l'interconnectivité, un système ternaire composé de poly (acide lactique-Co-glycolique) (PLGA 50/50)/poly (éthylène-glycol) (PEG) /ethanol (C_2H_5OH) /CO_2 a été écumé par CO_2 à des conditions sous-critiques. En changeant la concentration de PEG dans le mélange et en écumant les échantillons soit à la pression étanche ou la température étanche, une structure poreuse reliée ensemble a été produite. L'étude a démontré que le mélange de (PLGA 50/50)/PEG dans les rapports de 95/5, 90/10, 75/25, 50/50 et 33/67 par poids peuvent être écumé pour produire un variété de tailles de pore de 10 à 500 μm ainsi que des ouverture de 5 au 250 μm. La géométrie produite d'échafaudages dans les systèmes étudiés furent de grosse structure poreuse varié entre partiellement ouvert à complétement ouvert, bien relier ensemble, homogènes et hétérogènes. Les échafaudages ont des applications potentielles dans la technologie de tissu.

Acknowledgements

I would like to express my gratitude for the contributions of the following people to the development of my work. First of all, Prof. Xudong Cao who not only gave immense professional support and thorough guidance but also unconditional helped me grow academically and personally as a mentor and a friend, giving me advice and guidance in the most difficult times during the last 2 years. Deep appreciation to Dr. A. Victoria Nawaby for her professional guidance and the unselfish help on the use of lab facilities and materials.

To Mr. David Kingston and Jim Margeson for the help and with SEM techniques and the friendly and enjoyable atmosphere. To Dr. Pamela Whitfield and Dr. Jiangfu Ding for their assistance with X-ray and GPC data, respectively. To Mr. Gilles Robertson on the assistance of DSC operation and analysis.

To my colleagues Susan Badel, Nan Cheng, Cathy Goubko, Angela Melhuish, Brenda Green, Chae-Ho Yim for so many good moments together, the daily smile and all the support. To Xia Liao and Baisheng Yao for interesting and stimulating discussions and valuable suggestions along the way.

I am extremely grateful to my parents, for their constant love, motivation, encouragement. Finally to my beloved wife for her love, support, and motivation.

Table of contents

List of figures

List of tables

Abbreviations and symbols

Abbreviations

Abbreviation	Name
BDNF	Brain derived neurotrophic factor
bFGF	Basic fibroblast growth factor
CAD	Computer aided design
CAM	Computer aided manufacturing
CFC	Chlorofluorocarbon
CNS	Central nervous system
CS	Chondroitin sulfate
CT	Computed tomography
DSC	Differential scanning calorimetry
EVA	Ethylene vinyl acetate
FDM	Fused deposition modeling
FTIR	Fourier transform infrared spectroscopy
GAG	Glycosaminoglycan
GF	Gas foaming
GPC	Gel permeation chromatography
HFM	Hollow fiber membranes
LA/GA	Lactic acid/glycolic acid
LMWH	Low molecular weight heparin
MSB	Magnetic suspension balance
MSC	Mesenchymal stem cell

MRI	Magnetic resonance imaging
NGF	Nerve growth factor
NT-3	Neurotrophin-3
PCL	Poly(caprolactone)
PDGF	Platelet-derived growth factor
PEG	Poly(ethylene glycol)
PGA	Poly(glycolic acid)
PL	Particulate leaching
PLA	Poly(lactic acid)
PLCL	Poly(lactic-co-caprolactone)
PLGA	Poly(lactide-co-glycolide)
PMMA	Poly(methyl methacrylate)
PNS	Peripheral nervous system
PPO	Poly(propylene oxide)
PS	Poly(styrene)
PVA	Polyvinyl alcohol
QCM	Quartz crystal microbalance
SCI	Spinal cord injury
SEM	Scanning electron microscope
THF	Tetrahydrofuran
Tg	Glass transition temperature
VA	Vinyl acetate
VEGF	Vascular endothelial growth factor

VOC	Volatile organic solvent

Symbols

Symbol	Name	Unit
A	Aarea of the micrograph	cm^2
A_f	Constant related with the sample radius, sample weight and the total CO_2 mass saturated in polymer	-
B	Langmuir affinity constant	-
C	Concentration	-
C_1	Concentration of gas molecules, is	-
C_D	Molar concentration sorbed by ordinary dissolution	-
C_H	Molar concentration sorbed by hole filling	-
C'_H	Langmuir capacity constant	-
C_t	CO_2 concentration in a polymer at time t	-
C_0	CO_2 concentration in a polymer	-
D	Diffusivity	cm^2 /s
D_d	Desorption diffusivity	cm^2/s
f_0	is frequency factor for gas molecules joining the nucleus	-
f_1	Frequency factor for gas molecules joining the nucleus	-
ΔG^*_{het}	heterogeneous activation energy for heterogeneous nucleation	J
ΔG^*_{hom}	Homogeneous activation energy for homogeneous nucleation	J

k	Boltzman's constant ($1.3806503 \times 10^{-23}$)	m^2 kg /(s^2 K)
k_D	Henry's law constant	-
M_0	Sample mass before CO2 soaking experiment	mg
M_n	Average number molecular weight	-
Mp	Peak molecular weight	-
M_w	Average weight molecular weight	-
M_X	Magnification	-
M_t	Sample mass measured at time t	mg
n	Number of pores in the micrograph	-
N_0	Nucleation rate	nuclei/cm^3.s
N_f	Cell density	number of cells/cm^3
P	Pressure	MPa
Pc	Critical pressure	MPa
P*	Characteristic pressure	MPa
ΔP	Pressure difference generated in the foaming process	MPa
t	time	s
T	Temperature	K
T*	Characteristic temperature	K
Tg	Glass transition temperature	^oC
Tc	Critical temperature	K

w_1	Polymer one weight percentage in the blend	-
w_2	Polymer two weight percentage in the blend	-
W_A	Mass of solid body in air	g
W_B	Mass of solid body when immersed in test liquid (water)	g
γ_{bp}	Interfacial tension of the polymer–bubble interface	N/m
δ_{ij}	Binary interaction parameter	-
ε	Porosity	-
η	Inherent viscosity	Pa.s
θ	Contact angle of polymer-additive-gas interface	^{o}
ρ	Density	kg/m^3
ρ_0	Density of test liquid (water)	g/cm^3
ρ_f	Density of foamed polymer sample	g/cm^3
ρ_p	Density of the unfoamed polymer sample	g/cm^3
ρ^*	Characteristic density	kg/m^3

1. Introduction

1.1 Scaffolds for tissue engineering

Tissue engineering is "an interdisciplinary field that applies the principles of engineering and life sciences toward the development of biological substitutes that restore, maintain, or improve tissue function or a whole organ" [1]. Cells or drugs are often implanted or seeded into an artificial structure capable of supporting three-dimensional tissue formation. These structures are typically called scaffolds. The scaffolds offer the possibility of the regeneration of tissues damaged by disease or trauma and to create new tissues and replace failing or malfunctioning organs [2] [3]. This is typically done through the use of degradable biomaterials to either induce surrounding tissue and cell ingrowths or to serve as temporary scaffolds for transplanted cells to attach, grow, and maintain differentiated functions[4] [5].

1.2 Scaffold requirements

To achieve the goal of tissue reconstruction, scaffolds must meet some specific requirements. The scaffolds serve at least one of the following requirements [6-8]:

1. Biocompatibility: The scaffolds must be biocompatible with cells and human bodies in order to allow cell attachment and migration.

2. Porosity: The scaffolds must have enough porosity to deliver and retain cells and other biologically active ingredients, such as growth factors. A high porosity and an adequate pore size are necessary to facilitate cell seeding and diffusion throughout the whole structure of both cells and nutrients.

3. Mechanical property: The scaffolds must have certain mechanical property to act

as a physical support. The surrounding tissue compresses the scaffold continuously, so that the scaffold must be strong enough to maintain its shape and porosity in order to supply the environment for the cell growth and new tissue regeneration.

4. Biodegradability: Biodegradability is another essential factor since scaffolds need to be absorbed by the surrounding tissues without the necessity of further surgical removals. The rate at which degradation occurs has to coincide as much as possible with the rate of tissue formation: this means that while cells are producing their own natural matrix structure around themselves, the scaffold is able to provide structural integrity within the body and eventually it will break down, leaving newly formed tissue to take over the mechanical load.

1.3 Scaffold materials

Based on the requirements of the scaffolds, many different materials (natural and synthetic, biodegradable and permanent) have been investigated [9-12]. Most of these materials have been known in the medical field for a long time, such as materials used in bioresorbable sutures and meshes.

1. Naturally occurring materials: Commonly used natural materials for scaffolds include [7]: protein materials, such as collagen and fibrin; and polysaccharidic materials, such as chitosan and glycosaminoglycans (GAGs). All of those materials have been proven to be suitable in terms of cell compatibility; however some issues with potential immunogenicity still remain.

2. Synthetic materials: A commonly used synthetic material in tissue engineering is biodegradable poly(α-ester), such as poly(lactic acid) (PLA). This is a type of polyester which degrades within the body to form lactic acid, a naturally occurring chemical which is easily removed from the body. Similar materials are poly(glycolic acid) (PGA) and poly(ε-

caprolactone) (PCL): their degradation mechanism is similar to that of PLA, but they exhibit respectively faster and slower degradation rates compared to PLA [13].

3. New functional synthetic materials: In order to improve the scaffold properties, new biomaterials have been engineered to have ideal properties such as injectability, biocompatibility, and non-immunogenicity. For example, PuraMatrix, originated from the MIT laboratories of Zhang, Rich, Grodzinsky and Langer, is one of these new biomimetic scaffold families which have now been commercialized and have already shown great clinical promises in tissue engineering [14]. PuraMatrix is a synthetic 16-amino acid polypeptide which assembles into a 3-D extracellular matrix hydrogel to support the growth of many different types of cells in tissue culture. Furthermore, a lot of research is concentrated on the synthesis of hybrid materials which combined the advantages of several selected materials together for special applications. For example, Salomon et al. synthesized a new tri-block copolymer poly(ε-caprolactone)/poly(L-lactic acid)/ poly(ε-caprolactone) (PCL/PLA/PCL). The tri-block copolymers displayed enhanced mechanical properties; at the same time, these copolymers degrade faster than their respective homopolymers. The degradation can be adjusted by changing the PLA block length [15]. It is also possible to improve the scaffold performance by adding functional groups in the polymers. In Rabolt's work, poly(ethylene glycol) (PEG) functionalized with low molecular weight heparin (LMWH) was fabricated into poly(lactide-co-glycolide) 75:25 (PLGA 75/25) fibers for application in drug delivery. They compared the basic fibroblast growth factor (bFGF) binding on electrospun fibers between PLGA 75/25, (PLGA 75/25)/LMWH and (PLGA 75/25)/PEG-LMWH. They observed the significant improvement in the binding of (bFGF) to the electrospun PLGA 75/25 fibers functionalized with PEG-LMWH [16]. The result shows that there are significant differences in bFGF binding between the LMWH/ (PLGA 75/25)

and PEG-LMWH/ (PLGA 75/25) fibers because the retention of PEG-LMWH on the PLGA 75/25 fibers is longer than LMWH alone. Instead of synthesizing new materials, blending of different existing materials with desired properties is a likely simple way to optimize material properties in order to satisfy tissue engineering scaffold design requirements. To this end, for example, Li et al. electrospun fibrous composite scaffolds composed of PLGA 90/10, gelatin and elastin. Their results show that the resultant scaffolds offered a combined desired characteristic of each individual composing components, rendering the newly blended material biodegradable, biocompatible, hydrolysis resistant and cell adhesive [17].

1.4 Scaffolds perspective in drug and cell deliveries

The ideal scaffold design and the corresponding potentials of the scaffold are mainly determined by the tissue engineering specific applications [18, 19]. In fact, as the demand of new and more sophisticated scaffolds develops, materials are being designed to have a more active role in guiding tissue development [20]. Instead of merely holding cells in place, these matrices are designed to accomplish other functions through the combination of different format features and materials [21]. In one case, heart cells were cultured on collagen scaffolds and induced to synchronously contract using electrical pacing designed to mimic those in native heart tissue. The electrical stimulation resulted in the *in vitro* development of cardiac constructs with a remarkable level of ultra structural organization 8 days later. Another good example of new scaffold design is the use of drug delivery devices that can act simultaneously as scaffolds for cell growth. For example, the combination of microspheres or nanospheres (with encapsulated cells, growth factors or other therapeutic agents) within a polymeric matrix will facilitate the cell growth and drug delivery [22]. This type of multifunctional device can also be designed to act as an injectable material, with the

advantage of allowing minimal invasive surgery procedures for their implantation in the body.

Drug delivery profiles of the drug concentration in plasma against time can be used to compare traditional methods of drug delivery (e.g. oral, intravenous) and the controlled release by using scaffolds. Figure 1.1 is based on a figure from a review by Holland and Tighe [23] and illustrates typical drug delivery profiles, showing the advantages of the controlled drug delivery. The drug release system in a scaffold involves incorporation of the active substance into a scaffold, which is implanted into the patient in various ways, and a diffusion mechanism produces the maintained drug release followed by bulk hydrolysis of the polymer.

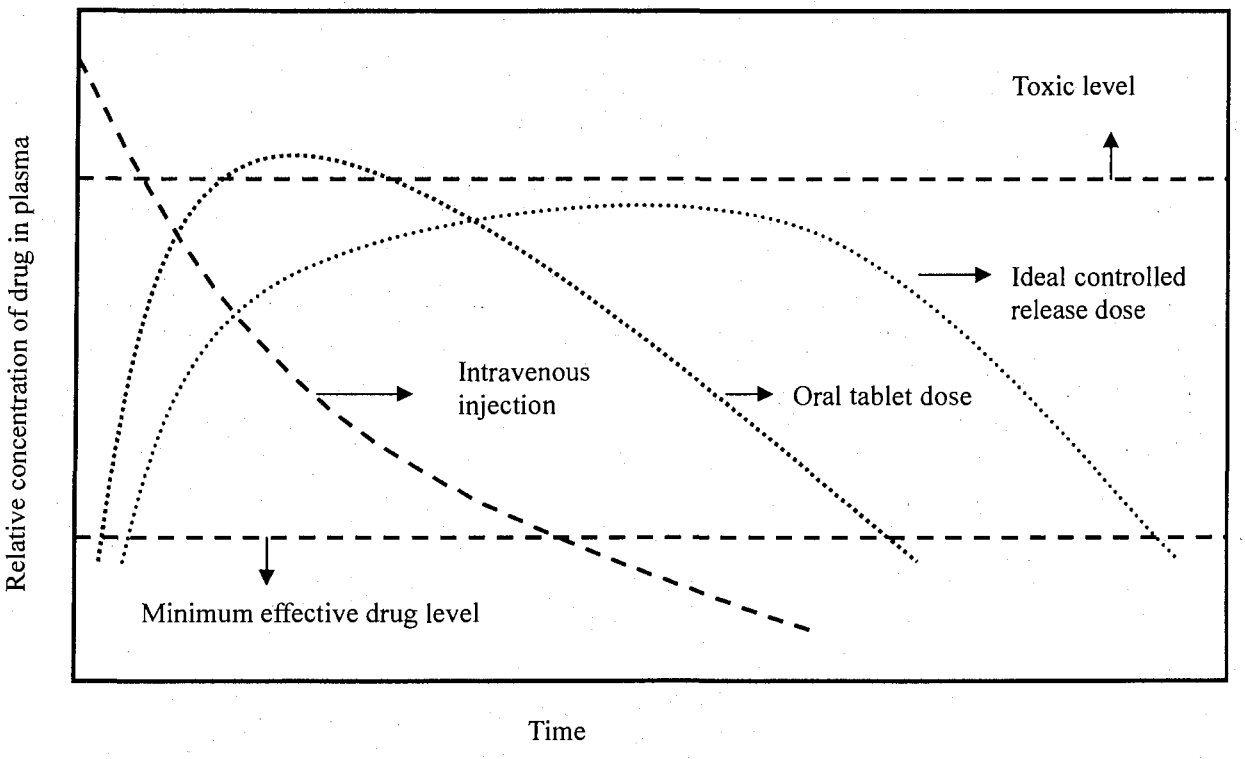

Figure 1.1. Drug release profile comparison [23]

Beside single use of growth factor or other drugs, combined use of multiple drugs in a scaffold preceded with cells to accelerate tissue regeneration. Richardson and Mooney

published their research on a dual drug delivery system in which vascular endothelial growth factor (VEGF) and platelet-derived growth factor (PDGF) loaded in PLGA 80/20 scaffold can direct the formation of a mature vasculature, as compared to the delivery of VEGF or PDGF alone [24]. This process allows for sustained protein delivery and maintains the biological activity of incorporated and released growth factors. The polymeric scaffold developed to allow controlled, dual release of two distinct proteins could provide a powerful tool to study a wide array of other developmental processes in biology and medicine.

Now researchers are attempting to combine new techniques with scaffold design to apply on the tissue regeneration, such as stem cells and gene therapy[25] [26]. For example, DNA has been incorporated into polymeric scaffolds to enhance gene transfer by delaying clearance from the desired tissue. The scaffold can protect DNA from degradation and an immune response, providing sustained delivery and extending opportunities for internalization. Nie et al. loaded DNA in Poly (lactide-co-glycolide) (PLGA)/Hydroxylapatite (HAp) composite scaffolds via two ways: naked DNA and encapsulation of DNA/chitosan nanoparticles into scaffolds [27]. The results demonstrate that sustained DNA release in DNA/chitosan nanoparticles with negligible immunological effects. Also the cell culture experiments show that the scaffolds with encapsulated DNA/chitosan nanoparticles have higher cell attachment, higher cell viablility and desirable transfection efficiency of DNA.

One important consideration for the most widely studied tissue engineering approaches is the cell source and the ability to control cell proliferation and differentiation [28]. The recent identification of stem cells [29] [30] [31] – cells that can give rise to essentially all cell types in the body, depending on the culturing conditions – offers probably the most exciting alternative source of cells for tissue engineering. These recent

developments in the stem cell field have impacted significantly on the progress of tissue regeneration and scaffold design. For example, Levenberg et al. studied the human embryonic stem (hES) cells differentiation on three-dimensional scaffolds fabricated from degradable poly(α-hydroxyl esters) including poly(lactic-co-glycolic acid) and poly(L-lactic acid) [32]. They succeeded in the enhanced Neuronal differentiation by using the factors in the medium ((e.g., retinoic acid (RA), nerve growth factor (NGF), and neurotrophin 3 (NT-3)). This may be beneficial for the treatment of diseases such as Parkinson's, spinal cord injury, and glaucoma.

1.5 Nervous system and regeneration

1.5.1 Nervous system and injuries [33]

The nervous system is classified into two main subsystems: the central nervous system (CNS) and the peripheral nervous system (PNS). The CNS consists of the brain and the spinal cord. The PNS consists of all other nerves and neurons that do not belong to the CNS. The PNS consists of nerve fibers that receive information from the external environment and carry signals to and from the brain and spinal cord. Neurons (nerve cells) are the core components of the brain, spinal cord and peripheral nerves. Neuron is typically composed of a soma, or cell body, a dendritic tree and an axon. Neurons are electrically excitable cells in the nervous system that process and transmit information [34].

Physical injury to the nervous system, such as crush or transection, represents one of the major causes of nervous system injury. As mature neurons are non-proliferative, injury to the cell bodies lead to neuron death and consequently to loss of function. Injury to the PNS normally causes a loss of function in the muscles and sensory organs. Injury to the mature CNS will leave patients permanently paralyzed below the site of injury. There is no accepted

treatment to restore impaired sensory or motor function due to the inability of the axons to repair or regenerate by themselves [35, 36].

1.5.2 Nerve regeneration strategies

The biology of the PNS and CNS are different and thus the approaches required achieving regeneration of the PNS and CNS can not be the same.

In the PNS, the severed processes spontaneously regenerate by extending axons through nerve bundles from proximal to distal ends, which can result in successful regeneration and functional recovery. A major problem in PNS regeneration is that the distance of healing is limited to very short gaps [37]. For repair of large gaps (i.e. gaps longer than 5 mm), nerve autografts are currently accepted as the standard of care [38]. To overcome the limitations associated with the autograft approach, researchers [39] [40] [41] have engineered biomimetic artificial grafts to improve the possibility of peripheral nerve regeneration, especially over long gaps. Most of the strategies have focused on using a conduit that is filled with either a matrix, such as diluted collagen or neurotrophic factors to promote regeneration.

The inhibitory environment of the injured CNS (including both physical and chemical barriers) must be overcomed in order to repair spinal cord injury. The chemical barrier and glial scar have been demonstrated to be two major factors to prevent regeneration in the CNS [42]. One strategy involves stem cell transplantation to replace injured neurons and glial cells with new healthy cell populations, and to activate endogenous cells to provide "self-repair" [43]. Additionally, neurotrophic factors, such as nerve growth factor (NGF) [44], neurotrophin-3 (NT-3) [45, 46], brain derived neurotrophic factor (BDNF) [47] and the combination of NT-3 and BDNF [48], have been delivered into the CNS to promote nerve

fiber regeneration after injury.

1.5.3 Scaffold design for the nerve regeneration after spinal cord injury (SCI) [42]

To overcome SCI, the inhibitory glial environment and the limited regenerative capacity of the mature CNS neurons has to be reversed with judicious intervention, such as the use of the biomimetic regeneration device. To enhance regeneration, Cao and Shoichet have investigated the effect of haptotactic and chemotactic cues on the nerve regeneration. Haptotactic cues involve polymer surface/bulk modification with cell adhesive peptides. Chemotactic cues involve guiding axons with concentration gradients of neurotrophic factors. They demonstrated a nerve regeneration model in which the cell-adhesive and cell-nonadhesive regions were created and the neurotrophic factor gradient was also included in the system (Figure 1.2).

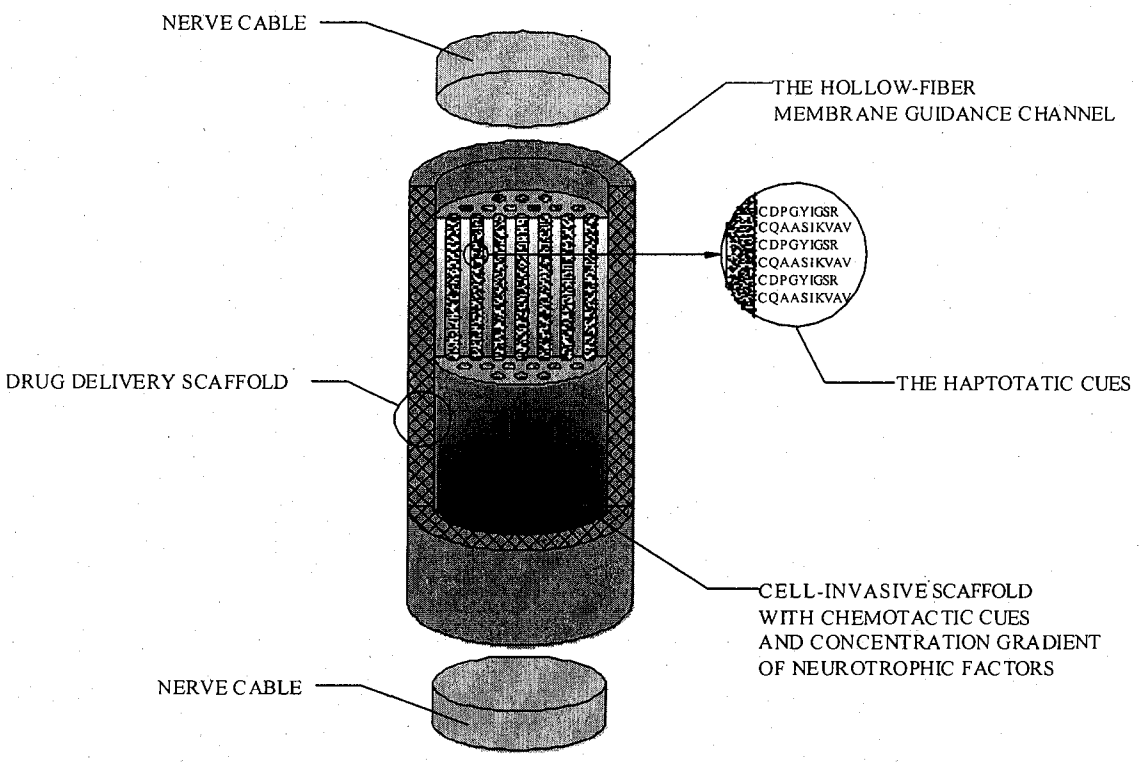

Figure 1.2. Design of biomimetic device for nerve regeneration after SCI [42].

To mimic natural repair in the body, recent studies have focused on the use of various approaches to create ideal nerve guidance channels that combine multiple stimuli in an effort to better mimic the complex signals normally found in the body. Wang et al. fabricated tubular scaffolds with knitted outer wall and controllable inner structure [49]. Chitosan fiber-based yarns were used to create porous hollow tubes, which served as the outer wall of the scaffolds. The inner matrices with multiple axially oriented macrochannels and radially interconnected micropores were fabricated by a special molding technique. The cell culture experiment showed that the neuro-2a cells (mouse neuroblastoma) proliferated and grew along the aligned microchannels. Zhang and Wen fabricated semipermeable hollow fiber membranes (HFM) by using the wet phase inversion process [50]. The HFMs have aligned

grooves on the inner surface of HFMs. The dorsal root ganglion (DRG) regeneration assay was carried out *in vitro*. Their studies showed that both the alignment and outgrowth rate of regenerating axons increased significantly on HFMs with aligned textures compared to those on HFMs with a smooth inner surface. Moore et al. produced biodegradable scaffolds with multiple-channel geometry by a simple injection molding/solvent evaporation technique [51]. Poly(lactic-co-glycolic acid) (PLGA) with copolymer ratio 85:15 was used for the experiments. The scaffold channels were seeded with Schwann cells and the Schwann cells survived for at least 48 h *in vitro*. Schwann-cell containing scaffolds implanted into transected adult rat spinal cords. They demonstrated the axon regeneration by the three-dimensional reconstruction of serial histological sections.

According to the work introduced above, we can conclude that the scaffold design and fabrication for the nerve regeneration is a systematic engineering. Besides the general properties required as a common scaffold, the ideal tubular scaffold for nerve regeneration should have some special attributes. The shell of the scaffold should have enough mechanical property to endure the compress from the surrounding tissue, and also the shell should be used as a drug carrier to support and promote the nerve or cell growth. The inner matrix should be used to guide and promote the nerve growth. The optimized design of the inner matrix should contain haptotactic and chemotactic cues. In our project, one of the goals of the research is to demonstrate a tubular structure which can be used as the shell of tubular scaffolds for nerve regeneration to guide and promote nerve growth.

1.6 Project goals

1. Multilayered films will be prepared by using different polymers and their blends. Polymer films will be made by using solvent (chloroform)-casting technique and dried on

glass petri-dishes layer-by-layer. The different molecules should have strong interactions, especially in the interfaces between layers. Meanwhile, the solvent vaporization should be fast enough to avoid the upper layer polymer solution dissolving the polymer films underneath.

2. Multilayered films will be foamed at sub-critical CO_2 conditions and the porous structures will be studied. Because different polymers will foam differently, the scaffolds with gradient porous structures will be fabricated.
3. The interconnected (open) porous structures will be fabricated by using a tertiary system composed of poly (dl-lactic-co-glycolic acid) (PLGA 50/50), poly (ethylene glycol) (PEG), and ethanol; and then the system will be soaked at a sub-critical CO_2 condition and foamed by a pressure quench or temperature quench method. The different PEG concentrations and different foaming conditions will be studied.
4. The polymer tubes will be fabricated by a dip-coating technique. Then polymer tubes will be foamed at a sub-critical condition to obtain tubular scaffolds. By using this method, the gradient tubular structure can be realized.

1.7 Hypotheses

1. A porous scaffold with porosity gradient can be formed from a multi-layered film using a sub-critical CO_2 foaming process.
2. The interconnected (open) structures can be obtained by selecting appropriate polymer blend system and suitable processing conditions.

2. Literature survey

In this project, the research direction is on the scaffold fabrication. The involved background includes the survey of biomaterials, such as biomaterial synthesis and other related biomaterial properties. We also need to investigate the scaffold fabrication methods, thus we can compare them and make our choice. The scaffolds will be intended to apply in cell and drug delivery, especially for the nerve regeneration. Therefore, the tube fabrication and the resulting typical structures are surveyed and compared. We finally decided using CO_2 gas foaming technique to make scaffolds because of its advantages superior to other fabrication techniques based on the whole comparisons. As a result, the CO_2 gas foaming technique related theory, processing, and testing are also investigated and discussed. The drawback of CO_2 gas foaming technique, i.e. the lack of interconnectivity in scaffolds and the existence of skin layer on scaffold surfaces, is also investigated and discussed.

2.1 Synthesis of biodegradable polymeric biomaterials (Poly(α-esters)) [52] [53] [54]

Linear polyesters of lactide (PLA) and glycolide (PGA) have been used for more than four decades for a variety of medical applications. They were among the first synthetic degradable polymers to find application as surgical suture materials, controlled drug release devices, as well as orthopedic and reconstructive implants. Low molecular weight PLA and PGA are prepared by the direct condensation of lactic and glycolic acid, respectively. Poly (ε-caprolactone) (PCL) was synthesized from the anionic, cationic or coordination polymerization of ε-caprolactone. Poly (lactide-co-glycolide) (PLGA) is obtained by the condensation of both lactic and glycolic acids with or without catalysts. High molecular weight polymers are all produced by the ring opening method with a catalyst such as dialkyl

zinc. For example, PLGA is synthesized by means of random ring-opening co-polymerization of two different monomers, the cyclic dimers (1, 4-dioxane-2, 5-diones) of glycolic acid and lactic acid. Common catalysts used in preparation of this polymer include Tin(II) 2-Ethylhexanoate, Tin(II) Alkoxides or aluminum isopropoxide. During polymerization, successive monomeric units (of glycolic or lactic acid) are linked together in PLGA by ester linkages, thus yielding linear aliphatic polyester as a product. Because the ratio of monomeric units (glycolic acid and lactic acid) will affect the property of the polymer, PLGA is usually written as PLGA m/n. The m/n indicates the molar ratio between monomeric unit of lactic acid and glycolic acid in the polymer.

Having an asymmetric carbon atom, lactic acid has two optical isomers. Therefore, its polymer consists of L (levorotation)-, D (dextrorotation) - and D, L- lactic acid in which the L or D- polymers have a crystalline form, and D, L- polymers are amorphous and more rapidly degraded.

The industrial synthesis of PLA, PGA, PLGA m/n and PCL is shown as follows:

Table 2.1 The industrial synthesis of PLA, PGA, PLGA m/n and PCL

PGA	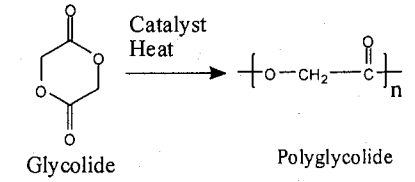
PLA	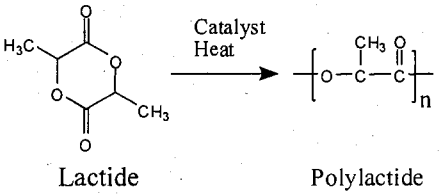

PLGA m/n	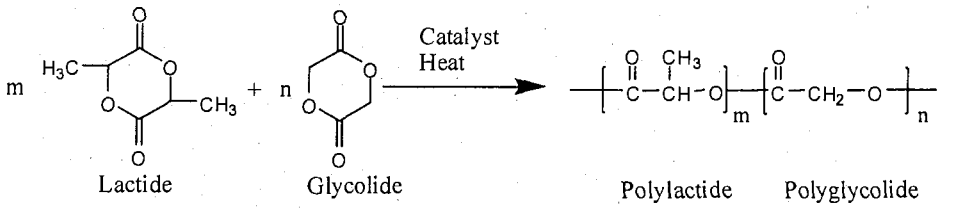
PCL	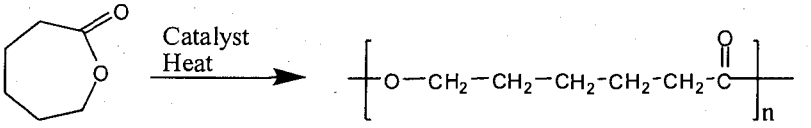

2.2 Degradation[55]

Degradation of PLA, PGA, PLGA and PCL has been studied extensively both *in vitro* and *in vivo*. Degradation can be followed by change in mass, molecular weight, morphology, mechanical strength as well as in glass transition temperature (Tg) and crystallinity. The polymers and copolymers of glycolide, lactide, and ε-caprolactone degrade by simple hydrolysis. When these polymers are exposed to aqueous media such as buffer or tissue, water is absorbed and reacts with the ester linkages, thus breaking the polymer backbone. One hydroxyl group and one carboxylic acid group forms for each ester linkage that is hydrolyzed. Because the ester linkages are cleaved randomly along the polymer backbone, relatively few water-soluble fragments form initially. Rather, long polymer chains are broken to form shorter ones. As a result, the reduction in molecular weight produces an increase in hydrophilicity but little change initially in physical properties or polymer mass. As degradation proceeds, the reduction in molecular weight leads to a reduction in physical properties and the formation of water-soluble fragments. These water-soluble fragments diffuse away from the polymer matrix and finally these fragments are ultimately hydrolyzed to glycolic and lactic acids, which are processed through normal metabolic pathways. The

rate of hydrolysis depends on factors such as the size and hydrophilicity of the particular polymer implant, the monomer composition and the degree of crystallinity of the polymer, the pH, and temperature of the environment.

2.3 Biocompatibility

PLA, PGA, PLGA 50/50 and PCL have good biocompatibility and now are being used clinically in human therapy, such as sutures and bone fracture devices [56]. Grayson et al. studied the tissue reaction to PLA, PGA and PLGA 50/50 films [57]. In their research, the *in vivo* biocompatibility and both *in vivo* and *in vitro* degradation of these materials were characterized using several techniques. The total leukocyte concentration measurements showed normal acute and chronic inflammatory responses to the PGA. Low-molecular-weight PLGA 50/50 was resolved by 21 days, while the normal inflammatory responses to the PLA and high-molecular-weight PLGA 50/50 were resolved at slower rates up to 21 days. They found that there was normal inflammatory reaction to the polymers and these polymers have suitable biocompatibility and biodegradation rates for implantable drug-delivery devices. Another experiment was conducted by Bini et al. in an attempt to extend the application of degradable PLGA 10/90 polymers into neurosurgery [58]. Poly (L-lactide-co-glycolide) (10:90) polymer fibers were used for the fabrication of conduits. One week after implantation of the conduit into the right sciatic nerve of rat, a thin tissue capsule was formed on the outer surface of the conduit, indicating good biological response of the conduit. One month after implantation, 9 of 10 rats showed successful nerve regeneration. None of the implanted tubes showed tube breakage. This showed that there was no inflammatory response to the PLGA 10/90 in rat bodies.

2.4 Scaffold fabrication

There are many methods invented and materials used for different applications. The fabrication methods have been described in many literatures for preparing porous structures to be employed as tissue engineering scaffolds. The detailed reviews of the scaffold processing are reviewed elsewhere [28] [59] [60]. The major methods are generally descripted and discussed as follows:

2.4.1 Electro spinning [61-63]

Electro spinning technique is able to produce continuous fibers from the submicron diameter down to the nanometer diameter. A high electric voltage is applied to the polymer viscoelastic solution. A solution jet comes out from the tip of spinneret by the aid of the high electric voltage. A grounded target is used to collect the resultant fibers which are deposited in the form of a nonwoven mesh. Figure 2.1 illustrates the schematics of the process. The factors affecting the process include solution viscosity, conductivity, applied voltage, spinneret tip-to-collector distance, and solution concentration. Overall, most of the electro-spinning research is focused on the development of nanofiber membranes and scaffolds as new materials for applications. For example, Zhong et al. obtained a novel nano fibrous collagen–glycosaminoglycan (GAG) scaffold by electro spinning collagen and chondroitin sulfate (CS). The electrospun collagen–GAG scaffold exhibited a uniform fiber structure in nano-scale diameter. The scaffolds exhibited a high biostability from the collagen digestion test. Its excellent biocompatibility was demonstrated by standard cell proliferation assay and cell morphology studies [64]. The advantage of the technique is that highly interconnected scaffolds can be obtained. The shortcoming of the method is that the residue of solvent in scaffolds may affect the cell proliferation.

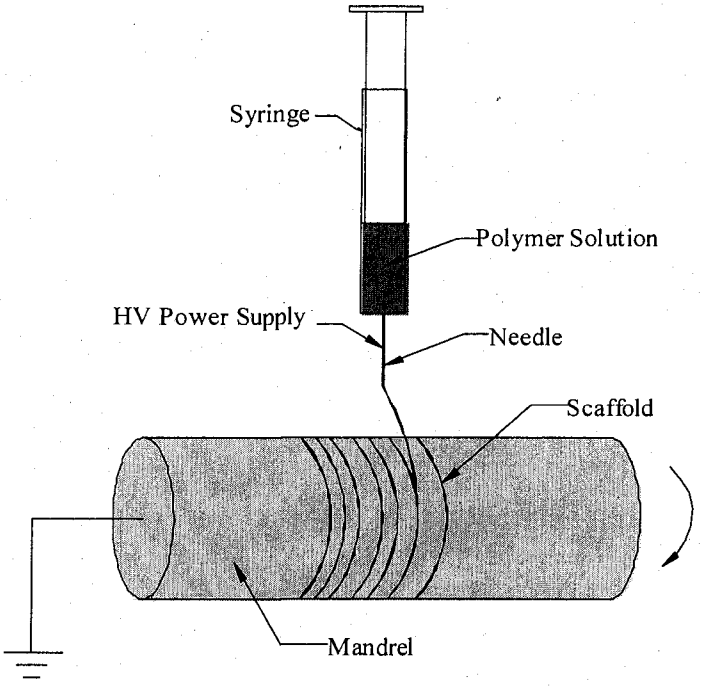

Figure 2.1 Electro spinning process [64]

2.4.2 Solvent Casting & Particulate Leaching [65] [66]

This is a simple scaffold fabrication method although the scaffold morphologies are generally worse than those made by other methods. First the polymer is dissolved into a suitable organic solvent (e.g. poly(lactic acid) could be dissolved into dichloromethane), and then the solution is cast into a mold filled with porogen particles. Such porogen can be an inorganic salt like sodium chloride, crystals of saccharose, gelatin spheres or paraffin spheres. After the polymer solution has been cast, the solvent is allowed to fully evaporate. Then the composite structure in the mold is immersed in a bath of a liquid suitable for dissolving the porogen. Once the porogen has been fully dissolved, a porous structure is obtained. Figure 2.2 illustrates the process schematics. Draghi et al. investigated the effect of three different porogens (gelatin microspheres, paraffin microspheres and sodium chloride crystals) on the

scaffold morphologies and properties [67]. Highly porous scaffolds were obtained with all porogens and well defined spherical pores resulted from microspheres leaching. Furthermore, scaffolds with spherical pores showed better mechanical performance and lower flow resistance. The size of the porogen particles will affect the size of the scaffold pores, while the polymer to porogen ratio is directly correlated to the amount of porosity of the final structure. This approach allows the preparation of porous structures with regular porosity, but with a limited thickness. The uneven distribution of salt particles and the extraction of the salt are two major concerns in the technique. In order to overcome this disadvantage, normally this technique will be combined with other technique, such as freeze drying technique [68]. By using this technique, the porogen can be easily frozen evenly in the polymer solution, thus the limit of the thickness of scaffolds should be diminished. Another drawback of the technique lies in its use of organic solvents which must be fully removed to avoid any potential damage to the cells seeded with the scaffold.

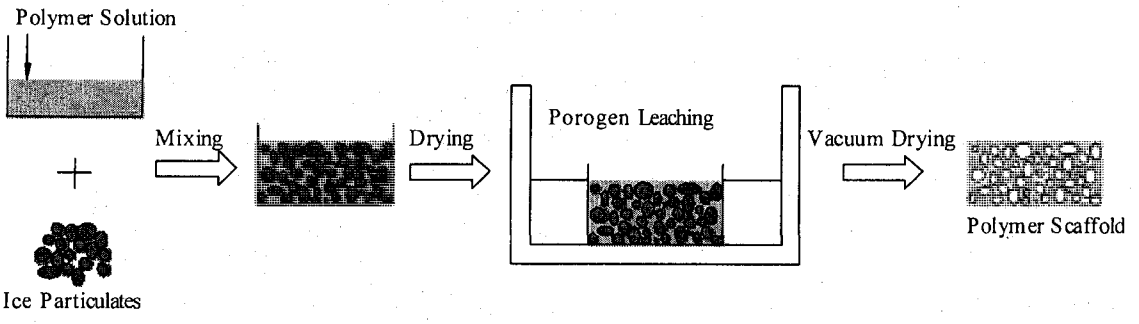

Figure 2.2. Solvent Casting / Particulate Leaching process [66]

2.4.3 Emulsification/Freeze-drying [69] [70] [71]

First a polymer is dissolved into a suitable solvent (e.g. polylactic acid in

dichloromethane) then a poor solvent (e.g. water) is added to the polymeric solution and the two liquids are mixed in order to obtain an emulsion. Before the two phases separate, the emulsion is cast into a mold and quickly frozen by means of immersion into liquid nitrogen. The frozen emulsion is subsequently freeze-dried to remove the dispersed water and solvent, thus leaving a solidified, porous polymeric structure. Figure 2.3 shows the schematic process of emulsion/freeze drying technique. The emulsification and freeze-drying is a faster process in comparison with solvent casting & particulate leaching, since it does not require a time consuming leaching step. However, it still requires the use of potentially harmful organic solvents. Moreover the pore size is relatively small and the porosity is often irregular.

Emulsion/Freeze-drying is a commonly employed technique for the fabrication of scaffolds. The control on the polymer concentration, solvent type and freezing speed are all very important on the final scaffold morphologies. By using the freeze-drying technique, Cho et al. fabricated porous alginate/polyvinyl alcohol (PVA) scaffolds to improve cell compatibility as well as flexibility of the scaffolds [70]. The scaffolds exhibited highly porous, inter-connected structures. The average pore sizes ranged from 190 μm to 290 μm, and the porosity was 85% approximately.

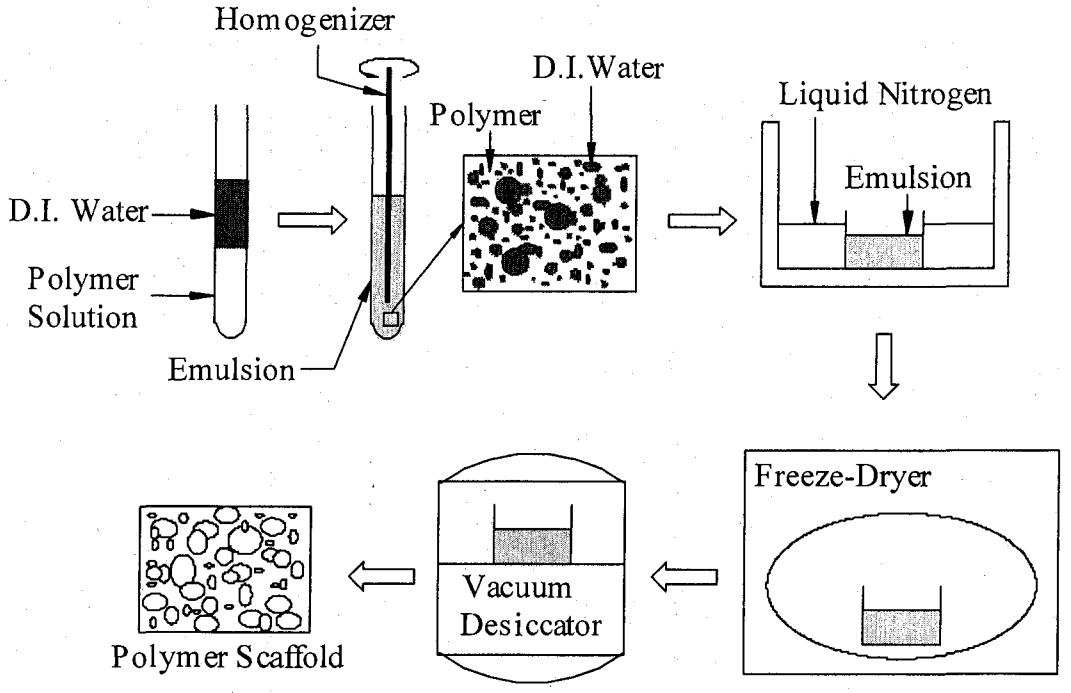

Figure 2.3. Emulsification/Freeze-drying process [70]

2.4.4 Liquid-liquid phase separation [72, 73]

The phase separation technique is based on thermodynamic de-mixing of a homogeneous polymer solvent solution into a polymer-rich phase and a polymer- poor phase, usually by either exposure of the solution to another immiscible solvent or cooling the solution below a binodal solubility curve. The phase separation procedure requires the use of a solvent with a low melting point that is easy to sublime. The quenched polymer solution below the freezing point of the solvent is subsequently freeze-dried to produce porous structure. Figure 2.4 schematically described the liquid-liquid phase separation process. For example dioxane could be used to dissolve PLA, then phase separation is induced through the addition of a small quantity of water: a polymer-rich and a polymer-poor phase are

formed. Following cooling below the solvent melting point and some days of vacuum-drying to sublime the solvent, a porous scaffold is obtained. Hua et al. used PLGA–dioxane–water ternary systems to fabricate regular and highly interconnected macroporous scaffolds ranging in size from 50 to 150 μm [74]. The effect on scaffold morphology of processing parameters including quenching temperature, polymer concentration, solvent composition, molecular weight, and quenching time. They showed that most commercial PLGAs have different characteristics including molecular weights and LA/GA ratios; therefore they will exhibit different phase transition and solution properties. Hence, the optimum quenching conditions should be tested for each PLGA in order to effectively fabricate porous scaffolds for cell culture. One of the advantages of this technique is that various porous structures can be obtained by adjusting various thermodynamic and kinetic parameters. Liquid-liquid phase separation presents the same drawbacks of emulsification/freeze-drying, including difficulties in controlling the morphology of the resulting scaffolds and the residue of the organic solvents in the foams.

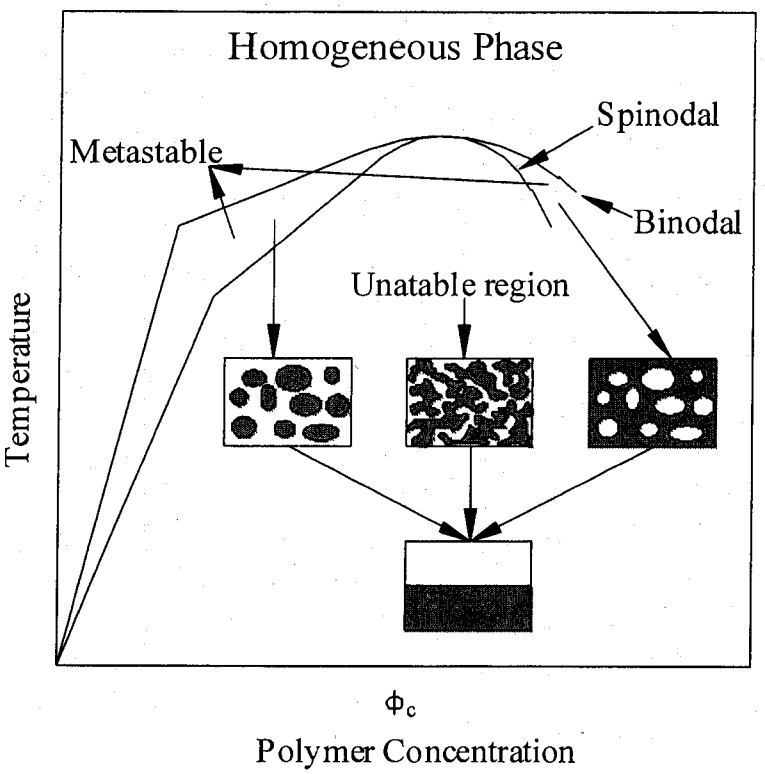

Figure 2.4. Liquid-liquid phase separation process [73]

2.4.5 CAD/CAM Technology [75-77]

Computer aided design (CAD) and computer aided manufacturing (CAM) become more and more popular because of the development of the computer technology and the mechanical technology. Since most of the approaches described above are limited to the control of porosity and pore size, computer assisted design and manufacturing techniques have been introduced to tissue engineering scaffold designs. First a three-dimensional structure is designed using CAD software, and then the scaffold is realized by using ink-jet printing of polymer powders or through fused deposition modeling (FDM) of a polymer melt. Figure 2.5 shows the schematic process of the FDM fabrication technique. Sun et al. introduced the computer aided design and applications in tissue engineering, including

biomimetic design, analysis, simulation and freeform fabrication of tissue engineered substitutes [78]. The advantage of this technique is that scaffolds can be fabricated into complicated tissue morphologies, such as skull, tooth and bone. The whole process of tissue reconstruction includes 3 steps: obtaining the tissue image via computed tomography (CT)/ magnetic resonance imaging (MRI) first, then 3D modeling (CAD), and final application-CAM (the fabrication of scaffolds). However, the smallness of the powder particles or binder drops is limited to a few hundred microns. The accuracy of the printing nozzle is also limited [79].The other disadvantage of this technique is that the high temperature used in the process. Most materials used in heat-based fabrication are synthetic polymers which have to withstand high temperatures while retaining their desired properties such as degradation and biocompatibility.

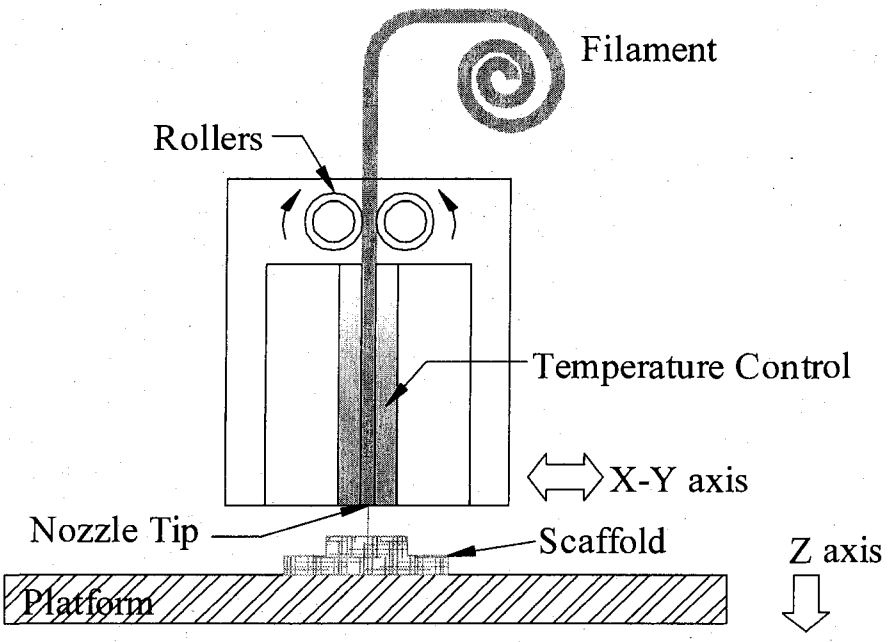

Figure 2.5. A schematic diagram of the FDM extrusion and deposition process **[76]**

2.4.6 CO_2 Gas Foaming [80] [81] [82]

First, polymer films are prepared by means of compression molding using a heated mold. The films are then placed in a chamber and exposed to high pressure CO_2 for certain time. This will allow CO_2 molecules to diffuse into polymer matrix. At the end of the process, the pressure inside the chamber is released to the normal atmospheric pressure. During this procedure, the pores are formed by the carbon dioxide molecules that abandon the polymer matrix due to the thermal dynamic instability, resulting in a sponge like structure. Figure 2.6 shows a CO_2 gas foaming process schematics. Alternately, the polymer films containing CO_2 molecules can be put in higher temperature environment to generate the nucleation and finally to obtain porous structures. The main problem related to the technique is that the pores normally do not form an interconnected structure and the existence of non porous skin layer on the foam surfaces. Beckman et al. studied the skin formation in poly(methyl methacrylate) (PMMA) during the foam formation [81]. They explain that the skin formation in the foaming process is attributed to the CO_2 molecules near the edge of polymer films diffusing out of films faster then the speed that they can form nuclei. The CO_2 concentration near the edge of the films is too low to nucleate and grow into pores. Colton et al. investigated the relationship between openings and the processing conditions [83]. They indicate that surface tension and viscosity of a polymer are very important to affect the success of the open structure formation. The surface tension affects the nucleation density and therefore determines the saturation pressure requirements, and the viscosity affects the rupture time and therefore determines the required foaming time. They used poly(styrene) (PS) to test their theory and found that the open structure can be obtained at a saturation pressure of 17.2 MPa and foamed at a scaled time of 1-2 s at 200°C.

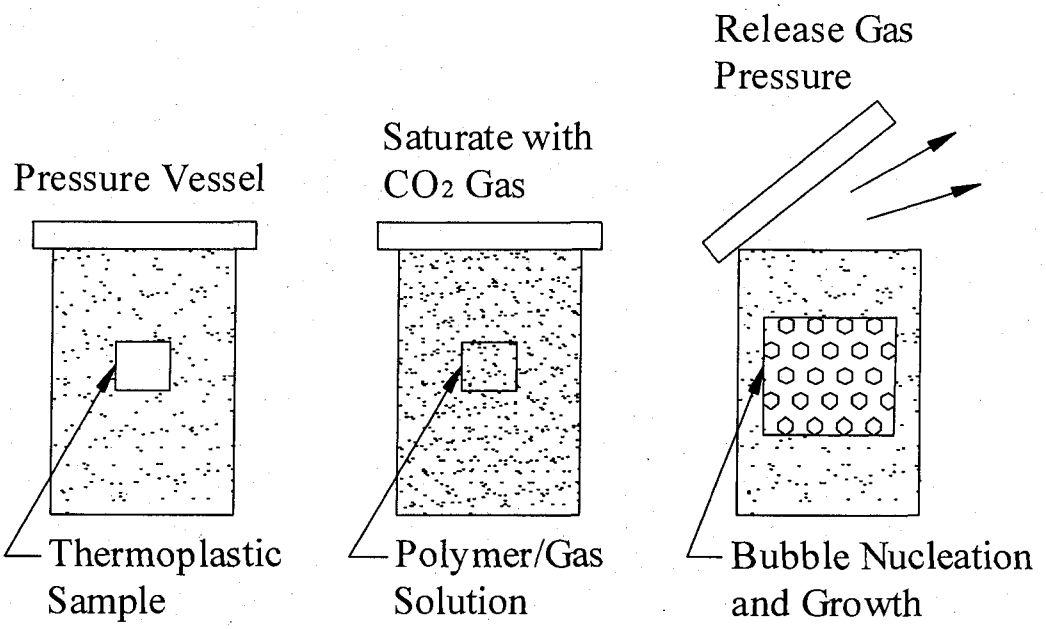

Figure 2.6. The gas foaming method (pressure quench) [82]

To summarize, each scaffold fabrication technique has its pros and cons. The major advantages and disadvantages of these techniques are listed as follows:

Table 2.2. Polymer scaffold fabrications and their characteristics for tissue engineering [1] [60]

Processing	Advantages	Disadvantages
Electro spinning	--Highly porous scaffolds with interconnected pores	--Use solvents which are poisonous to cells immersed in them for a long time
Solvent Casting & Particulate Leaching	--Controlled porosity, up to 93% --Independent control of porosity and pore size	--Limit to membranes up to 3-mm thick --Lack required mechanical strength for the load-bearing tissues --Use solvents which are poisonous to cells immersed in them for a long time

Emulsification/Freeze-drying	--Interconnected porous structure	--User and technique sensitive --Solvent residue maybe harmful
Liquid-liquid phase separation	--No decreased activity of the bioactive molecules	--Difficult to control precisely --Use solvents which are poisonous to cells immersed in them for a long time
CAD/CAM Technology	--No thickness limitation. --Enhanced control over pore structure, porosity, etc. -- Independent control of high porosity and pore size. --Macro shape control	--precise control the deposition. -- High temperature required for non amorphous polymer
CO_2 Gas Foaming	No organic solvents	--Mostly a nonporous surface. --Closed-pores structure inside the polymer matrix.

2.5 Methodology of tube fabrication

There are many methods which are used in the fabrication of micro-tubular structure. The widely used method in industry is extruding [84]. The continuous production can be processed by using the extruder. Polymer and polymer blends can be extruded using a round ring shape die, thus a polymer tube can be formed followed by a tube cooling unit. The tube casting is another technique used in study and industry [79]. The melting polymer can be filled into tubular molds. Then the mold/polymer temperature is cooled down. Finally the polymer tube can be obtained after the separation of the polymer tubes from the molds. Other methods include freeze drying [85], solvent casting and leaching [86], which are normally used for making porous tubular structures. But these methods can not avoid their disadvantages mentioned above—solvent residue. The rotational melt molding is a special technique to fabricate the polymer tubes [87]. The molten polymer is coated in rotating molds at high temperature. The coating time in the oven is critical. If the time is too long, the polymer will start to degrade which will negatively impact the mechanical property of the material. If the coating time is too short, the polymer melt may be incomplete, resulting in

large bubbles in the polymer tube. Dip coating is another method that can be used to cast polymer into tube [88]. The polymer solution is coated on a spinning mandrel layer by layer. Finally the solvent is vaporized and the polymeric tube is obtained. This is a simple method to make micro tubes because there is no complicated instrument needed in the process. In this project, we will use this method to fabricate tubes.

2.6 Structures with porosity gradients [89]

In order to fabricate structures with porosity gradients, Harley et al. used a spinning method combined with freeze drying technique [90]. The collagen-glycosaminoglycan suspension was spun at 5,000-30,000 rpm in a copper cylindrical mold to accomplish relative component separation (liquid and solid phases). The spinning suspension was then rapidly frozen in liquid nitrogen to lock the component separation achieved via spinning, and then the frozen solvent phase was removed via sublimation. The resulting the tubular scaffold had a gradient structure with denser structure at outer wall and more porous structure inside. The structure was created to facilitate drug or cell deliveries in tissue engineering. However, the drawback of this technique is the difficulties to control the gradient structure because the temperature, the spinning speed, and the cooling rate are all critical to the final morphology.

Another example is that the electro-spinning technique was used for the fabrication of the gradient structures. Pham et al. fabricated layered scaffolds by changing the poly(ε-caprolactone) (PCL) fiber diameter from 2-10 micron meter to 20-45 micron meter [89]. Mesenchymal stem cells (MSCs) were chosen to test the scaffold properties. Cell attachment after 24 h did not increase with increasing number of nanofibers, but the presence of nanofibers enhanced cell spreading. Additionally, increasing the thickness of the nanofiber layer reduced the infiltration of cells into the scaffolds.

Wang et al. fabricated a gradient tubular structure by using fiber knitting and special molding technique [49]. Chitosan fiber-based yarns were first used to create porous hollow tubes, which served as the outer wall of the scaffolds, through an industrial knitting process. Then, an inner matrix was molded with multiple axially oriented macrochannels and radially interconnected microspores. Acupuncture needles were used as mandrels during molding to improve the safety and controllability of the process. The results showed the scaffolds processed the suitable mechanical strength, porosity and biodegradability. The neura-2a (mouse neuroblastoma) cells attachment and proliferation results showed that the cells grew into the scaffold interior and along the oriented microchannels.

The conventional homogenous scaffolds will result in an even distribution of cell and drug concentration in all directions. However, scaffolds with gradient porous structure will provide a better control over distribution of cells and drug deliveries, such as drug concentrations and targeted areas, which means the higher efficient drug delivery environment compared to those with homogeneous structures. Gradient structures are promising and challenging. To date, there is no published paper or patent related with the fabrication of micro tubular gradient structures by using the CO_2 gas foaming technique.

2.7 Supercritical fluids [91] [92]

A supercritical fluid is defined as a substance for which the temperature and pressure are above their critical values and which has a density close or higher than its critical density. Supercritical fluids generally are compressed gases, which combine properties of gases and liquids in a chemically interesting manner. Supercritical fluids have physicochemical properties in between a liquid and a gas. They can have gas-like low viscosity and high diffusivity and, like a liquid, can easily dissolve many chemicals and polymers. The typical

values of physical properties of gases, supercritical fluids and liquids are listed and compared in Table 2.3.

Table 2.3. Comparison of typical values of physical properties of gases, supercritical fluids and liquids, where ρ, η and D stand for density, viscosity and diffusivity, respectively [91].

Properties	Gas	Supercritical fluid	Liquid
ρ (kg m^{-3})	1	100-800	1000
η (Pa s)	0.001	0.005-0.01	0.05-0.1
D (m^2 s^{-1})	$1 \cdot 10^{-5}$	$1 \cdot 10^{-7}$	$1 \cdot 10^{-9}$

In Table 2.4, the critical properties of some compounds which are commonly used as supercritical fluids are shown as follows.

Table 2.4. Critical conditions of several substances [92]

Solvent	T_c(K)	P_c (MPa)	Solvent	T_c(K)	P_c (MPa)
Acetone	508.1	4.70	Hexafluoroethane	293.0	3.06
Ammonia	405.6	11.3	Methane	190.4	4.60
Carbon dioxide	304.1	7.38	Methanol	512.6	8.09
Cyclohexane	553.5	4.07	n-hexane	507.5	3.01
Diethyl ether	466.7	3.64	Propane	369.8	4.25
Difluoromethane	351.6	5.83	Propylene	364.9	4.60
Difluoroethane	386.7	4.50	Sulphur hexafluoride	318.7	3.76
Dimethyl ether	400.0	5.24	Tetrafluoromethane	227.6	3.74
Ethane	305.3	4.87	Toluene	591.8	41.1
Ethylene	282.4	5.04	Trifluoromethane	299.3	4.86
Ethane	308.2	6.14	Water	647.3	22.1

Supercritical fluid technology encompasses a very broad field, which includes various reactions, separations, and material formation. In this project, we will only focus on the CO_2 gas foaming technique.

Supercritical fluids in general exhibit interesting physical properties, specific interest in CO_2 is magnified by its perceived 'green' properties—carbon dioxide is non-flammable, relatively non-toxic, and relatively inert. In addition, unlike water, the supercritical regime of CO_2 is readily accessible, given its critical temperature of only 304 K and critical pressure only 7.4 MPa [93]. In various traditional methods of polymer processing, environmentally

hazardous volatile organic solvents (VOCs) and chlorofluorocarbons (CFCs) are generally used. Due to the enormous increment of hazardous solvents emissions and generation of aqueous waste streams, chemists and chemical engineers are seeking new and cleaner methods for the processing of polymers [93]. The most widespread use of supercritical CO_2 is in extraction processes for the food and pharmaceutical industries with several large extraction units in operation in the United States and in Europe, i.e. decaffeinating coffee and tea, extracting flavours and essential oils from hops, spices, and herbs. Other applications are reported in recrystallization, purification, cleaning, degreasing, and as a substitute for organic diluents in spray painting and coating processes.

2.8 Supercritical CO_2 and CO_2 foaming technology

The supercritical CO_2 is used as a processing solvent or plasticizers, therefore people have already used the supercritical CO_2 as a foaming agent to replace other organic solvents. For microcellular foaming technique, supercritical CO_2 is dissolved into a polymer at a certain pressure and temperature. Upon pressure release, the CO_2 transforms from the supercritical to the gas phase. This results in super saturation, which gives the thermodynamic instability needed for nucleation. The foaming temperature, the saturation pressure, and the depressurization rate (pressure drop per unit time) mainly determine the number of the cells (cell density), the cell size, and the cell size distribution in a product [94] [95]. The classical homogeneous nucleation theory is widely used to describe the start of foaming process (nucleation) [95]:

$$N_0 = C_0 f_0 e(-\Delta G^*_{\text{hom}} / kT)$$

$$\Delta G^*_{\text{hom}} = \frac{16\pi\gamma_{bp}}{3\Delta P}$$

where N_0 is the nucleation rate, C_0 is the concentration of gas molecules, f_0 is the frequency factor for gas molecules joining the nucleus, k is Boltzmann's constant, T is temperature in K, ΔG^*_{hom} is the homogeneous activation energy for homogeneous nucleation, γ_{bp} is the interfacial tension of the polymer–bubble interface, ΔP is pressure difference generated in the foaming process. The equation is exponential with respect to the activation energy barrier (ΔG^*_{hom}).

The heterogeneous nucleation normally happens in polymer/additive systems. The nucleation appears at the interface between polymer and additive interface [92], which can be described as follows:

$$N_0 = C_1 f_1 e(-\Delta G^*_{het} / kT)$$

$$\Delta G^*_{het} = \frac{16\pi\gamma^2_{bp}}{3\Delta P}\left(\frac{1}{4}\right)(2+\cos\theta)(1-\cos\theta)^2$$

where C_1 is the concentration of gas molecules, f_1 is the frequency factor for gas molecules joining the nucleus, k is Boltzmann's constant, T is temperature in K, ΔG^*_{het} is heterogeneous activation energy for heterogeneous nucleation, γ_{bp} is the interfacial tension of the polymer–bubble interface, ΔP is the pressure difference generated in the foaming process, θ is the contact angle of polymer-additive-gas interface.

After the nucleation, the cells start to grow and finally a porous structure is formed. Colton et al. illustrated how the parameters in foaming process will affect nucleation, cell growth, and cell rupture [83]. The pressure drop and pressure drop rate, foaming temperature, foaming time and CO_2 concentration are key factors to decide the foaming result because these factors determine the viscosity, solubility and diffusivity.

2.9 Methodology of CO_2 foaming technique [96]

Ordinarily, we can separate the CO_2 gas foaming technique into two series: batch foaming and continuous foaming. For batch foaming, polmer/CO_2 melts can be injected into molds and finally expanded and solidified into shaped foams in molds. This technique is usually used in research works, e.g., tissue engineering. For example, polymers are soaked in high CO_2 pressure vessel and foamed by pressure quench method (super saturation is generated by pressure difference) or temperature quench method (super saturation is generated by temperature difference). In comparison, the continuous method is usually used in industry to produce large amount of products. In industry, different foaming agents and materials are always added into polymers to adjust the final foaming result in order to match the market demands.

2.10 The CO_2 solubility in polymers

Because the CO_2 uptake in a polymer matrix is the fundamental element that decides the formation of a scaffold during the CO_2 gas foaming process, the survey of the CO_2 solubility is necessary to be conducted. The solubility of CO_2 in a polymer is an index to show the relationship between polymer and CO_2 under certain conditions, which also reflects a phase equilibrium status between the polymer and CO_2.

2.10.1 The effect of temperature and pressure [97] [98]

The solubility of CO_2 in polymer increases with increasing pressure. In contrast, the solubility of CO_2 in polymer decreases with increasing temperature. At higher CO_2 density region and lower temperatures, more CO_2 can be adsorbed into polymer. Pantoula et al.

measured the CO_2 solubility in PS/CO_2 system [97]. The sorption of CO_2 in PS is about 4% (wt%) at 132°C and at 10MPa, about 11% (wt%) at 35°C and at 10MPa. Once the pressure increases from 10MPa to 25MPa, the sorption of CO_2 in PS can reach 8% (wt%) at 132°C and 16% (wt%) at 35°C. However, the solubility of N_2, He, H_2, and O_2 in polymer may increase with the increase of the temperature, especially at high temperature conditions, which is called reverse solubility [99].

2.10.2 The effect of functional groups [100] [101]

The affinity of CO_2 for a polymer is associated with the interaction between CO_2 and the polymer molecules. The functional groups such as polyolefin have the weak interaction with CO_2, whereas the other functional groups, such as carboxylic groups, have the stronger interactions between CO_2. As a result, the CO_2 solubility will be higher in polymers with carboxylic groups than that in polyolefin. Generally, the solubility of CO_2 increases with the increasing content of polar groups in the polymer. Berens and Huvard pointed out that sub-critical CO_2 behaves like a polar, highly volatile organic solvent when interacting with polymers [100].Several researchers used FTIR (Fourier transform infrared spectroscopy) to investigate the interaction of CO_2 with polymers [102] [103] [104]. For example, Eckert and co-workers find that polymers containing carbonyl groups act as electron donors and exhibit specific interactions with CO_2 as electron acceptors rather than as electron donors. Mawson et al. suggests that the interaction of CO_2 with polymers possessing acrylate groups (containing carbonyl groups) may be of a Lewis acid-base nature [105]. Shieh and Lin reviewed the interactions between CO_2 and polymers and studied the effects of carbonyl group content and crystallinity on the equilibrium solubility of CO_2 in rubbery ethylene vinyl acetate (EVA) with different vinyl acetate (VA) content [101]. Their study suggests that the

sorption process at or below critical pressure was mainly driven by the carbonyl groups and above critical pressure by the degree of crystallinity such that the higher the degree of crystallinity, the lower the normalized CO_2 sorption concentration in the polymer. Also, the specific interactions between CO_2 and the dipoles of the C-F bonds or fluorine were proposed to explain the increased solubility of CO_2 in fluorine-containing polymers in comparison with polyolefin.

The pendant groups, such as methyl group, as a kind of steric hindrance, will prevent the CO_2 uptake. On the other hand, the pendent group will also increase the free volume in the polymer matrix, which will also increase the CO_2 uptake. The final CO_2 uptake will be affected by both factors. Tomasko et al. presented that the solubility of CO_2 in PLGA m/n increases with the increase of the lactic group ratio (m) because of the increased free volume [106].

2.10.3 The effect of molecular weight

When CO_2 is dissolved into a polymer, the mobility of the polymer chains is increased due to disentanglement of the polymeric chains. As a result, the free volume inside the polymer is increased and the swelling of the polymer takes place. The polymer with higher molecular weight will have stronger molecular entanglement; therefore the accessibility of CO_2 to the free volume or to functional groups will be more difficult [107]. Elvassore et al presented that PLGA 53/46 with a molecular weight of 27 kDa has higher CO_2 sorption in comparison with PLGA 53/46 with a molecular weight of 47 kDa. At a 313K and 2.0MPa condition, PLGA 53/46 with a molecular weight of 47 kDa has a solubility of 3.06% (wt%), whereas PLGA 53/46 with a molecular weight of 27 kDa has a solubility of 3.34% (wt%) [105].

2.10.4 Correlation and Prediction of Solubility of CO2 in Polymers.

The sorption isotherms of CO_2 in polymers exhibit different pressure dependencies below and above the glass transition temperature (Tg). Below Tg, the dependence of sorption on pressure is represented by a curve concave to the pressure axis, described by the dual-mode sorption model [108]:

$$C = C_D + C_H = k_D p + C_H' \frac{bp}{1+bp},$$

where C and p are the molar concentration and pressure, respectively, C_D is the molar concentration sorbed by ordinary dissolution, C_H is the molar concentration sorbed by hole filling, k_D is Henry's law constant and C_H' and b are the molar Langmuir capacity and Langmuir affinity constant, respectively.

The sorption occurs in two modes: the dissolution mode obeying Henry's law and the adsorption mode obeying the Langmuir equation. Above Tg, the dependence of sorption on pressure is generally linear in the low pressure range and can be described accurately by Henry's constant, that is, C_H' is zero and the model reduces to the dissolution mode.

This model successfully characterizes the sorption behaviour of CO_2 inside polymers and correlates the solubility of CO_2 in polymers, but the three parameters in the model are all functions of temperature. The Henry's law constant k_D is also considered as a function of total absorbed concentration C at high pressures, which makes the model of limited use in extrapolating to higher pressure and temperatures.

The Sanchez-Lacombe equation of state [109] is perhaps the most widely used model to describe the solubility of CO_2 in polymers due to its simplicity, well-defined physical meaning, and the ability to extend available data to high temperature and pressures.

According to the lattice theory [110], the polymer molecules are ordered according to a lattice structure. The sorption of gas in polymer can be explained as that the gas molecules diffuse into the polymer lattice and finally the chemical potentials between gas phase and solid phase reach equilibrium. It is particularly adept at correlating mixtures containing molecules of widely different sizes using three characteristic parameters per molecule (T^*, P^*, and ρ^*). Typical characteristic parameters for gases and polymers have been published [111] [112]. Mixtures are handled using volume fraction-based mixing rules and an adjustable binary interaction parameter, δ_{ij}, is typically introduced into the mixing rule. Unfortunately, very limited interaction parameter data for CO_2 and polymers are available in literatures, and those are in a limited pressure or temperature range. Although the Sanchez-Lacombe equation of state can correlate the solubility of CO_2 in polymers very well, it cannot be relied upon to extrapolate to other temperatures and pressures. Kirby and McHugh [113] show that a good representation of the phase behaviour is obtained only if the binary mixture parameters are allowed to vary with temperature.

2.11 Open structures obtained by CO_2 gas foaming technique

In tissue engineering, a highly interconnected and porous structure is desired in order to achieve cell seeding and growth within the scaffold, and to facilitate the transportation of nutrients and oxygen for subsequent cell proliferation and differentiation. Microcellular biodegradable thermoplastic scaffolds are composed of pores (or cells), and open structures mean there are the holes existing on the pores. The controlled fabrication of open structures and the accurate characterization of pore size and opening size are important on specified applications. However, many researchers working with CO_2 foaming technique believe that

the technique results in the formations of highly porous scaffolds, but with limited connectivity between pores and with a skin layer on the scaffold surface [114]. The reason is believed to be that the CO_2 on the polymer surface is easier to diffuse out from the polymer matrix, but not nucleate and foam [115].

Researchers tried to solve the problem by using gas foaming/salt leaching (GF/PL) technique [116]. Porogen (salt) was first blended with polymer and soaked in high pressure CO_2 environment. Once the foaming process is finished, the porogen was leached out, thus an interconnected porous structure can be obtained. The GF/PL process results in matrices with two levels of porosity: interconnected macropores are created by leaching of the salt (NaCl) particles, and smaller, closed pores are created by the nucleation and growth of gas pores within the polymer matrix. Although the partly open scaffolds can be fabricated, salt or porogen particle sizes limit the morphology of the scaffold, i.e. salt size limit. The salt residue may also affect the cell growth. Especially it is difficult to disperse the salt particle homogenously in the polymer matrix.

Other researchers tried to change polymer chemical structures to obtain open structures. For example, Nawaby et al. grafted metal ligand on polymer chain so the polymer's properties will change and lead to the open structures at a mild processing condition [117]. The other development in this research direction includes the change of crystallinity in the foaming process [118]. The different plasticization or crystallization rate in the CO_2 soaking process will affect the CO2 solubility and polymer physical properties, and therefore the open cellular foam morphologies may be generated.

Rodeheaver and Colton developed a theoretical model related with the open-cellular foam production [83]. They divided the process into two stages: the cell impingement and the bubble coalescence. In microcellular foam, a single bubble nucleates and grows until it

contacts other bubbles on all sides. To form an open-celled structure, the thin walls between cells must break spontaneously. The rupture of thin walls is modeled as two bubbles that coalesce to form one bubble. The nucleation density, surface tension and viscosity are three important factors to decide the open structures. Higher pressure and higher temperature will increase the CO_2 nucleation density, therefore the cell impingement is easier to be realized. At the same time, the higher pressure and higher temperature will decrease the surface tension and the viscosity in the system, therefore the bubble coalescence can be reached. To sum up, the higher foaming temperature and pressure condition will beneficial for obtaining open structures.

High pressure condition means higher equipment investment and high temperature means high energy consumption, and sometimes the high temperature and pressure condition cause the porous structure to collapse or can not maintain the original shape due to the polymer melting condition. It is also possible that the higher temperature will de-activate therapeutic ingredients loaded in the polymer scaffolds.

In our project, one goal is to fabricate interconnected porous scaffolds. Because of the disadvantages of high pressure/temperature conditions, we want to find a simple solution to obtain interconnected scaffolds at mild pressure/temperature conditions.

2.12 The plasticization effect

The plasticizers are very important on the polymer physical properties. They are widely used to improve the processing properties [119]. In fact, in the CO_2 gas foaming process, CO_2 is a plasticizer [120]. Plasticizers work by embedding themselves between the chains of polymers, spacing them apart, and thus significantly lowering the glass transition temperature for the plastic and making it softer. It has been known for many years that the

dissolution of CO_2 lowers the Tg of amorphous polymers dramatically. Not only CO_2 molecules, but other small molecules, such as water, ethanol, poly(propylene oxide) (PPO) and poly(ethylene glycol) (PEG) (with low molecular weight) can also lubricant the polymer molecules and plasticise the polymer system [121]. In theory, the small molecules will increase the free volume in the polymer matrix due to the increase of the flexibility of the polymer chains [122].

Since there are so many molecules that can be used as plasticizers like CO_2, the open porous structure may be solved at mild conditions by the combination of CO_2 and other plasticizers.

2.13 The measurement of the CO_2 uptake

Generally speaking, there are 3 kinds of methods to measure the CO_2 uptake in polymer.

2.13.1 Barometric (Pressure decay) Method [123]

The apparatus in the pressure decay method is inexpensive and simple. The mass of gas absorbed by a polymer sample is obtained from the difference between the amount of gas initially contacted with the polymer and the amount remaining in the gas phase after equilibration. However, this method needs a large amount of sample (about 5 g), which in turn requires a long time for the polymer to equilibrate with CO_2. Also, it is difficult to apply at high temperatures for polymer melts because of the lack of suitable pressure sensors. If the measurement is carried out at high temperature (e.g., 200 °C for polystyrene (PS)), degradation becomes a concern. Further, a very accurate equation of state for the gas phase is needed and the volume of the system needs to be very accurately calibrated.

2.13.2 Gravimetric Method [124]

The CO_2 solubility is obtained by measuring the weight change of a polymer sample after being removed from a high pressure cell to a microbalance at ambient conditions. Based on the analytical solution to diffusion from a flat plate, the time-dependent weight change can be extrapolated to time zero to give an estimate of the solubility. In this project, we will use this simple method to measure the CO_2 solubility in polymers. More precisely, the mass of the polymer sample plus CO_2 is directly measured with a sensitive microbalance in high CO_2 pressure environment. The gravimetric method requires an accurate equation of state for the gas phase and the estimate (or measurement) of the swelling of the polymer phase to diminish the buoyancy effect. The swelling of polymers can be either measured or predicted using the Sanchez-Lacombe equation of state. The basic principle for measuring the swelling of polymers in CO_2 is to determine swelling by measuring the change in one or more dimensions of a polymer sample. The other common type of microbalance is the magnetic suspension balance (MSB) [124]. The sample and balance are mechanically isolated in MSB. The sample is magnetically levitated inside a high-pressure vessel while the balance electronics are at ambient conditions. This makes it suitable for the measurement of gas solubility and diffusivity in polymers at high temperatures and pressures. But the buoyancy correction is also important for this type of balance.

2.13.3 Frequency Modulation Method [125]

Quartz crystal microbalance (QCM) is used in the frequency modulation method to measure the CO_2 solubility. It is an accurate technique to measure gas solubility in polymers at high pressures. The QCM is composed of a thin quartz crystal coated with the polymer

(sample) and sandwiched between two metal electrodes, which establish an alternating electric field across crystal, causing vibrational motion of the crystal at its resonant frequency due to the piezoelectric effect. The resonant frequency decreases linearly as the mass of the coating increases, which works very well for small mass gains in well-adhered films. The challenge of this technique is the preparation of well-adhered films on the crystal.

3. Experimental

3.1 Materials

Poly(D, L-lactic-co-glycolic acid)(50:50) (PLGA 50/50) with different molecular weights of 125, 000 g/mol, 76, 000 g/mol and 45, 000 g/mol were purchased from Durect Corporation (Pelham, AL); Poly(ε-caprolactone)(PCL)(Mw=123,000 g/mol) and poly(D, L-lactic-co-caprolactone)(80: 20)(PLCL 80/20)(Mw=175,000 g/mol) were also obtained from Durect Corporation. Anhydrous ethanol (≥99.8%) was purchased from Commercial Alcohols Inc. (Toronto, ON). Deionized distilled water was obtained from Milli-RO 10 plus and Milli-Q plus system (Bedford, MA) and used at 18MΩ resistance. Bone-dry 99% pure CO_2 was purchased from BOC Gas Canada Ltd. (Whitby, ON). All other chemicals were purchased from Sigma-Aldrich (St. Louis, MO) and used as received unless indicated otherwise.

Polymer molecular structures are listed below:

Poly(D, L-lactic-co-glycolic acid) (PLGA 50/50)

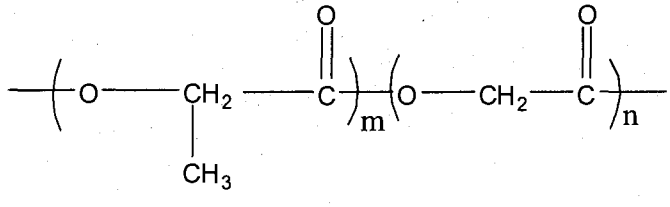

m: n=50: 50

Poly ε-caprolactone (PCL)

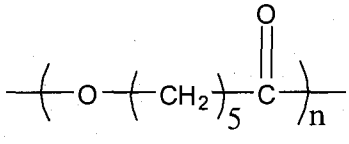

Poly(D, L-lactic-co-caprolactone) (PLCL 80/20)

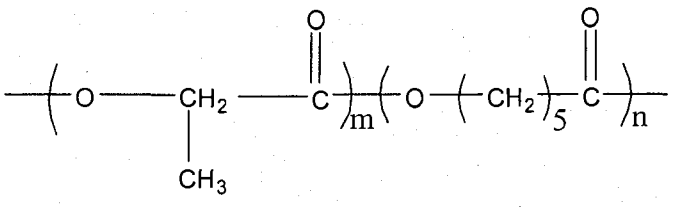

m: n=80: 20

Poly(ethylene glycol) (PEG)

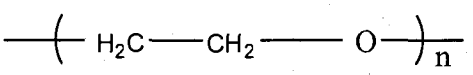

The major chemical and physical properties of the polymers were provided by Durect Corporation (Pelham, AL) and are listed in Tables 3.1 and 3.2.

Table 3.1 Polymer physical properties-1 [126]

Polymer Type	Inherent Viscosity (dL/g)	Melting Point (°C)	Glass Transition Temperature (°C)	Concentration* At 5% w/w	Approximate Resorption Time (Months)
PLGA 50/50	0.55 - 0.75	Amorphous	45 - 50	1,2,3,4,5,6	1 - 2
PCL	1.1 - 1.3	58-63	-65 - -60	1,4,5,6	>24
PLCL 80/20	0.70 - 0.90	Amorphous	20	1,4,5	16

* Solvents (partial listing only):

1 = dichloromethane

2 = tetrahydofuran

3 = ethyl acetate

4 = chloroform

5 = hexafluoroisopropanol

6 = acetone

Table 3.2 Polymer physical properties-2 [126]

Polymer Type	Specfic Gravity (g/ml)	Tensile Strength (MPa)	Elongation (%)	Modulus (MPa)
PLGA 50/50	1.34	41.37 – 55.16	3 - 10	1.38×10^3 -2.76×10^3
PCL	1.11	20.68 – 34.47	300 - 500	2.07×10^2 - 3.45×10^2
PLCL 80/20	1.22	~5.17	~150	4.13×10^2 - 1.38×10^3

3.2 Methods

3.2.1 Film casting

Biodegradable polymers and their blends were dissolved in 5 ml chloroform to form 10% (w/v) solutions. The solutions were then cast in Petri dishes (diameter=6 cm) (VWR International, Mississauga, ON) and subsequently air dried for 3 days, followed by placing the samples in a vacuum oven at 45 °C for 7 days. The resulting films (thickness ~200μm) were peeled off carefully in liquid nitrogen. The multilayered films were made in a similar fashion except that the film was dried first and then cast layer by layer for several times with different polymer solutions for different layers. The films were stored in vacuum till they were used for other experiments.

3.2.2 Compress molding

To compare and study the morphology and CO_2 uptake of the polymers, the polymer pellets or films were compress molded into even round thin films. The compress molding setup is shown in Figure 3.1:

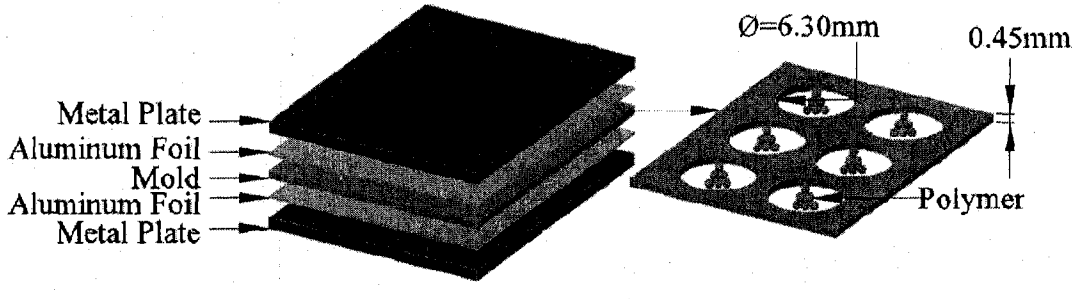

Figure 3.1. Compress molding setup

Briefly, a sheet of aluminum foil was placed on a steel plate. A mold of desired thickness was subsequently placed on top of the foil along with the polymer pellets or films. This was followed by layering a second sheet of aluminum foil on top of the polymer and a second steel plate was placed on the top. The entire setup was pressed in a compression molding machine (Fred S. Carver Inc., Wabash, IN) at 100°C at pressures increasing from 3.45-17.24 MPa in 3.45 MPa increments, with each pressure being applied for about 1 minute. Finally the setup was removed from the machine. The hot plates were then removed, and the aluminum, mold and polymer were left at room temperature for cooling. Once cooled, the sheets of aluminum foil were carefully peeled off from the mold. The film thickness was measured using a micrometer. The final films were compress molded into round films with a diameter of 6.30 mm and a thickness of 0.45 mm. The resulting compress molded films were ready for other experiments.

3.2.3 Tube fabrication

The Dip coating technique was used to make polymer tubes. The glass pipette (diameter=1.4 mm) as a mandrel spinning at 20 rpm was dipped into a polymer solution (10% g/mL) for 5 s and was then pulled out. This resulted in the polymer solution sticking on the glass pipette outer surface. The glass pipette was then rotated in horizontal position and spun for 4 h until the polymer solution was dry on the pipette surface forming a thin polymer film. After repeating the same procedure on the glass pipette for ~20 times, a certain thickness polymer tube was made (thickness~0.2 mm). Soaked in the liquid nitrogen, the glass pipette and polymer tube can be readily separated. The multilayered polymer tube was made by using different polymer solutions to get different polymer layers on the glass pipette.

When the dip-coating was finished, the polymer tube was put into a vacuum oven to dry for one week. Finally the dried tube was soaked in a supercritical CO_2 vessel and foamed. The dip-coating process schematics are shown below in Figure 3.2.

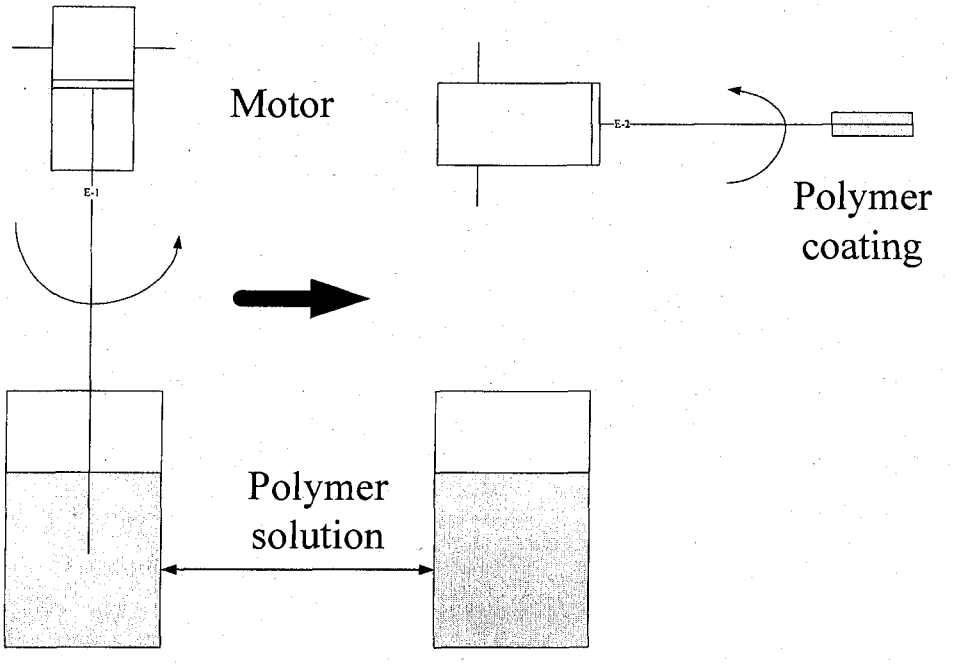

Figure 3.2. Dip coating process schematics

3.2.4 Sub-critical CO_2 Foaming

Films or tubes were saturated with CO_2 at pre-determined pressures (i.e. 1.38 MPa, 2.76 MPa, 4.14 MPa and 5.86 MPa) in a stainless vessel at room temperature for 24 h. Cellular morphologies were obtained by a pressure quench method (fast release the pressure to 1 atm within approx. 2-3 s) [82] or a temperature quench method (after the pressure quench method, the sample was immediately transferred in hot water to promote the nucleation and foaming) [127]. After rapid depressurization, the samples were foamed for 1 minute at room temperature and then cooled in ice water for 1 minute to solidify the foam microstructure. For the temperature quench method, the samples were pressure quenched

first, and then they were immediately put into 35°C water for 30 s, and finally cooled down in ice water for 1 minute to solidify the foam microstructures. Figure 3.3 shows the foaming process schematics:

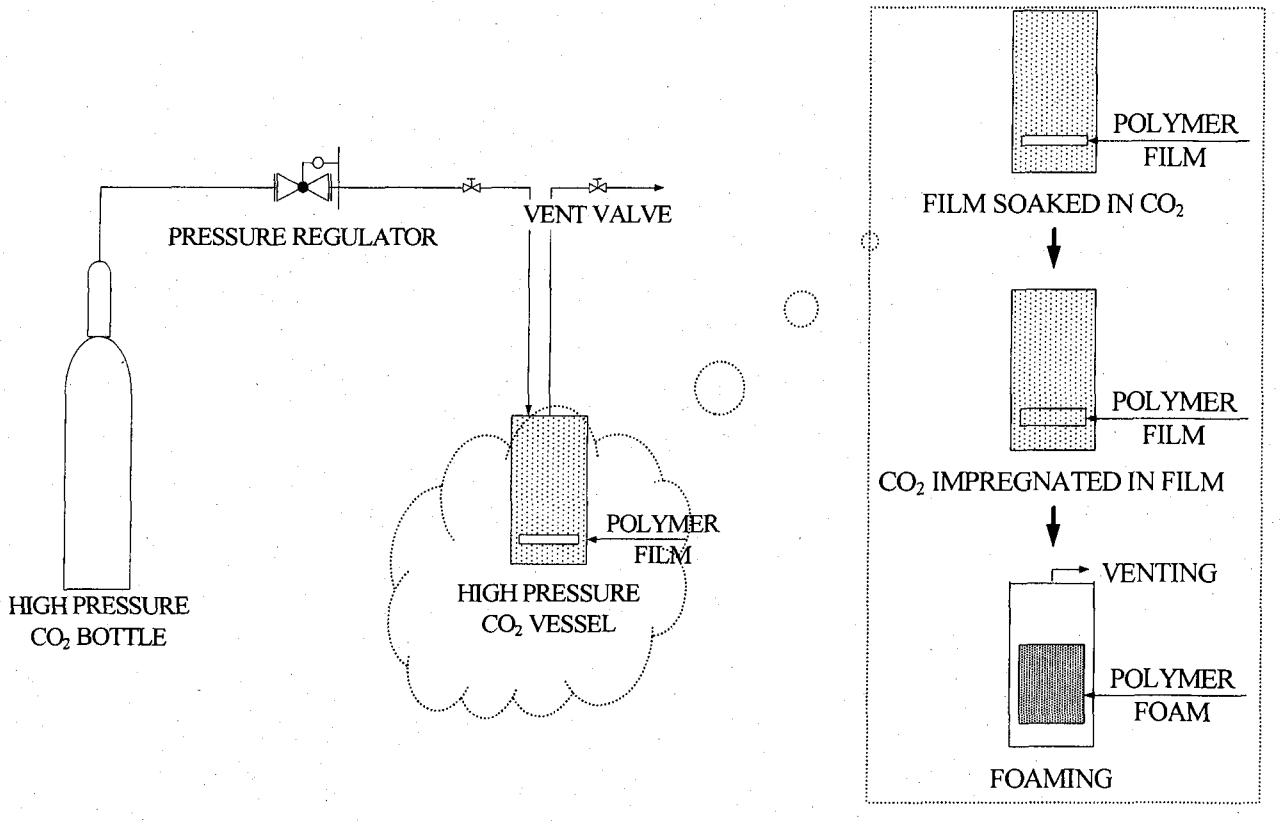

Figure 3.3. The foaming process schematics

In experiments that the CO_2 soaking process also involved ethanol or water solutions, the polymer films were soaked in ethanol or water solutions in glass vessels; the glass vessels were placed in a high pressure CO_2 container (Figure 3.4). The rest of the foaming procedures were the same as described above.

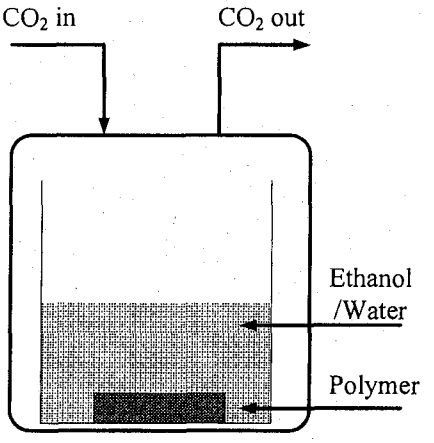

Figure 3.4. Polymer with ethanol/water system soaking and foaming process

3.2.5 CO_2 up-take measurements

CO_2 up-take was measured at room temperature and at 5.86 MPa and room temperature. PLGA 50/50, PLCL and PCL samples were prepared in round shaped films with a diameter of 6.30 mm and a thickness of 0.45 mm.Their weight and thickness were measured at first. The samples were then placed in the pressure vessel and saturated at the desired pressure and room temperature for 24 h. The CO_2 high pressure vessel was then vented, and the sample was removed from the vessel for weighing immediately. The difference in weight of the sample is equal to the amount of CO_2 absorbed by the polymer. In order to obtain the weight of the sample at time zero, a plot of sample weight versus the square root of time was carried. This should result in a straight line [105]. By extrapolating the straight line to the time zero, the sample weight time zero could be obtained. CO_2 up-take was calculated by dividing the difference in weight between the sample initial weight and the sample weight at the time of zero.

3.2.6 Scanning electron microscope (SEM)

Foamed samples were stored at room temperature for 3 days before they were fractured in liquid nitrogen and the surfaces were examined. The porous structures on the fractured cross section and surface were examined using a scanning electron microscope (SEM) (Hitachi S-4800 field SEM, Tokyo, Japan) with accelerating voltage 1.2 kV.

3.2.7 Gel permeation chromatography (GPC)

Polymer molecular weight and distribution were determined using GPC Viscotek TDA302 (VISCOTEK, Houston, TX). The GPC system is comprised of 2 ViscoGEL columns GMPWxl (Viscotek) coupled with a Viscotek on-line triple detector SEC3 system which included a four-capillary differential viscometer, right angle laser light scattering detector, and differential refractometer. The system was controlled with modular Windows TM-based OmniSEC™ 4.2 software (VISCOTEK, Houston, TX). Polymers were dissolved in tetrahydrofuran (THF) at a concentration of 1mg/mL. A sample size of 100 µl was injected and eluted at a flow rate of 1 ml/min. THF was used as mobile phase, and narrow distribution polystyrene standards (Mp=4, 000, 20, 000, 63, 000, and 200, 000, respectively. Polydispersity index=1.04, Polyscience, Warrington, PA) were used to construct a calibration curve. The molecular weight and poly distribution index of the sample polymers were then calculated by using OmniSEC™ 4.2 software.

3.2.8 Differential scanning calorimetry (DSC)

The thermal analysis of the polymers and their blends was verified by TA instruments DSC (TQC1000, TA instruments, New Castle, DE). Samples were scanned between -80°C and 100 °C at a heating rate of 10 °C /min. N_2 was used as a purging gas at a flow rate of 50 mL/min.

3.3 Characterization of scaffold

3.3.1 Image analysis and cell density

The pore sizes and distribution were counted and calculated by using Image-Pro Plus 5.0 software. (Media Cybernetics Inc., Silver Spring, MD). Cell sizes were measured from the SEM images. The number of cells/cm^3 (cell density) in the foam (N_f) was approximated by:

$$N_f = \left(\frac{nM_X^2}{A} \right)^{3/2}, [128]$$

where n, M_X, and A are the number of pores in the micrograph, magnification and area of the micrograph (cm^2), respectively.

3.3.2 Foam density and porosity

Foam density was characterized by the total immersion method using a Mettler ME-163 balance (Mettler-Toledo, Inc, Columbus, OH). According to the Archimedean Principle [129], a solid body immersed in a liquid loses as much of its own weight as the weight of the liquid it has displaced. The solid body is first weighed in air and then immersed in water. From these two weightings, density ρ is calculated as follows:

$$\rho = \frac{W_A}{W_A - W_B} * \rho_0 , [130]$$

Where

ρ = Density of solid body;

W_A= Weight of solid body in air;

W_B= Weight of solid body when immersed in test liquid (water);

ρ_0 = Density of test liquid (water) at a given temperature T. The density table for distilled water with temperature is attached in appendices.

The densities of the unfoamed (ρ_p) (polymer film density) and foamed (ρ_f) (polymer foam density) samples were both measured using the method mentioned above. The porosity (ε) was calculated by:

$$\varepsilon = 1 - \frac{\rho_f}{\rho_P}, \quad [8]$$

3.3.3 Scaffold sectioning and microscopy

Polymer scaffolds were soaked in Tissue-Tek solution (O.C.T. Compound) (Sakura Finetek, CA) in Peel-A-Way Disposable Embedding Molds (Polysciences, Inc., USA) and frozen at -25°C in Leica CM3050S Cryosectioning system (Leica Microsystems (Canada) Inc., ON). Then the solidified samples with Tissue-Tek (O.C.T. Compound) (Sakura Finetek, CA) were sectioned into 5μm thin layers on superfrost slices (VWR, USA).

The slices with thin-layered samples were dipped into water for 2 s to get rid of the Tissue-Tek solution. Finally the dried samples the on slices were checked under Motorised Research Microscope IX81 (Olympus, Japan).

3.3.4 Elemental analysis

The polymeric scaffold samples were dried in vacuum oven at room temperature for one week until weights are constant. The dried samples were analyzed by elemental analysis instrument (Flash 1112 Series EA, Italy) to obtain the atomic compositions of resulting scaffolds. Assume that the weight percentages of PLGA 50/50 and PEG in the resultant scaffolds are X and Y, respectively. According to the results obtained from the elemental analysis, by using the following formula, it is possible to calculate the value of X to Y (weight ratio of C to O). Then, according to the molecular weights of PLGA 50/50 and PEG, the weight ratios of PLGA 50/50 and PEG in resulting scaffolds could be obtained.

$$X * C\%_{(PLGA\ 50/50)} + Y * C_{\%(PEG)} = C\%$$

$$X * (100-C\%_{(PLGA\ 50/50)}) + Y * (100-C_{\%(PEG)}) = O\%$$

– $C\%_{(PLGA\ 50/50)}$: weight percentage of carbon in the compound of PLGA 50/50;

– $C\%_{(PEG)}$: weight percentage of carbon in the compound of PEG;

– C%: weight percentage of carbon in the resultant scaffolds, which was obtained from element analysis.

– O%: weight percentage of oxygen in the resultant scaffolds, which was obtained from element analysis.

3.3.5 Statistics

Data obtained from the image analysis were analyzed by Minitab 14 (Minitab Inc., State College, PA). Statistical analysis was carried out with 95% confidence. One-way ANOVA was employed to compare different groups.

4. Results

4.1 CO_2 uptake

Polymer films were placed into high pressure CO_2 vessel (5.86 MPa, room temperature) for 24 h to fully reach the saturation condition. Then the system is fast depressurized and the polymer samples were rapidly taken out to an external balance with 0.001mg accuracy (Sartorius, Germany). The weights of polymer samples as a function of time were recorded. The CO_2 concentration in a polymer sample as a function of square root of time is reported in Figures 4.1-A, 4.1-B and 4.1-C, indicating the CO_2 desorption profiles of PLGA 50/50, PLCL and PCL films, respectively.

The CO_2 concentration in a polymer at time t, $C_t = \frac{M(0) - M(t)}{M_P}$

where M(0) is the sample CO_2 uptake and $M(t)$ is CO_2 duffusion mass measured at time t, Mp is the mass of polymer measured before the experiment.

According to Fick's second law [131], the CO_2 concentration at time t can be described as

$$C_t = C_0 - A_f \sqrt{\frac{D_d * t}{\pi}}, \text{ [98]}$$

where C_0 is the CO_2 concentration at time zero; A_f is a constant related with the sample thickness, sample weight and the total CO_2 mass saturated in polymer; and D_d is the desorption diffusivity. The detail explanation of Fick's law is stated in Appendices (A4).

Therefore, Fick's law can be used to calculate the solubility of CO_2 by extrapolating the linear fitting to zero desorption time. Figure 4.1(A, B and C) indicate that the linear relationship between the concentration of CO_2 and the square root of desorption time validates the assumption that the polymer follows the Fick's diffusion. It is worthwhile to

note that typically about 30 s was needed to depressurize the system, open the cell and to place the sample on the external mass balance. As a result, there is no data between time zero and 30 s. If we can obtain more data near time zero, the more accurate results of CO_2 solubility can be obtained.

PLGA 50/50, PCL and PLCL has the solubility of 20.11 % (wt%), 15.49 % (wt%) and 16.63 % (wt%), respectively. The PLGA 50/50 has the highest solubility and PCL has the lowest solubility. From the slopes of the linear fitting lines, we find that PLCL has the fastest diffusion, and the PLGA has the lowest diffusion speed. The release behaviour (slopes) of carbon dioxide from the polymeric matrix during desorption is due to the chain mobility of the polymer. Also the slopes are related with sample size but which will not affect the calculation of the solubility. The solubility results are similar with that in other people's work, i.e., 20%(wt) CO_2 in PLGA 50/50 at 30 °C and 6 MPa [106], which demonstrate that the technique is feasible on measuring the solubility on these materials in this condition. It is worthy to note that this is a simple and rough method because it neglects the swelling.

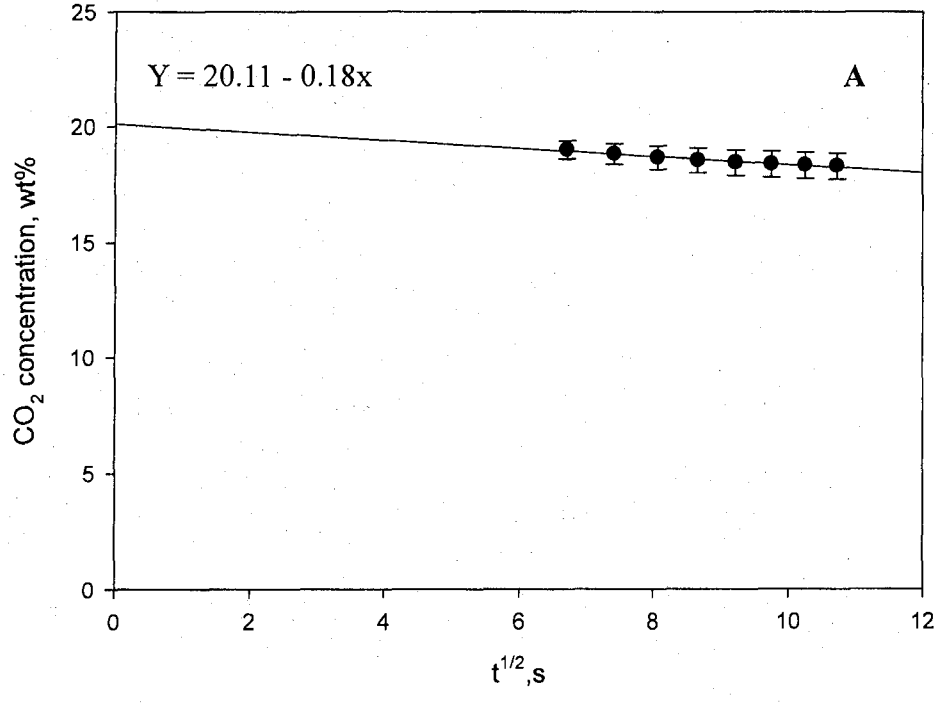

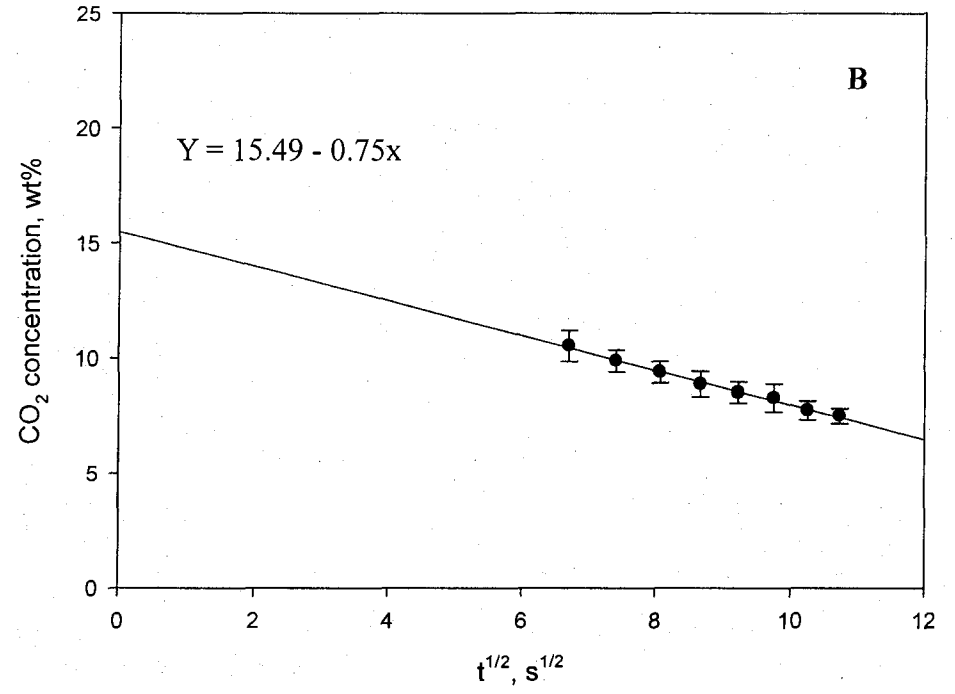

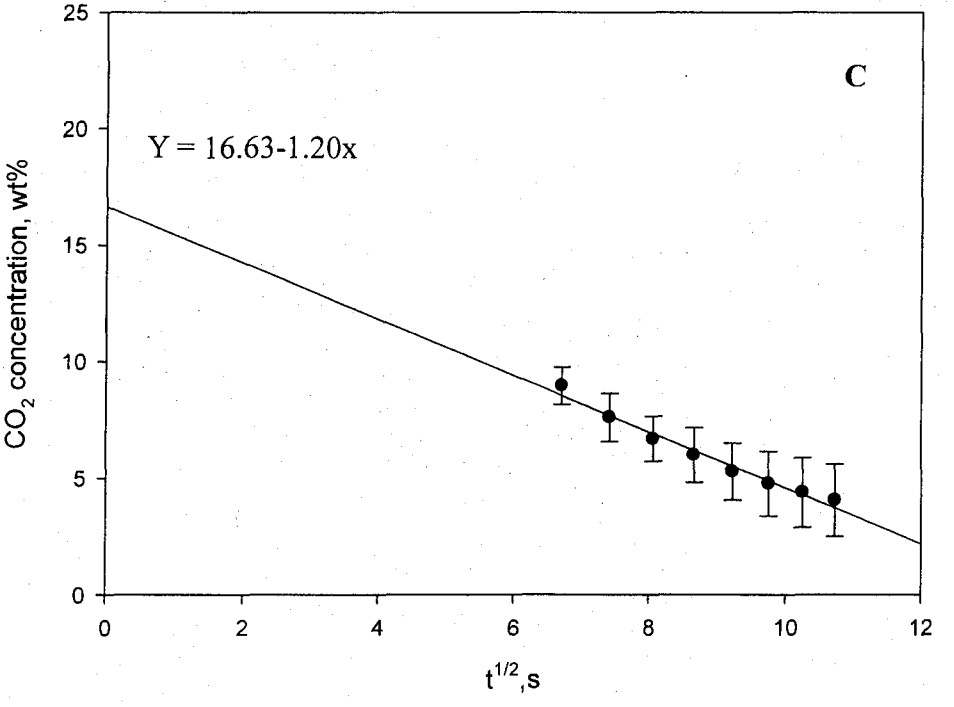

Figure 4.1 CO_2 release profile from PLGA 50/50 (A), PCL (B) and PLCL (C) films treated at 5.86 MPa and room temperature. Points are experimental measurements and lines are used to extrapolate CO_2 concentration to time zero. The standard deviation of the experimental data was calculated with three repetitions of the experiment.

4.2 Miscibility

It is not possible to get varieties of morphologies only relying on the pure limited polymers (PLGA 50/50, PLCL and PCL in our project). The use of polymer blends is a solution because the unlimited blend ratios can be created between the limited polymers and those blends of the limited polymers can be foamed into different morphologies due to their different physical properties. Since miscibility is an important element in polymer blends, so it should be tested before the foaming experiments. These experimental results are shown and discussed as follows:

A thermal analysis (DSC Figure 4.2.1) of the blends of PLGA 50/50 and PLCL shows that their Tg peaks come together. This indicates that they are partial miscible polymers and the Tg shift is due to the change of phase composition. When the (PLGA 50/50)/PLCL ratio is 1/3, the two peaks merge into one. If we calculate the Tg in the blend by using the Fox Equation [132],

$$\frac{1}{T_g} = \frac{w_1}{T_{g1}} + \frac{w_2}{T_{g2}},$$

where

w_1 – PLGA 50/50 weight percentage in the blend;

w_2 – PLCL weight percentage in the blend;

T_{g1} – PLGA 50/50 Tg;

T_{g2} - PLCL Tg;

T_g – The final merged glass transition temperature in the polymer blend;

The Tg of the (PLGA 50/50)/PLCL blend with a weight blend ratio of 1/3 (Tg=30.63°C) almost equals the theoretical value (Tg=32.92°C) calculated by the Fox equation, which means the two polymers are miscible and formed into a one-phase system.

The Tg difference between the experimental value and the theoretical value may be because the (PLGA 50/50)/PLCL blend ratio is not accurate enough or more complex models, such as the Couchman approach [133] should be applied in this case. We hypothesize that the good compatibility is due to the common lactic groups in PLGA 50/50 and PLCL (50% in (PLGA 50/50) and 80% in PLCL), respectively.

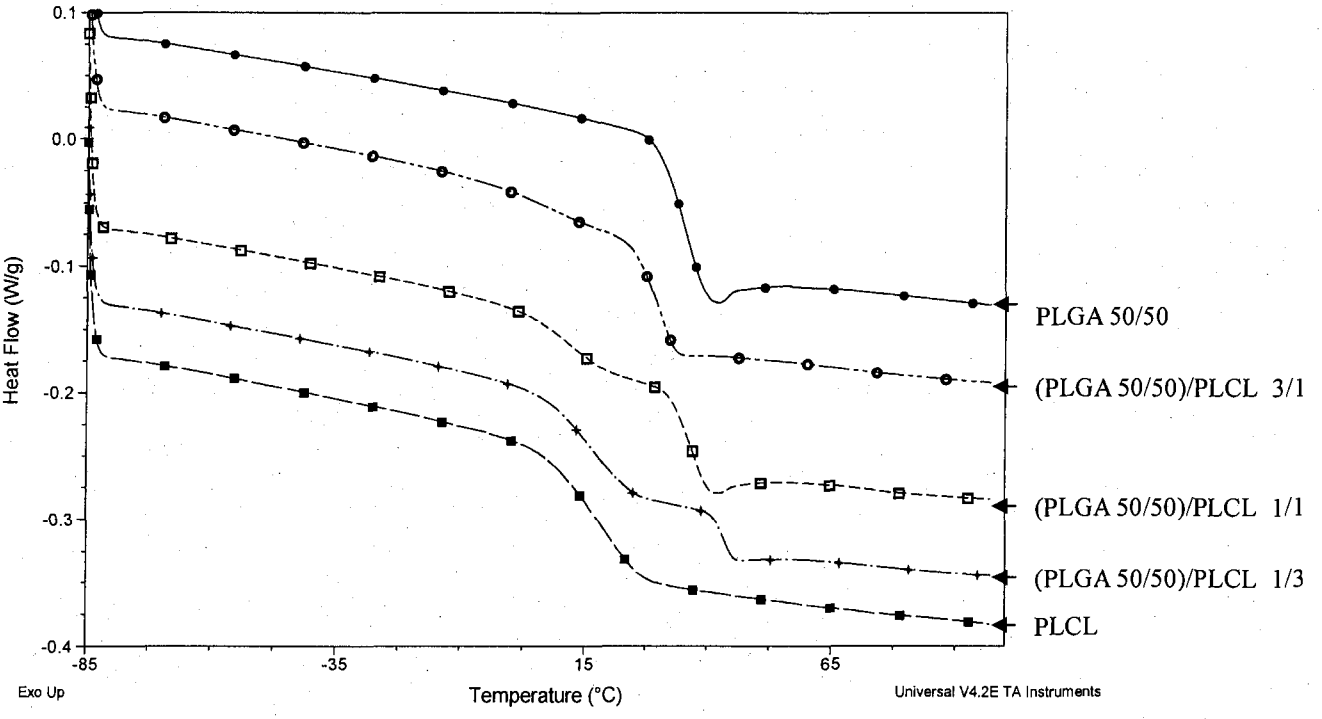

Figure 4.2.1 A thermal analysis of (PLGA 50/50) and PLCL blends

For the PLCL and PCL blends, Figure 4.2.2 shows that there is no PLCL Tg shift and the PCL Tg is not easy to observe due to the high crystallinity of PCL [134]. Therefore, it is difficult to predict the miscibility of PLCL and PCL using DSC. However, after the polymer films are prepared and foamed, these foams show homogeneous morphologies, suggests that these polymers mix very well. Both PLCL and PCL share poly-ε-caprolactone chain

segments in their backbones. Although the concentration of the segment is not very high in PLCL (20%), it is still possible to form homogeneous polymer blends using PLCL and PLCL.

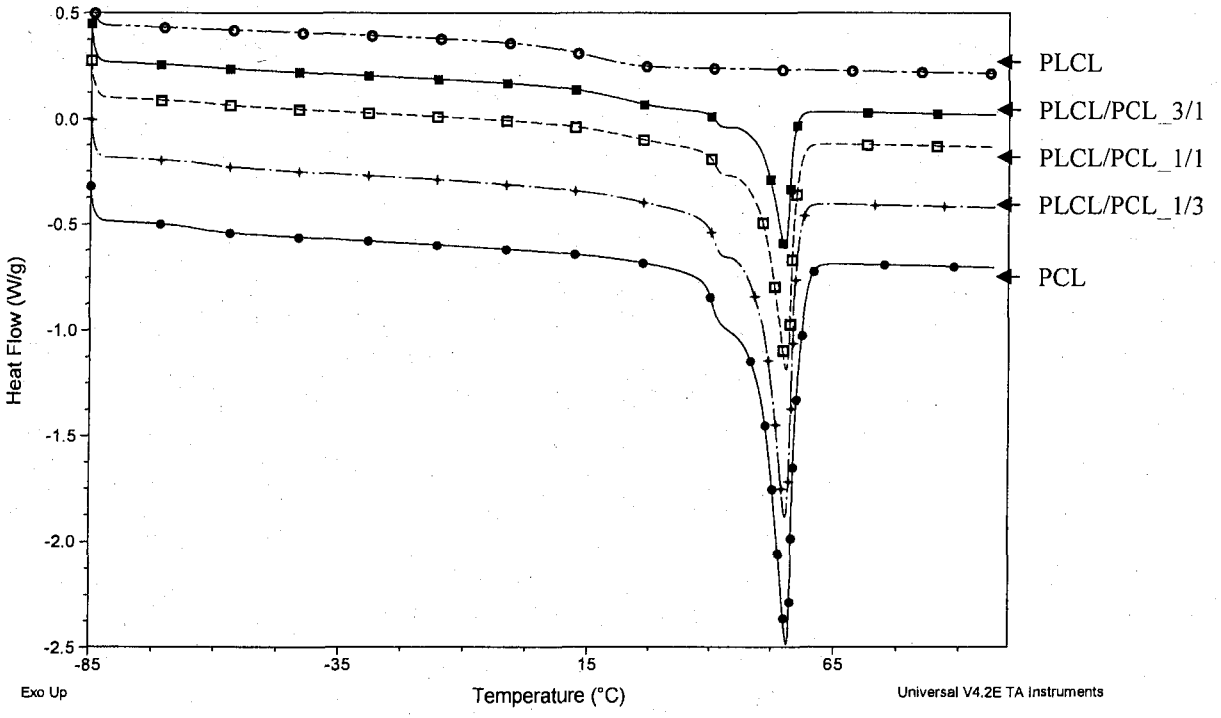

Figure 4.2.2 A thermal analysis of PLCL and PCL blends

The PCL/ (PLGA 50/50) blends are totally immiscible because even the blends solutions are separated automatically into two phases which are the PLGA 50/50 (brown color) solution and the PCL (transparent color) solution. The polymer films can also be found in two layers with a white color and a brown color. The DSC results shown in Figure 4.2.3 are only the simple combinations of their pure polymer thermal behaviors with different blend ratios.

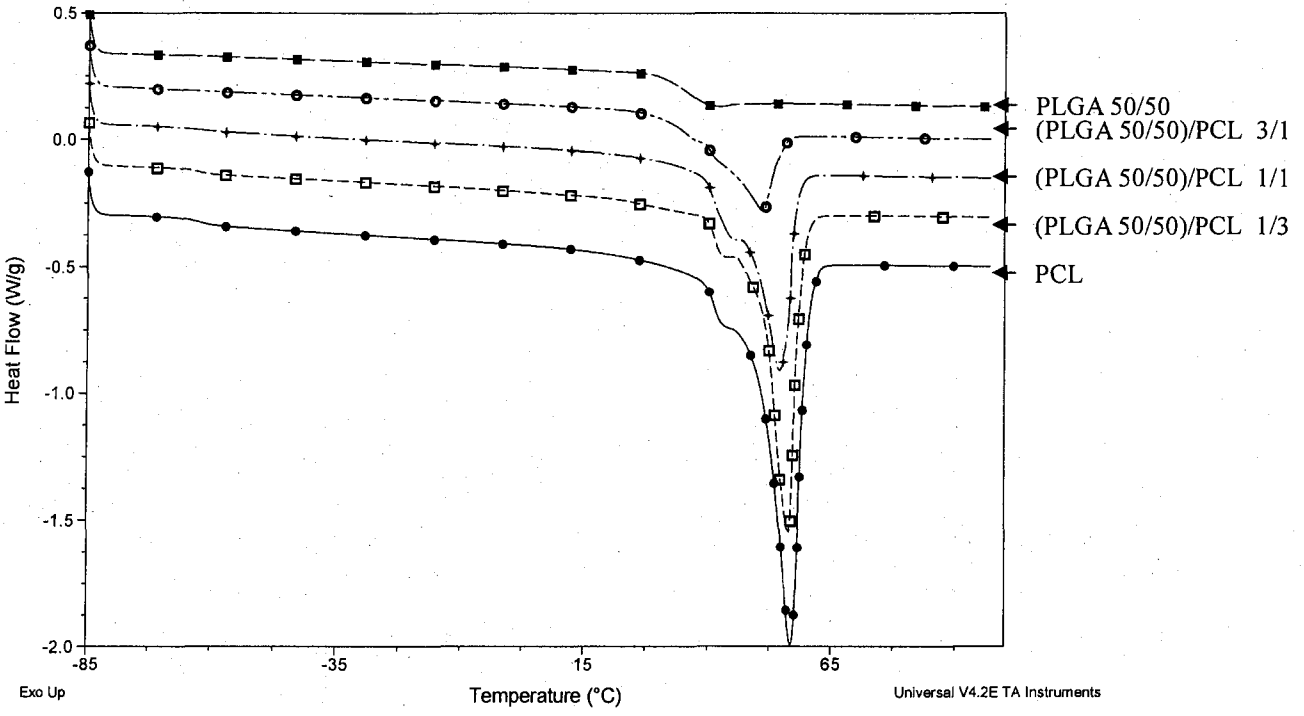

Figure 4.2.3 A thermal analysis of (PLGA 50/50) and PCL blends

4.3 Morphologies

4.3.1 Single layer scaffolds

Figure 4.3.1 shows PLGA 50/50, PLCL, and PCL foam morphologies obtained by using a pressure quench foaming method at 1.38 MPa, 2.76 MPa, and 5.86 MPa at room temperature.

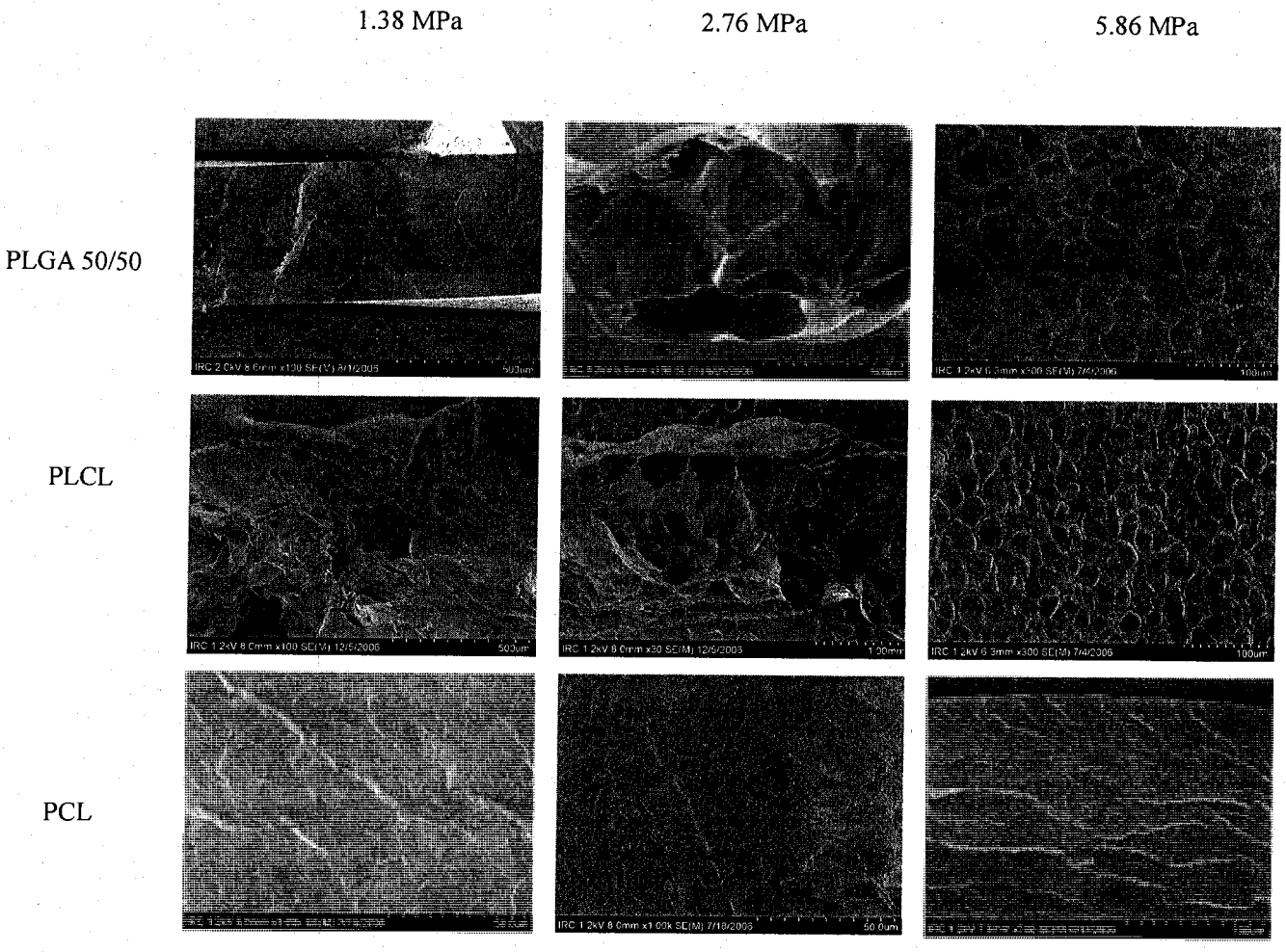

Figure 4.3.1 Morphologies of pure polymers (PLGA 50/50, PLCL and PCL) foamed by a pressure quench method at 1.38 MPa, 2.76 MPa, and 5.86 MPa at room temperature.

As shown in Figure 4.3.1, the PLGA 50/50 film cannot be foamed at 1.38 MPa. The CO_2 concentration is not high enough to relax the polymer molecules and to overcome the energy barrier to nucleate [92]. The PLCL film is easily foamed at 1.38 MPa because the Tg (~20°C) of the amorphous polymer is a little bit lower than room temperature. Once the CO_2 molecules diffuse into the PLCL matrix, the Tg of PLCL will be further decreased. Thus the polymer is easily relaxed and foamed at 1.38 MPa and room temperature. The PCL film cannot be foamed under 1.38 MPa, 2.76 MPa and 5.86 MPa, due to the polymer's high crystallinity. In theory, CO_2 molecules can not penetrate into crystals; therefore crystallized polymers cannot be easily foamed. To overcome this problem, people normally choose high temperatures and pressures (i.e., supercritical conditions) because the crystals are totally destroyed at these conditions [115]. The lower pressure means less nucleation sites and bigger pore sizes [114]. If the CO_2 pressure is higher, the pore size will decrease because of the higher CO_2 concentration and more nucleation sites generated afterwards. When the CO_2 pressure increases, PLGA 50/50 pore sizes decrease from 268 μm (2.76 MPa) to 20.4 μm (5.86 MPa) and PLCL pore sizes decrease from 231 μm (2.76 MPa) to 12.4 μm (5.86 MPa) (Table 3.1).

As shown in Figure 4.3.1, different polymers foam differently even at the same pressure. Therefore we believe that by blending different materials with good compatibilities, different blend morphologies can be achieved. To demonstrate this, PCL/PLCL blends at different ratios were foamed. Figure 4.3.2 shows the effect of blend ratios on the resulting foam morphologies.

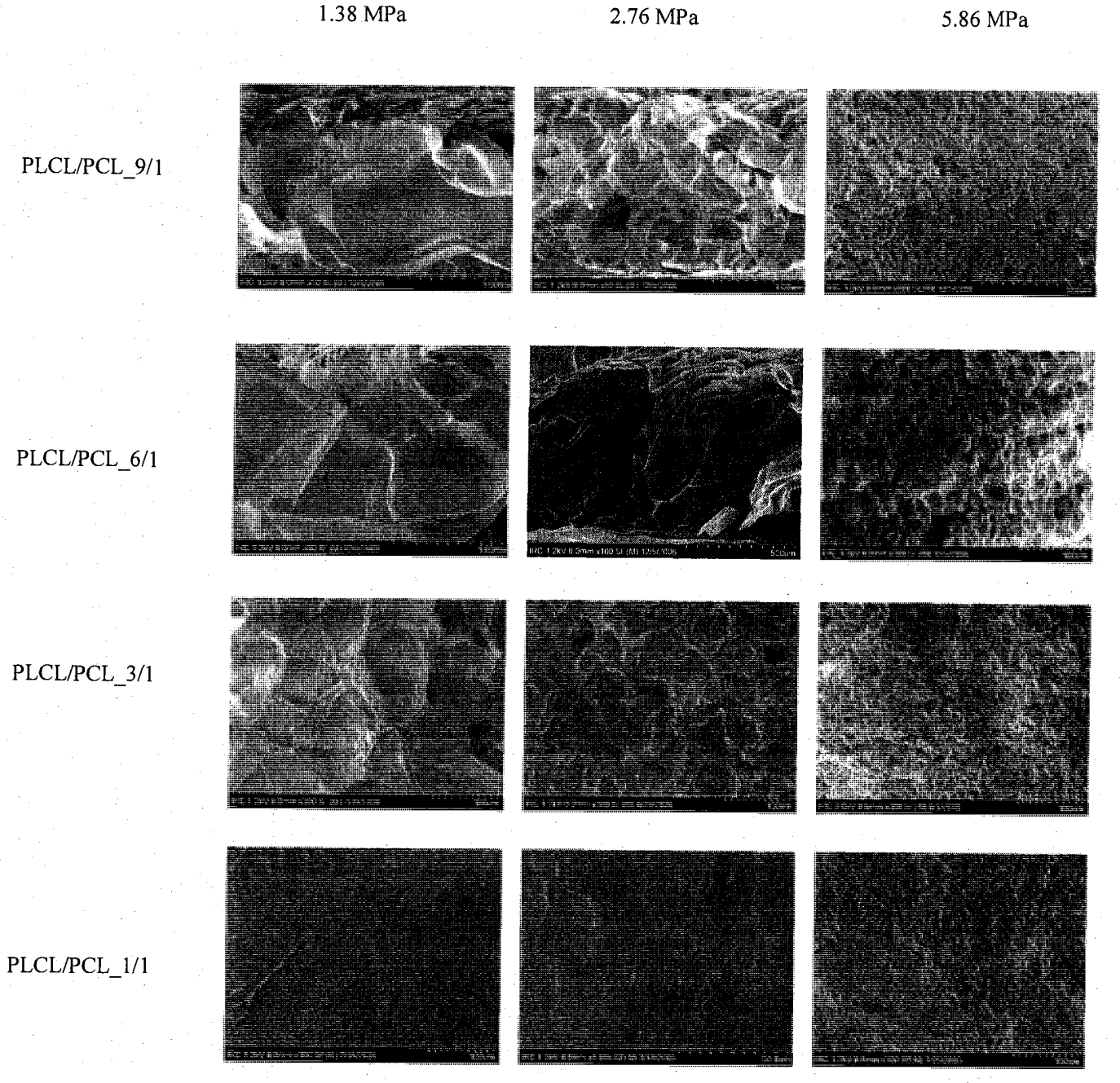

Figure 4.3.2 Morphologies of blend polymers PLCL/PCL foamed by a pressure quench method at 1.38 MPa, 2.76 MPa, 5.86 MPa and at room temperature.

With the increase of PCL in the blend system, the blends become more difficult to foam. When the pressure is higher, the number of nucleation sites increases. Therefore the foam morphologies show that these foams will have the smaller pore sizes (Table 4.1).

Table 4.1 Pore sizes of PLCL and PCL blends foamed by a pressure quench method at 1.38 MPa, 2.76 MPa, 5.86 MPa and room temperature.

	1.38 MPa		2.76 MPa		5.86 MPa	
	Pore size μm	Standard Deviation μm	Pore size μm	Standard deviation μm	Pore size μm	Standard deviation μm
PLCL	314	± 115	231	± 64.3	12.4	± 6.1
PLCL/PCL_9/1	735	± 202	196	± 47.5	10.2	± 5.47
PLCL/PCL_6/1	534	± 128	185	± 32.9	8.84	± 2.51
PLCL/PCL_3/1	67.2	± 22.9	34.5	± 12.5	5.79	± 1.26

It can be observed clearly that the foam shrinkage phenomenon appears during the PLCL/PCL foaming process due to the elasticity of the polymers. Because the CO_2 molecules can not support the shrinkage of cell walls, some of the pores shrink and collapse. The collapsing phenomenon becomes more pronounced when the pressure decreases. Therefore, the pore sizes can not be counted accurately in the foams foamed at 1.38 MPa. With the increase of PCL concentration in the PLCL/PCL blends, the shrinkage phenomenon in the foaming process becomes less pronounced.

The (PLGA 50/50)/PLCL blends are amorphous and they can be foamed into high porosity foams at 5.86 MPa. The pore sizes can be adjusted by the blend ratio between (PLGA 50/50) and PLCL (Figure 4.3.3).

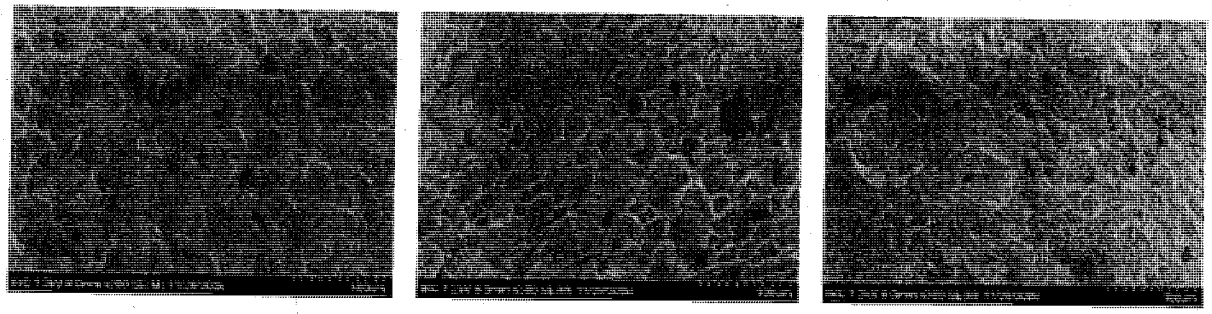

(PLGA 50/50)/PLCL_1/3 (PLGA 50/50)/PLCL_1/1 (PLGA 50/50)/PLCL_3/1

Figure 4.3.3 Morphologies of polymer blends (PLGA 50/50)/PLCL foamed by a pressure quench method at 5.86 MPa and room temperature.

The pore sizes of the blends ranges from 13.0 μm ((PLGA 50/50)/PLCL_1/3) to 18.6 μm ((PLGA 50/50)/PLCL_3/1) which are located between the pore sizes of pure PLCL (12.3μm) and that of pure PLGA 50/50 (20.4μm).

All these blends show that they have higher porosities and smaller pore sizes when the pressure increases (Figure 4.3.4). PLGA 50/50 foamed at 5.86 MPa yields a porosity of over 90%. The porosity decreases drastically when the PCL concentration increases in PLCL/PCL blends. As for (PLGA 50/50)/PLCL blends, the porosity ranges from 78% to 82%, between the porosity of PLGA 50/50 (92%) and that of PCL (76%).

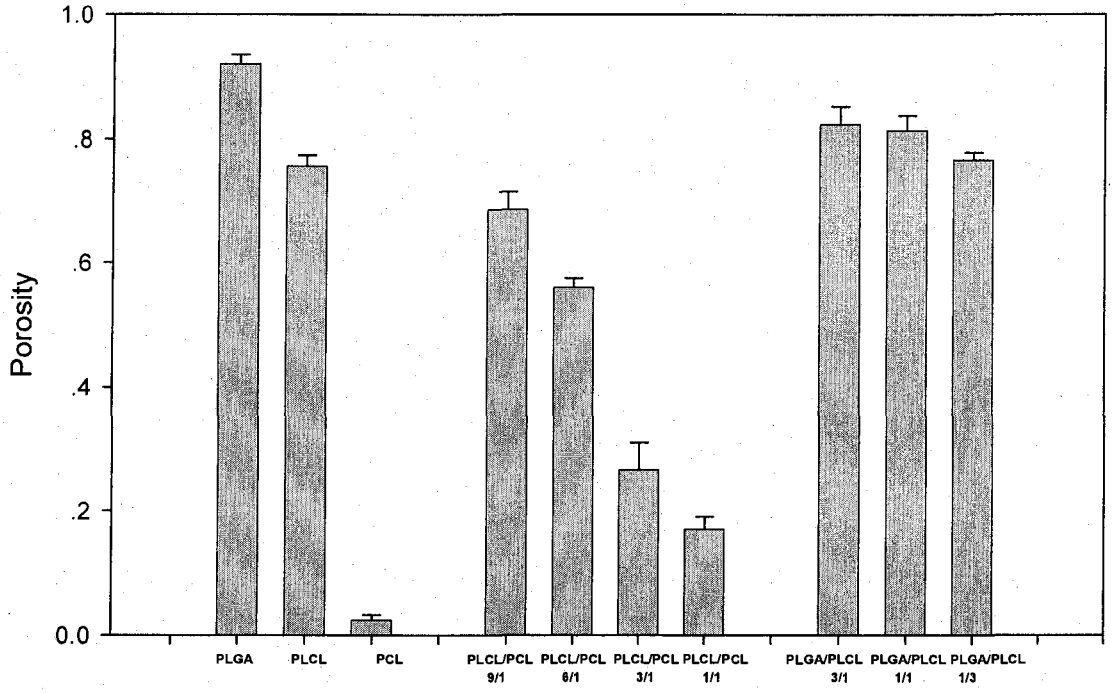

Figure 3.3.4 Porosities of polymer PLGA50/50, PLCL, PCL and their blends foamed by a pressure quench method at 5.86 MPa and at room temperature.

The effect of pressure on the foam morphologies is illustrated in Figure 4.3.5. It can be concluded that the porosities increase with increasing foaming pressure in the PLCL/PCL system. The PLCL foam has the highest porosity in the PLCL/PCL blend system whereas the PCL film can not be foamed at 5.86 MPa.

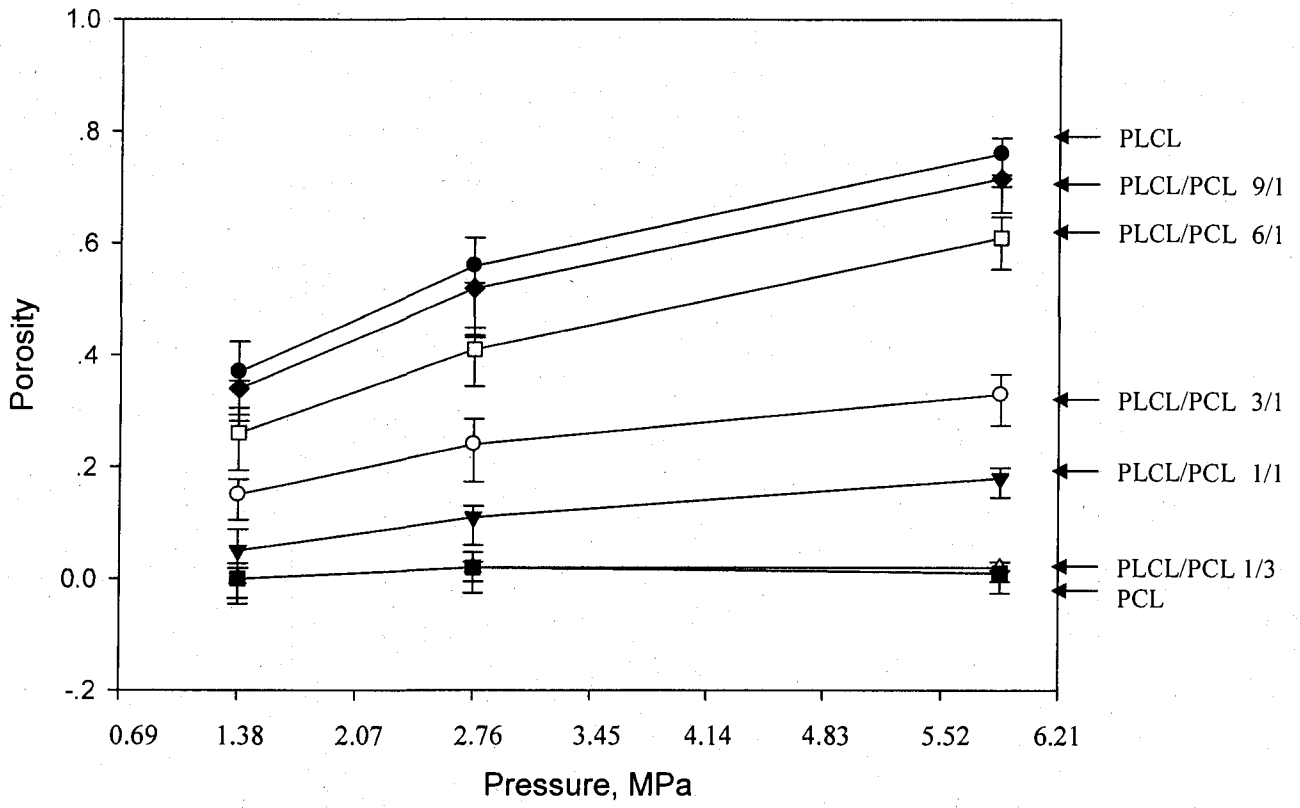

Figure 4.3.5 Porosities of PLCL/PCL blends foamed by a pressure quench method at 1.38 MPa, 2.76 MPa, and 5.86 MPa at room temperature.

4.3.2 Gradient (Multilayered) scaffolds

From the morphology results obtained, the high porosities and homogeneous structures can be generated at 5.86 MPa by a pressure quench method at room temperature. Therefore the multilayered foams were fabricated at this condition. The use of PLCL, PLGA 50/50, PCL is feasible to form the gradient structures because the polymers and their blends can form different morphologies with significant differences at the same foaming condition, as has been shown in section 4.3.1. The results shown in Figures 4.3.6-4.3.9 are two-layered structures and their pore size distributions foamed by a pressure quench method at 5.86 MPa and at room temperature.

The SEM micrographs show that there is no phase separation between the different morphologies within one scaffold, suggests that the solvent casting technique is good enough to make the molecules entangle each other into the neighbor layer. The different morphologies also show that the solvent vaporization is fast enough to avoid the layered films mixed into one homogenous phase. For PCL/(PLCL/PCL) two-layered films with one layer composed of the PLCL/PCL blend polymer and another layer composed of the PCL polymer, the PLCL/PCL ratio can be adjusted from PCL 100% to PLCL 100%. The two-layered scaffold without separation can be obtained likely due to the strong entanglement between PLCL and PCL molecules. The fabrication of the (PLGA 50/50)/ (PLCL/PCL) two-layered system is relatively difficult. When the PLCL/PCL ratio is less than 3/1, the two-layered scaffold will separate into two layers due to the weak entanglement and the bigger expansion difference in the foaming process.

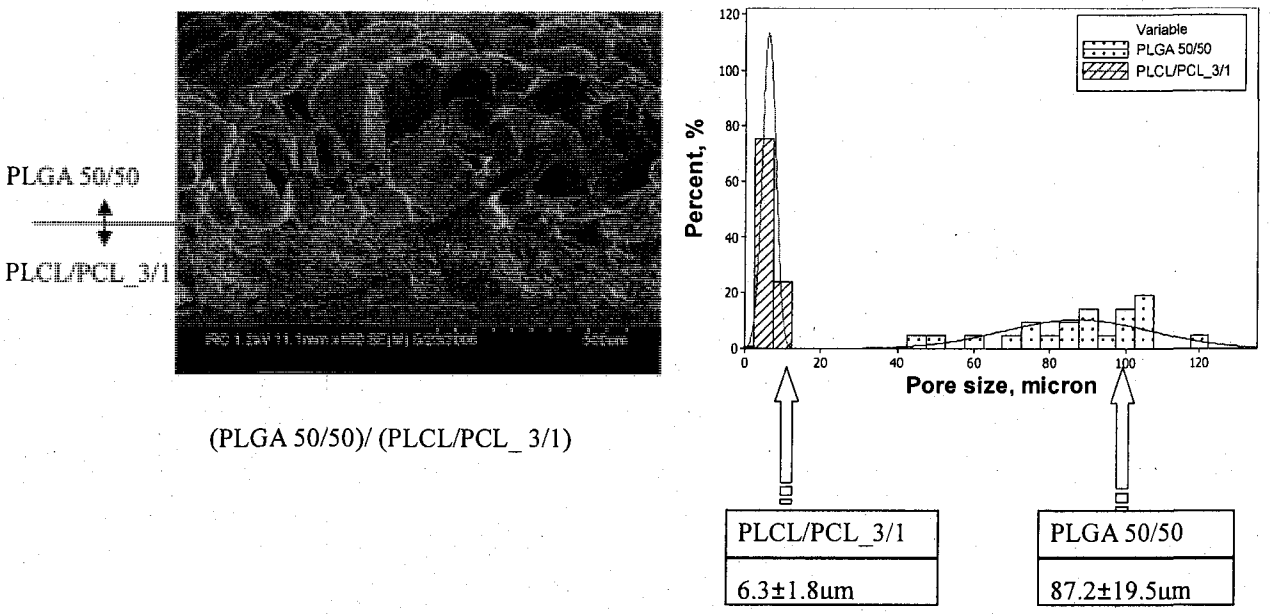

Figure 4.3.6 The two-layered foam morphology and pore size distribution—(PLGA 50/50)/ (PLCL/PCL_3/1) foamed by a pressure quench method at 5.86 MPa and at room temperature.

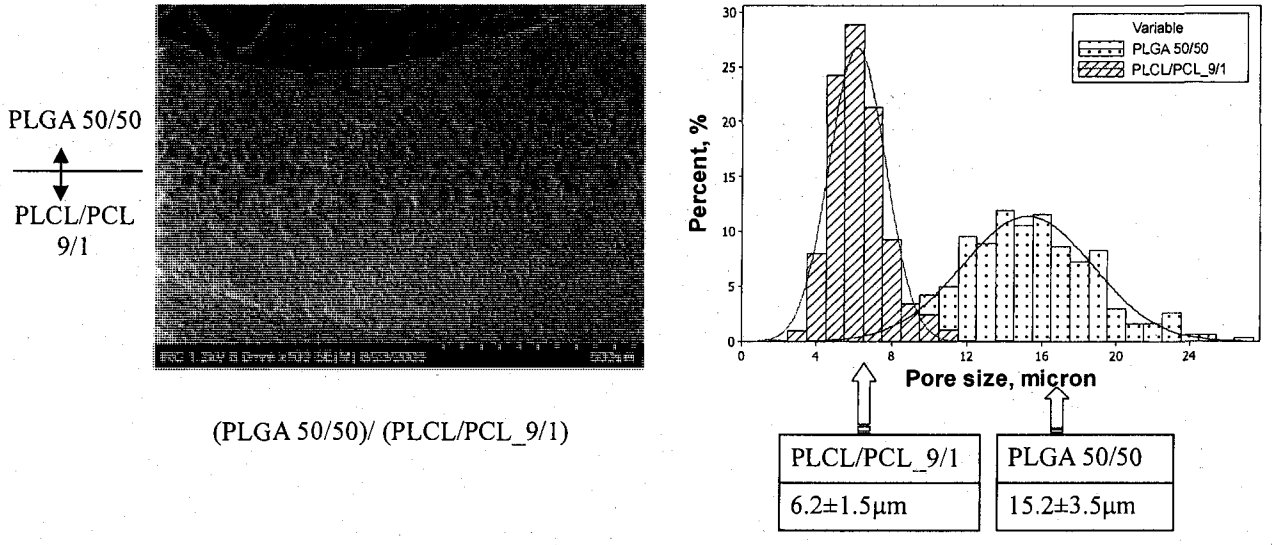

Figure 4.3.7 The two-layered foam morphology and pore size distribution—(PLGA 50/50)/ (PLCL/PCL_9/1) foamed by a pressure quench method at 5.86 MPa and at room temperature.

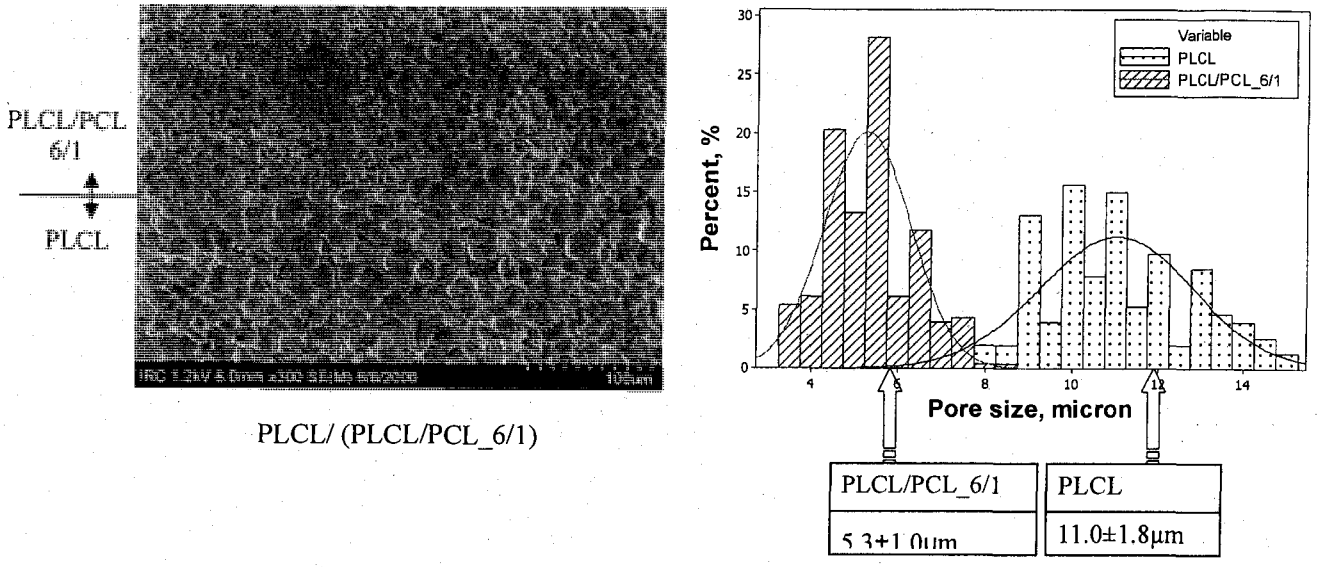

Figure 4.3.8 The two-layered foam morphology and pore size distribution—PLCL/ (PLCL/PCL_9/1) foamed by a pressure quench method at 5.86 MPa and at room temperature

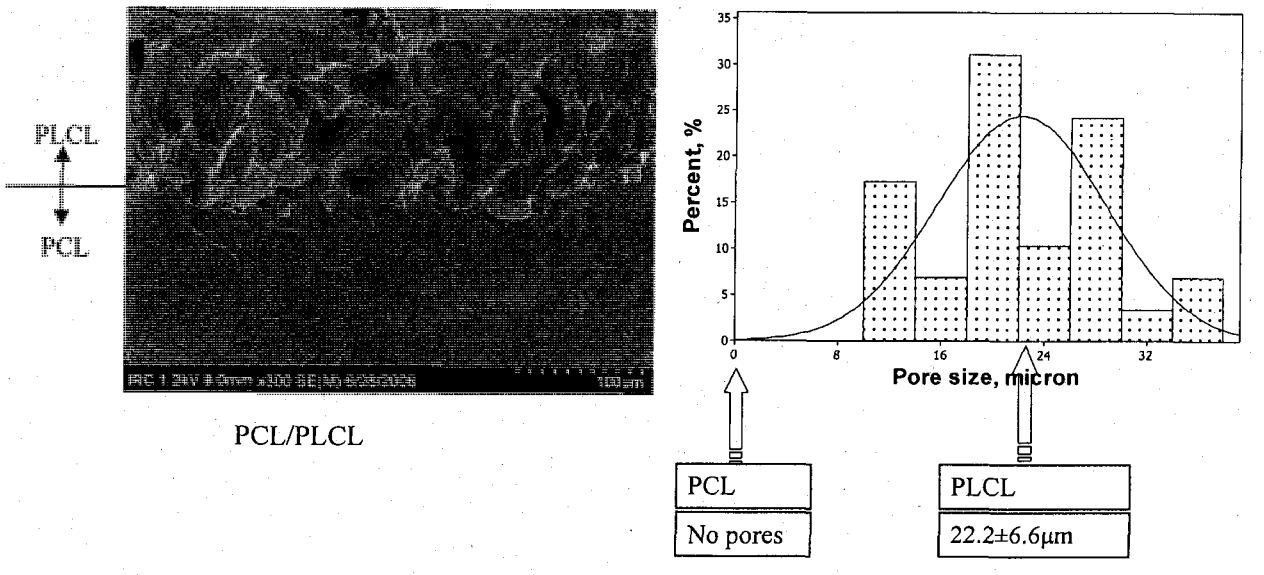

Figure 4.3.9 The two-layered foam morphology and pore size distribution—PLCL/PCL foamed by a pressure quench method at 5.86 MPa and at room temperature

Figures 4.3.10 and 4.3.11 show a three-layered and a six-layered scaffold with gradient structures. It is easy to find that the pore sizes and morphologies in the gradient structures are different in comparison with homogeneous scaffolds. Srinivas Siripurapu et al explain the phenomenon that the surface-constrained CO_2 foaming is totally different from the free film foaming on the nucleation, the pore growth, and the gas diffusion [135]. Once the foaming process starts, the CO_2 molecules will diffuse out from the polymer matrix. For the homogeneous polymer films, the gas diffusion happens evenly and freely to the entire film surface. For the layered gradient films, CO_2 molecules can only diffuse out easily from one side. Besides, the heterogeneous stretching of the gradient structures in the foaming process will also affect the CO_2 nucleation, the pore growth and the diffusion [135]. Figure 4.3.11 show the pore size's growth direction is from zero (in PCL layer) to very big (toward the PLCL layer). The anisotropic morphologies are most likely to be useful on one directional drug delivery.

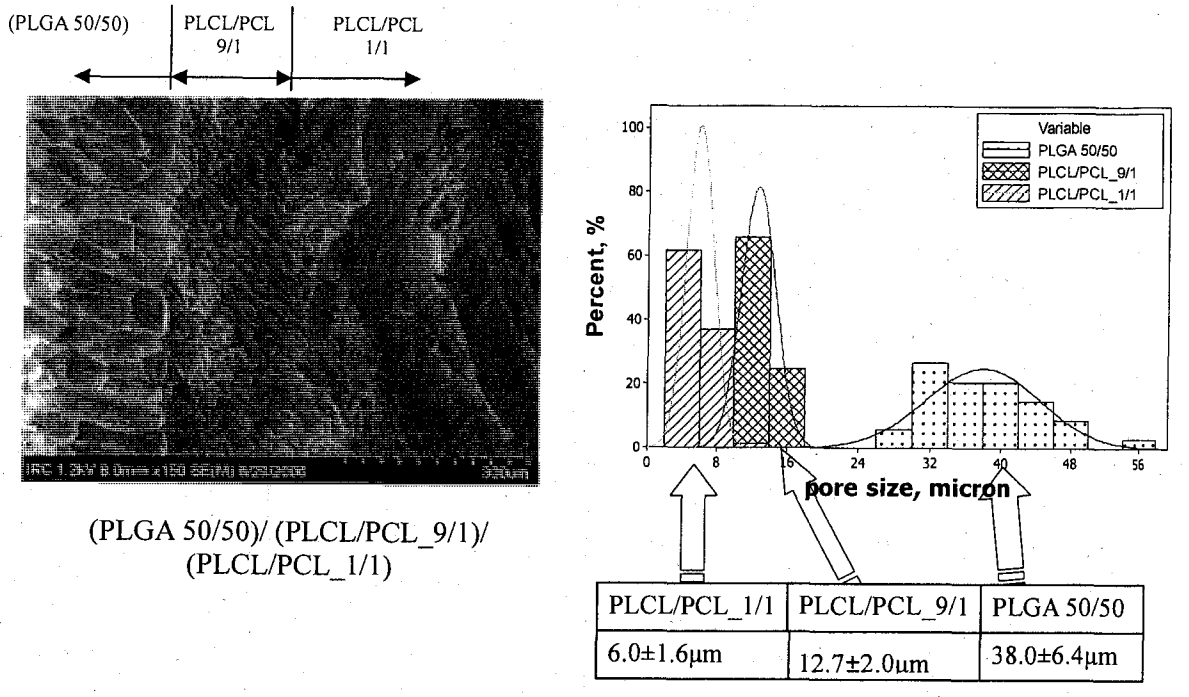

Figure 4.3.10 The three-layered foam morphology and pore size distribution—(PLGA 50/50)/ (PLCL/PCL_9/1)/ (PLCL/PCL_1/1) foamed by a pressure quench method at 5.86 MPa and at room temperature

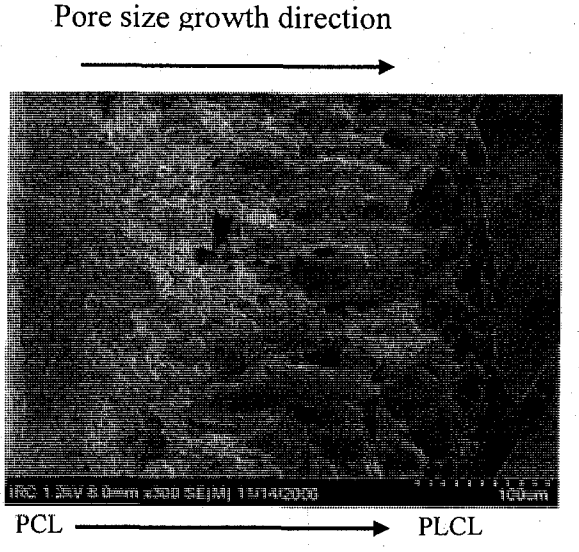

Figure 4.3.11 The six-layered foam morphology—PCL/ (PLCL/PCL_1/1)/ (PLCL/PCL_3/1)/ (PLCL/PCL_6/1)/ (PLCL/PCL_/9/1) /PLCL foamed by a pressure quench method at 5.86 MPa and at room temperature.

4.3.3 Multi-layered tubular structures

One of the objectives of this study is to fabricate porous, tubular scaffolds that display a gradient in the porosity along the tube radius, as well as a one-directional diffusion scaffold to facilitate the drug's migration characteristics, such as the nerve growth factor diffusion during the nerve regeneration. The outer layer of the scaffold with the dense phase structure will prevent the nerve growth factor migration, while the inner tube with a highly porous structure will provide fast nerve growth factor diffusion. A tubular scaffold with an inner tube of relatively lower densities and decreased pore sizes along the radial direction will make the transportation of the nerve growth factor to the drug target more effective. By using the dip coating technique, the multi-layered scaffolds with the porous gradient can be fabricated. Figure 4.3.12-A shows a two-layered tubular scaffold with an inner layer composed of PLGA 50/50 and an outer layer composed of PLCL/PCL_6/1. Figure 4.3.12-B shows that the enlarged interface between the two-layered scaffold. The inner layer has bigger pore sizes while the outer layer has smaller pore sizes. The outer layer pores were compressed and stretched because of the different expansion rate.

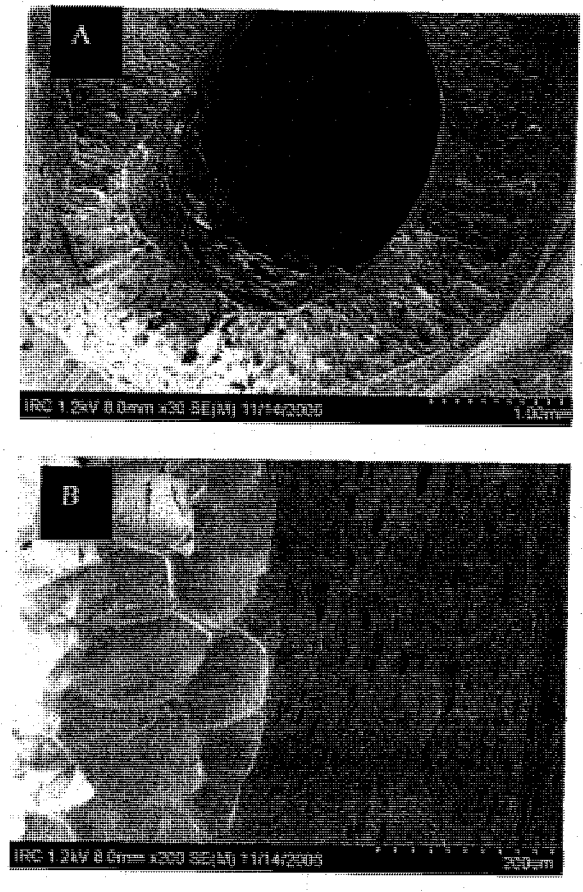

Figure 4.3.12 The two-layered foam morphology—a polymeric tube with an inner layer composed of PLGA 50/50 and an outer layer composed of PLCL/PCL_6/1 foamed by a pressure quench method at 5.86 MPa and at room temperature

4.4 Interconnected open structures

In order to improve the scaffold interconnectivity, a novel method was developed in this project. Our assumption is the combination of "the salt leaching" and the gas foaming at one step. The salt and solvent should both be used as components to enhance the CO_2 solubility. Plasticizers, such as PEG, water and ethanol, were selected in this project due to their plasticization effects and enhanced CO_2 uptakes [81] [121] [136]. PEG is a biocompatible material and it can be easily dissolved in water and ethanol, thus the residue of PEG in scaffolds will not be cytotoxic to the cells [137] [138].

The combination of water or ethanol, the (PLGA 50/50)/PEG system and the sub-critical CO_2 foaming technology in preparing biodegradable scaffolds with open structures is investigated. The open structures were only studied with PLGA 50/50.

4.4.1 The effect of small molecules(plasticizers)

In the CO_2 foaming process, the surface tension and viscosity significantly affect the porous morphologies [139]. Ethanol, water are small molecules which can be used as plasticizers to decrease the viscosity and enhance the CO_2 solubility [81] [140]. In order to check their effects on the foam morphologies, PLGA 50/50 films were first soaked and foamed in a CO_2 vessel with water or ethanol solutions under a sub-critical condition (5.86 MPa and room temperature).

As shown in both Figure 4.4.1 and Table 4.2, PLGA 50/50 scaffold morphologies will change by adding ethanol or water solutions.

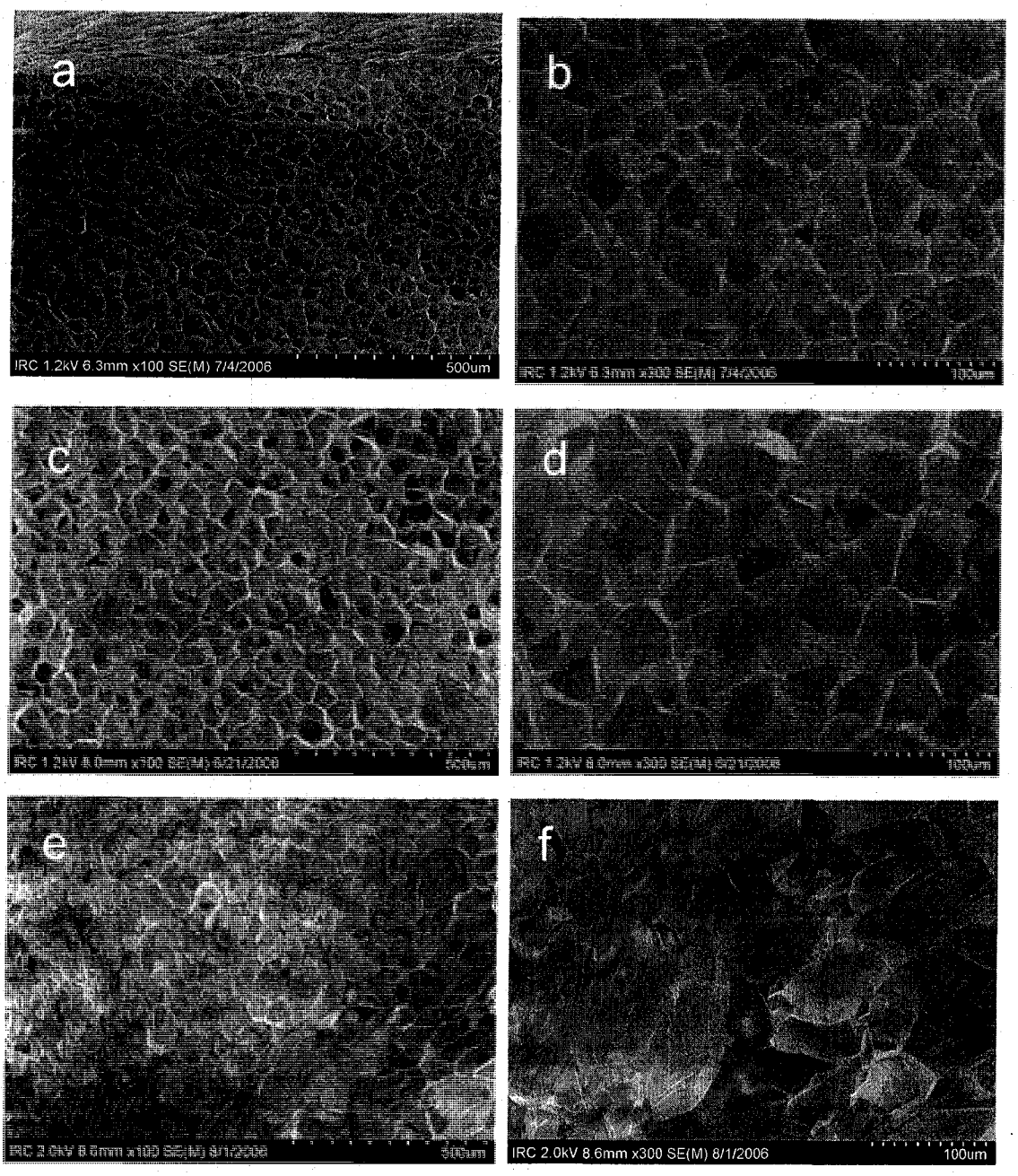

Figure 4.4.1 Morphologies of PLGA 50/50, (PLGA 50/50)/water and (PLGA 50/50) /ethanol foamed by a pressure quench method at 5.86 MPa and room temperature.
a, b: The PLGA 50/50 scaffold in low magnification (a) and high magnification (b);
c, d: The (PLGA 50/50)/water scaffold in low magnification (c) and high magnification (d);
e, f: The (PLGA 50/50)/ethanol scaffold in low magnification (e) and high magnification (f).

Table 4.2 PLGA 50/50, (PLGA 50/50)/water, (PLGA 50/50)/ethanol morphology analysis

	Pore size		Foam density		Cell density		Porosity	
	Diameter, μm	Standard deviation	g/cm^3	Standard deviation	$cm^{-3}/*10^6$	Standard deviation	%	Standard deviation
PLGA 50/50	20.4	± 3.0	0.0927	± 0.0108	382.29	± 48.08	93.08	± 0.81
(PLGA 50/50) /water	25.5	± 4.6	0.0419	± 0.0013	446.72	± 13.76	96.87	± 0.16
(PLGA 50/50) /ethanol	29.0	± 6.6	0.0545	± 0.0021	231.21	± 9.37	95.93	± 0.09

Using one-way ANOVA analysis of variances between groups, we find that there are statistically significant differences of the foam density, the cell density, and the porosity between PLGA 50/50, (PLGA 50/50)/water, and (PLGA 50/50)/ethanol systems. There are significant differences of pore sizes between PLGA 50/50 and (PLGA 50/50)/water systems or PLGA 50/50 and (PLGA 50/50) /ethanol systems, but there is no significant difference of their pore sizes between (PLGA 50/50) /water and (PLGA 50/50)/ethanol systems. Both (PLGA 50/50)/water and (PLGA 50/50)/ethanol systems get smaller foam densities and bigger pore sizes than pure PLGA 50/50 does. In addition, the (PLGA 50/50)/ethanol system obtains the smallest cell density. The possible reason is the effect of the surface tension introduced by the water (73dynes/cm, 20°C) or ethanol (22dynes/cm, 20°C) [141]. But there is still no open structures shown in these systems.

The use of (PLGA 50/50)/PEG blends is another promising issue because PEG is a plasticizer and the CO_2 uptake is much higher in PEG than that in PLGA 50/50 [142] [143] [144]. The (PLGA 50/50)/PEG series of films with different PEG concentration are soaked in a CO_2 vessel at 5.86 MPa for 24 h at room temperature and foamed by a pressure quench method to try to obtain an open structure.

The morphologies of these scaffolds are shown in Figure 4.4.2. The average pore size distribution is illustrated in Figure 4.4.3. The pore size decreases with the increasing concentration of PEG in polymer films. The pore sizes of (PLGA 50/50)/PEG 95/05 wt% and 90/10 wt% scaffolds have bigger pore sizes than the scaffold of pure PLGA 50/50, which indicates that the little amount of PEG will plasticize the polymer. As a result, cells are easy to swell and grow into bigger pores. However a higher PEG amount in polymer films will significantly enhance the nucleation, resulting in more small pores. The phenomenon may be explained by using heterogeneous nucleation theory [145, 146]. The free energy needed to generate nucleation in this (PLGA 50/50)/PEG blend system is much lower than that in PLGA 50/50, resulting in smaller pore sizes.

(PLGA 50/50)/PEG 95/05 wt%

(PLGA 50/50)/PEG 90/10 wt%

(PLGA 50/50)/PEG 75/25 wt%

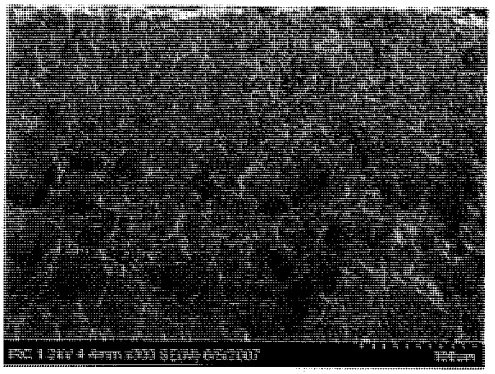

(PLGA 50/50)/PEG 50/50 wt%

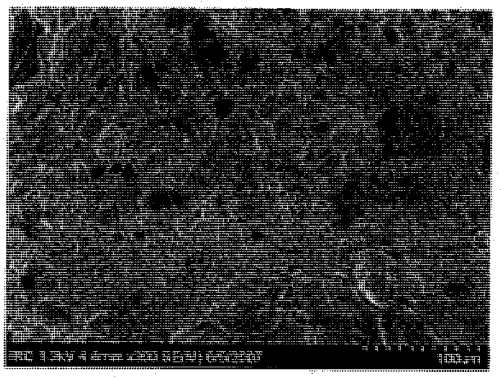

(PLGA 50/50)/PEG 33/67 wt%

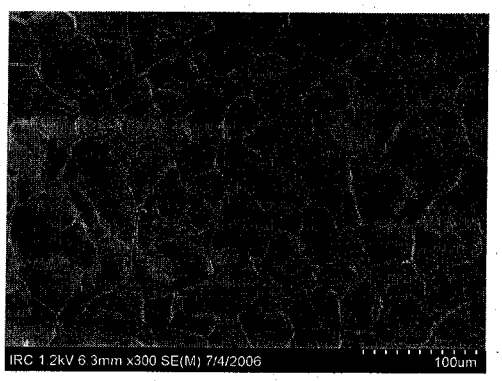

Control -- PLGA 50/50

Figure 4.4.2 (PLGA 50/50)/PEG blends foamed at 5.86 MPa and room temperature by pressure quench method

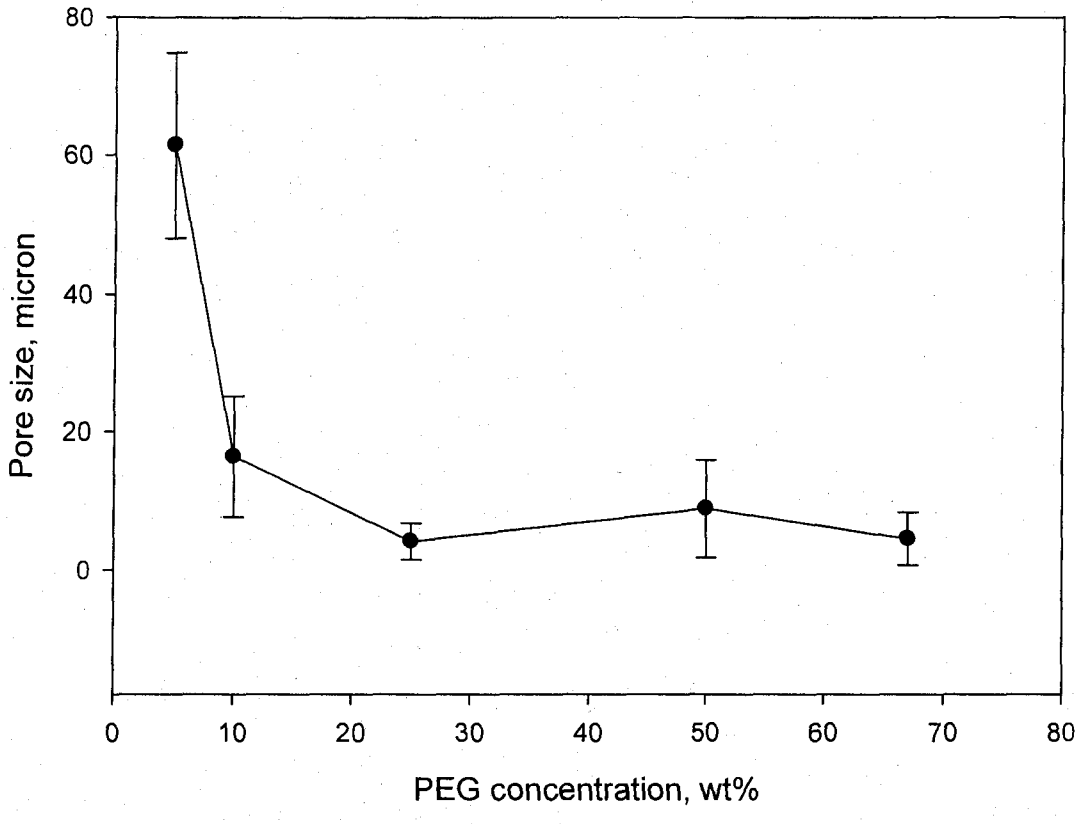

Figure 4.4.3 (PLGA 50/50)/PEG scaffold pore size distribution obtained at 5.86MPa and room temperature by pressure quench method.

4.4.2 The combination effect of Ethanol/Water/PEG on scaffold morphologies

In order to try obtaining open structures, small molecules, i.e., ethanol, water and PEG, are combined to foam. (PLGA 50/50)/PEG blend films are put in water, ethanol or water/ethanol (1/1) solutions. Then these films with solutions are soaked in the 5.86 MPa CO_2 environments for 24 h and foamed by a pressure quench method at room temperature. The results are shown in Figure 4.4.4.

Cross section (Low magnification) | Cross section (High magnification) | Surface

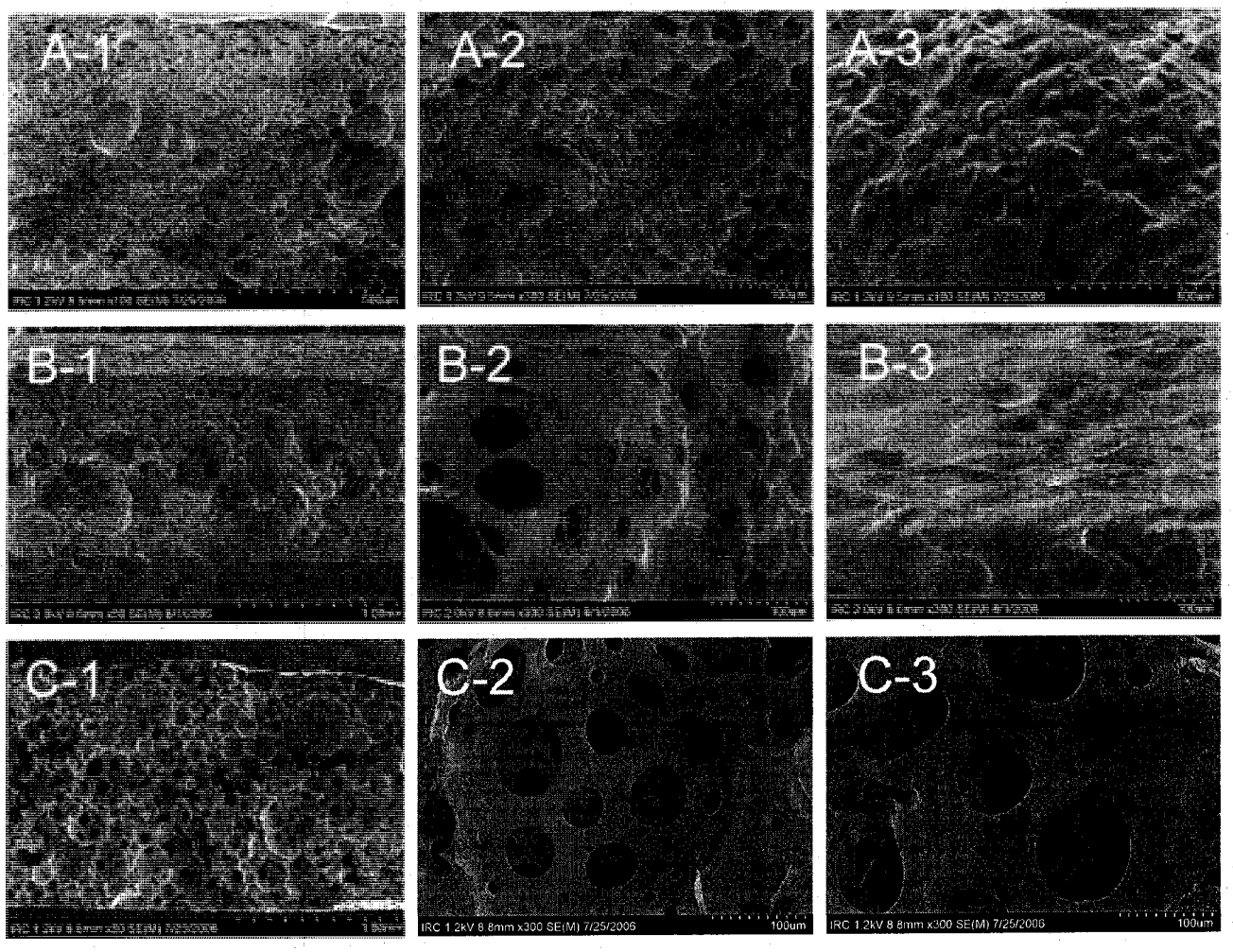

Figure 4.4.4 Morphologies of (PLGA 50/50)/PEG_33/67_wt% soaked in ethanol/water/CO_2 solutions and foamed by a pressure quench method at 5.86 MPa and room temperature.

A-1, A-2, A-3: The (PLGA 50/50)/PEG_33/67_wt% soaked in the water and CO_2 solution

B-1, B-2, B-3: The (PLGA 50/50)/PEG_33/67_wt% soaked in the water/ethanol 1/1 (v/v) and CO_2 solution.

C-1, C-2, C-3: The (PLGA 50/50)/PEG_33/67_wt% soaked in the ethanol and CO_2 solution.

The results illustrate that an open structure without the skin layer can be obtained by using (PLGA 50/50)/PEG_33/67_wt% plus ethanol (Figure 4.4.4-C). Once ethanol is changed to water, the scaffold shows a heterogeneous structure without interconnectivity (Figure 4.4.4-A). When the water/ethanol mixer with 1/1 volume ratio solution is used, the partly open structure scaffold can be made, but there is still no openings on the surface (Figure 4.4.4-B). The small molecules' plasticization effect and CO_2 uptake are both important to affect the final result. The surface tension of ethanol is much smaller than that of water, thus ethanol will decrease the polymer surface tension dramatically. This is helpful to obtain open structures. Besides, the CO_2 concentration can be 10 times higher in ethanol than in water especially in high pressures [147]. The higher CO_2 concentration will also significantly decrease the surface tension and viscosity of the polymer film. Also the existence of PEG is also helpful to get open structures due to its higher CO_2 uptake and plasticization effect. As a result, the interconnected open porous structures can be easier obtained by using the (PLGA 50/50)/PEG/**ethanol**/CO_2 system compared with the (PLGA 50/50)/PEG/**water**/CO_2 system.

4.4.3 (PLGA 50/50)/PEG/ethanol system and open structures

Based on the previous results, a series of (PLGA 50/50)/PEG blend films are made with different blend ratios of 95/05, 90/10, 75/25, 50/50 and 33/67 wt%. Then they are soaked in an ethanol/CO_2 environment for 24 h and foamed by a pressure quench method at 5.86 MPa and room temperature. A series of porous structures is shown as follows (Figure 4.4.5).

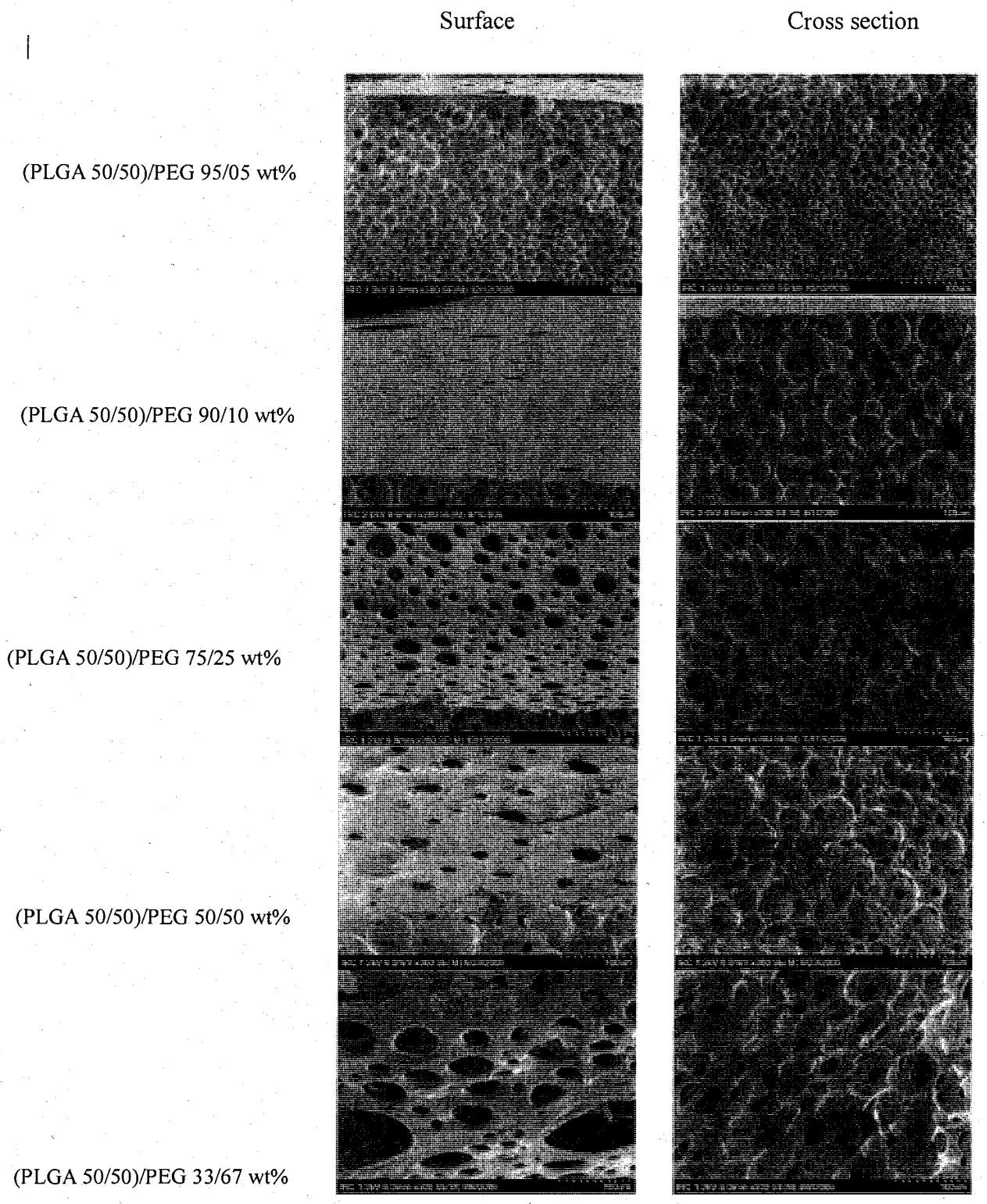

Figure 4.4.5 Morphologies of the (PLGA 50/50)/PEG/ethanol/CO_2 systems saturated at 5.86 MPa and room temperature and subsequently foamed by a pressure quench method.

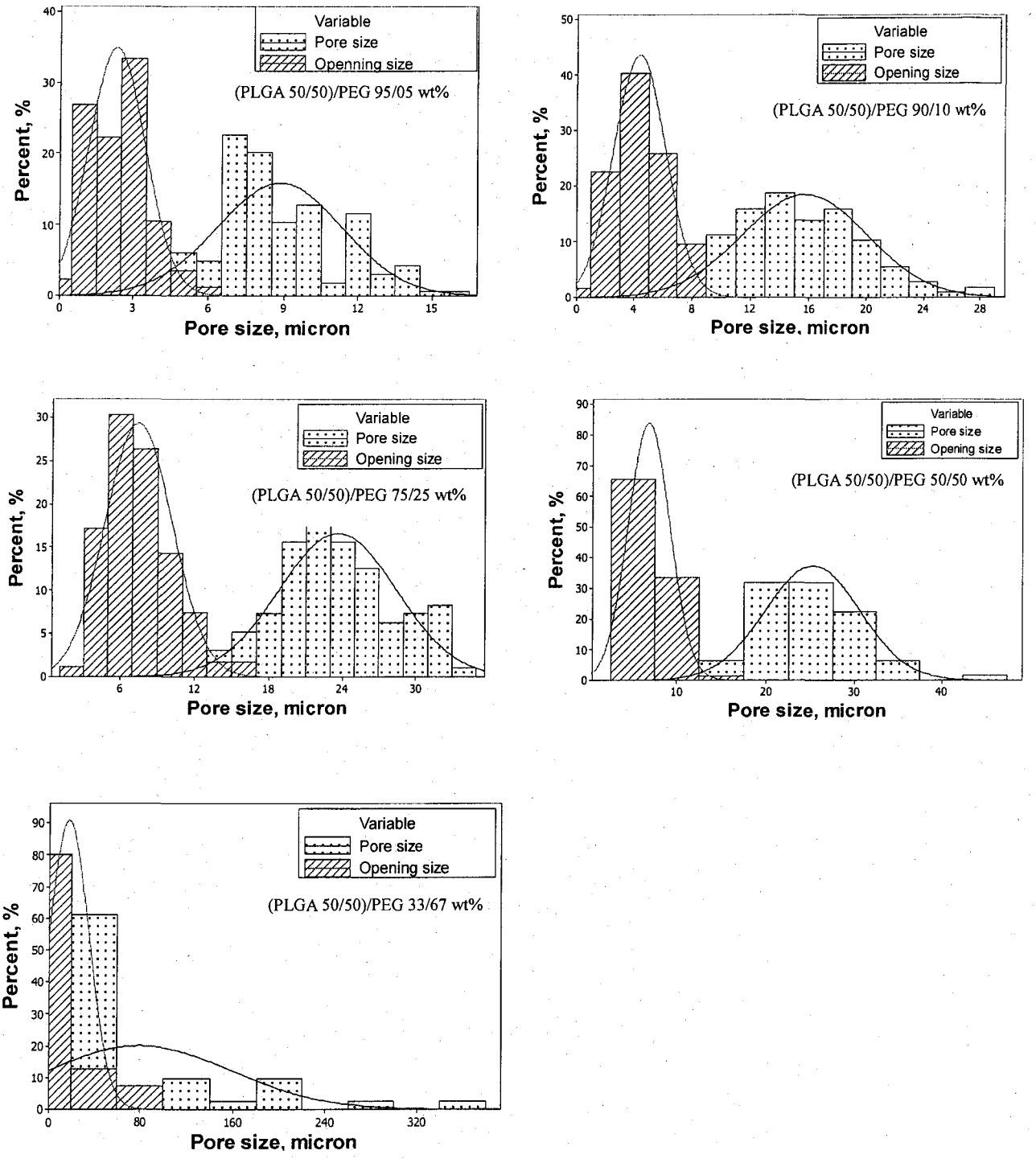

Figure 4.4.6 (PLGA 50/50)/PEG scaffolds pore sizes and opening sizes distributions (foamed by a pressure quench method at 5.86 MPa and room temperature).

From the SEM pictures, we can see clearly that pore sizes, openings and the degree of the openings on the surfaces will become larger when the PEG concentration increases in the polymer films. The pore sizes from 9 to 100μm, openings on the pore walls from 3 to 50μm and the openings on the surface from none to 100 μm are observed (Figure 4.4.6). The higher the PEG ratio, the easier it is to get open structures: bigger pore sizes, bigger openings.

If the temperature quench method is used, much more CO_2 can be nucleated [148]. It is evident in the SEM results (Figure 4.4.7) that the bigger pores and openings are obtained in comparison with the results foamed by the pressure quench method. The pore sizes from 16 to over 250μm, openings on the pore wall from 4 to 50μm, and the openings on the surface from zero to over 500 μm are made (Figure 4.4.8). With the increase of PEG ratio, more and more holes appear on the scaffold surfaces.

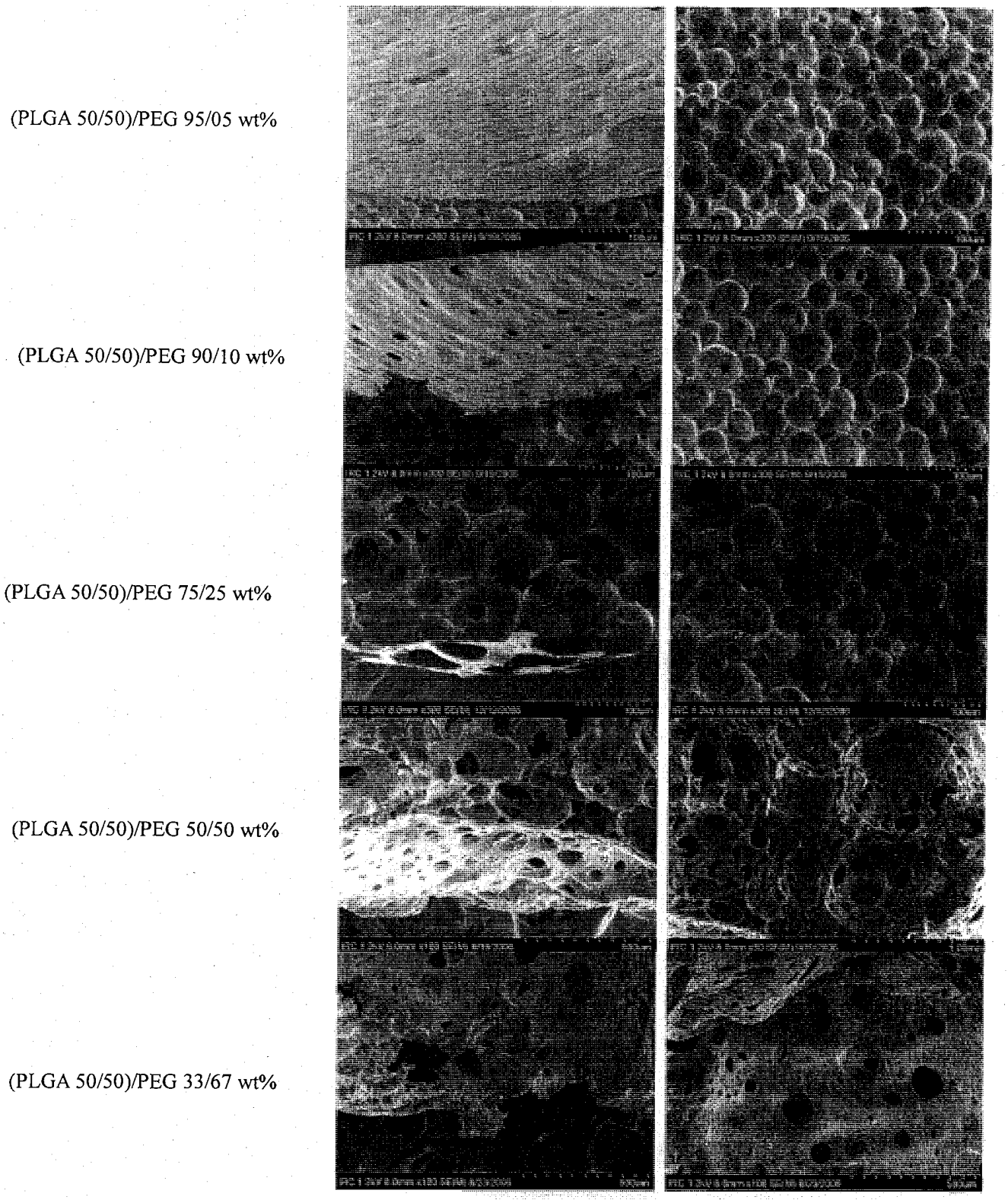

Figure 4.4.7 Morphologies of the (PLGA 50/50)/PEG/ethanol/CO_2 systems saturated at 5.86 MPa and room temperature and subsequently foamed by a temperature quench method (in a 35°C water bath for 30 s).

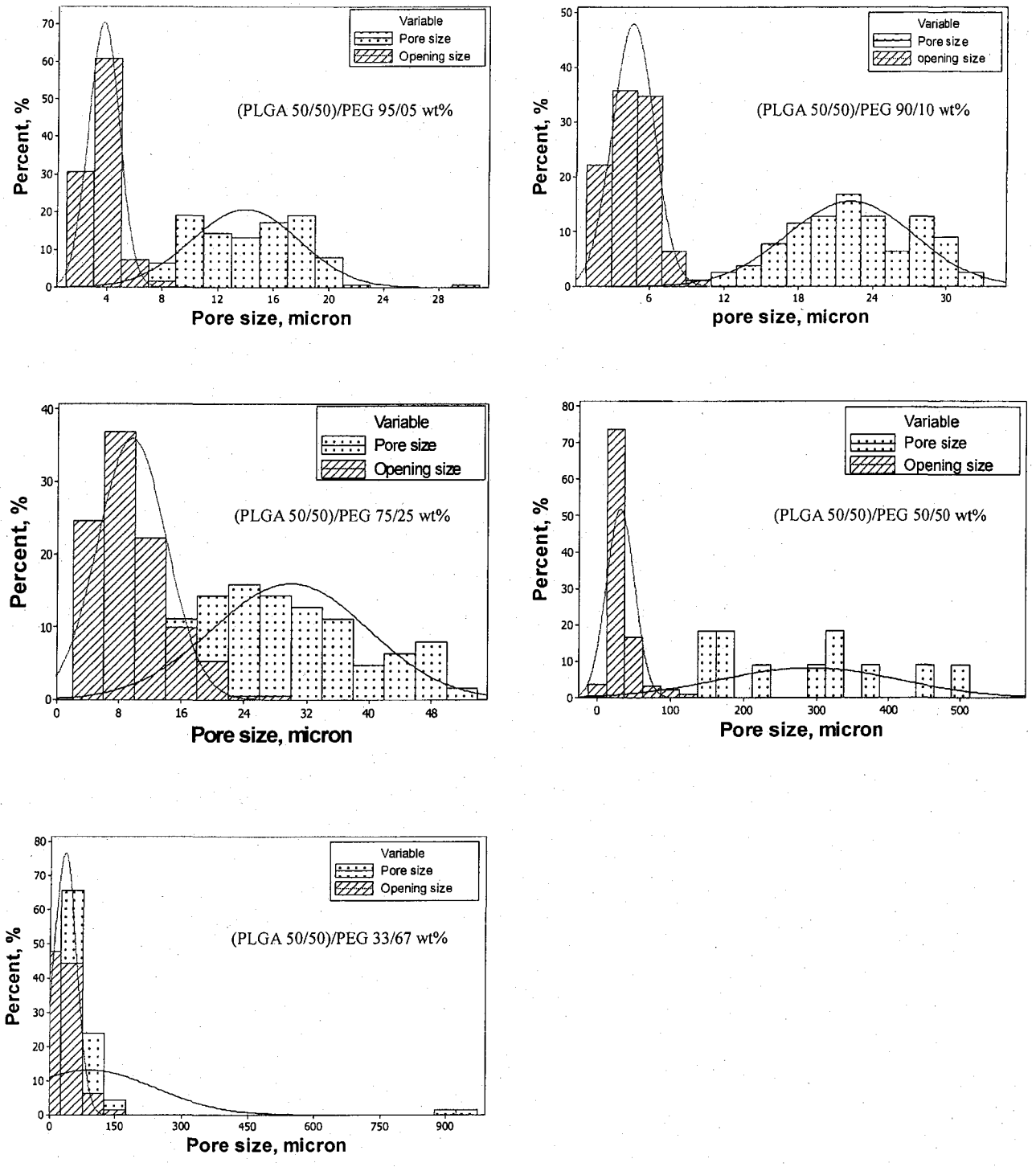

Figure 4.4.8 (PLGA 50/50)/PEG scaffolds pore sizes and opening sizes distributions (foamed by a temperature quench method (in a 35°C water bath for 30 s)).

In this system, once the pressure is released, the polymers will start to foam due to the low Tg and the high CO_2 concentration in the polymer matrixes. Subsequently, the foams are soaked in a 35°C water bath, which will initiate the second foaming immediately. The high temperature will soften the polymer matrix and CO_2 molecules entrapped in the pores will obtain the higher energy to swell the pore walls again. At the same time, the new nucleation sites will appear in the cell walls and grow into smaller pores. The softened pore walls, the increased strength of CO_2 in the pores, and the small pores appeared in the pore walls will all enhance the break of the cell walls. Figure 4.4.9 shows the second foaming schematics.

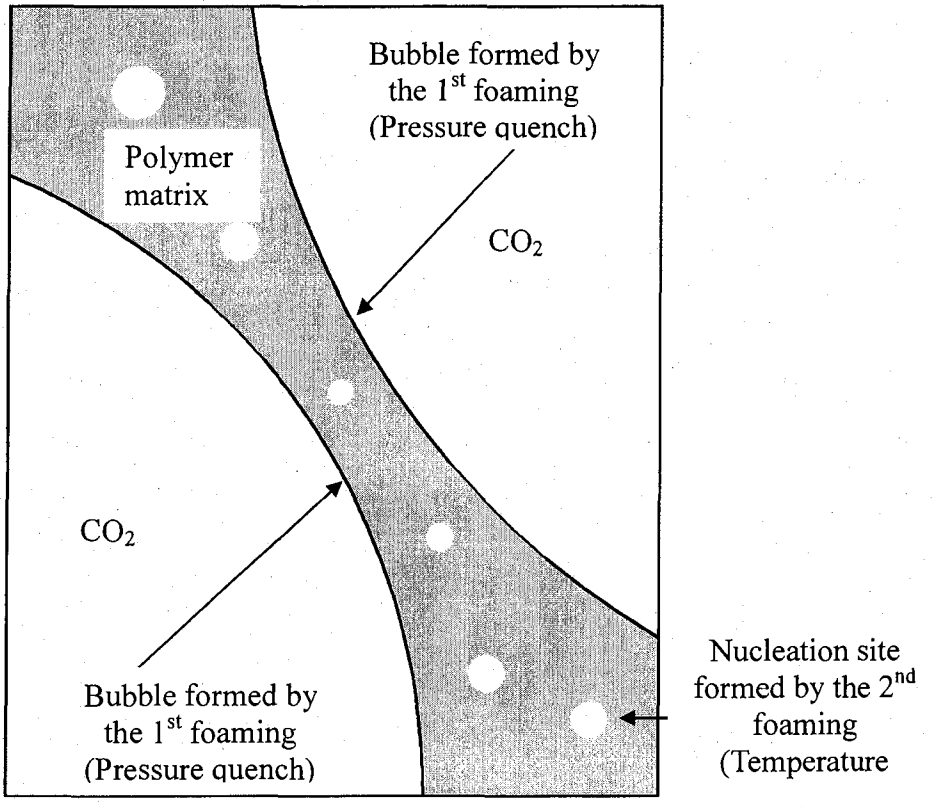

Figure 4.4.9 The second foaming (a temperature quench method in this process) schematics

It is very helpful to understand this phenomenon in Figure 4.4.7 of (PLGA 50/50)/PEG_50/50_wt% and (PLGA 50/50)/PEG_33/67_wt%, in which there are many micro holes and bubbles dispersed on the cell walls. The foaming process is so strong

that the morphology of the (PLGA 50/50)/PEG_50/50_wt% results in irregular pore shapes and many broken pores merge into some bigger pores. The CO_2 molecules burst almost all the pore structures in (PLGA 50/50)/PEG_33/67_wt%, so that the porous structure can not be distinguished very well on the pore openings and pore sizes.

4.5 Gradient interconnected structures

According to the gradient scaffold fabrication method described above, we can make layered interconnected scaffolds. Figure 4.5 shows two 2-layered scaffold SEM pictures. Layer I is a dense layer with smaller pore size and smaller openings, while layer II is a loose layer with bigger pores and bigger openings. Figures 4.5-A and 4.5-B show the different pore size gradients. Figure 4.5-A has a big difference on the pore size gradient between the two layers, while the Figure 4.5-B has a smaller pore size gradient. The pore sizes and opening sizes can be adjusted by controlling the PEG concentration in polymer blends. Therefore we can design controlled gradient structures for our future work by using this method.

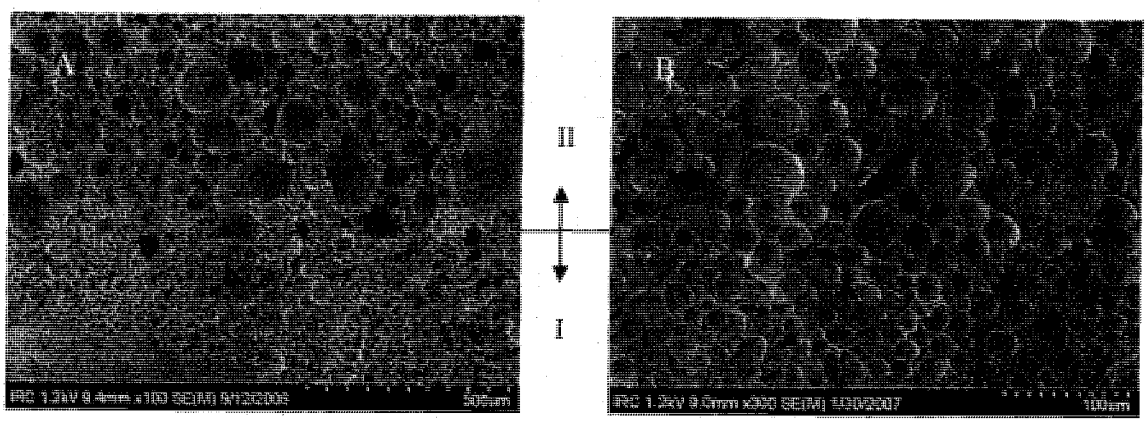

I: (PLGA 50/50)/PEG_90/10
II: (PLGA 50/50)/PEG_75/25

I: (PLGA 50/50)/PEG_95/5
II: (PLGA 50/50)/PEG_90/10

Figure 4.5 Morphologies of 2-layered interconnected gradient scaffolds

5. Discussions

5.1 The Mechanism of layered structures

To fabricate gradient structures by using the gas foaming technique, the coalescent force between different polymer layers should be considered to avoid phase separations. At least there are two factors related with the coalescent force. One is the expansion difference. The different polymer layers with different expansion rate and ratio will stretch each other, consequently the higher differences in between means more difficult it is to keep the gradient structure in one entire piece of scaffold. The other factor is that the interface between two layers should endure the stretching when the foaming happens, which means the entanglement of molecules in the interface should be strong enough to maintain the scaffold in one piece. The mutual effect of the two factors will result in the final morphologies. Figure 5.1.1 shows the gradient structure foaming schematics. Gradient structures without phase separations are our research goal.

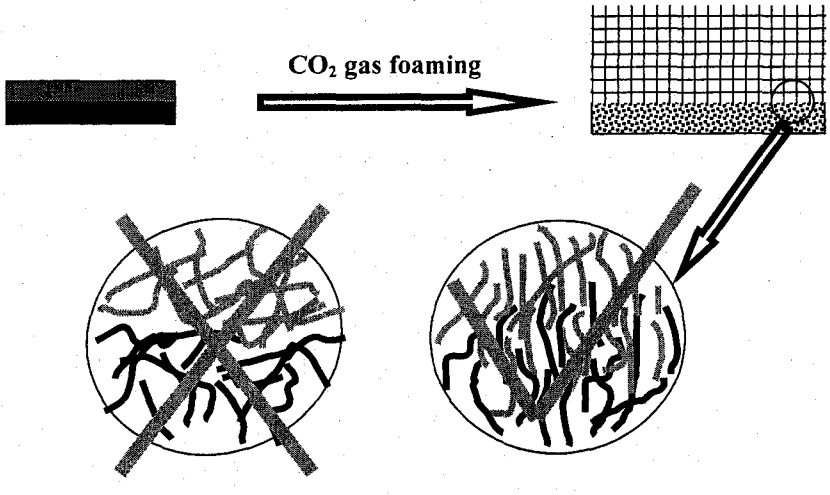

Figure 5.1.1 The gradient structure foaming schematics.

At beginning, we wanted to use PLGA 50/50 and PCL to get a two-layered scaffold in

which one layer is PLGA 50/50 with a high porosity and another layer is PCL with no pores at all. After we cast the films and foamed it, the scaffold separated into two pieces (Fig 5.1.2) due to the weak interaction between PLGA 50/50 and PCL molecules in the interface. Another reason of the layer separation is due to the big swelling strength generated by CO_2 molecules between different layers. If the expansions in different layers were significantly different, the polymers would stretch each other drastically.

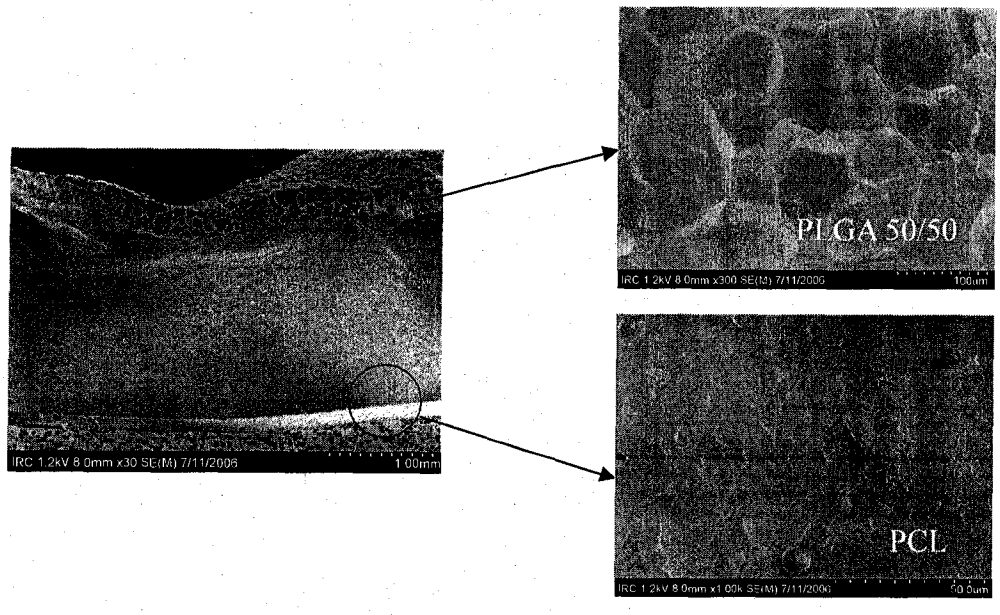

Figure 5.1.2 The 2-layered foam morphology—the phase separation due to the immiscibility and the big expansion difference between PLGA 50/50 and PCL.

In order to enhance the entanglement between PLGA 50/50 and PCL molecules, PLCL is selected as a molecular linker because it is a copolymer with one segment of PCL and another segment of PLA. The segments are included in PCL and PLGA 50/50 molecules (Figure 5.1.3).

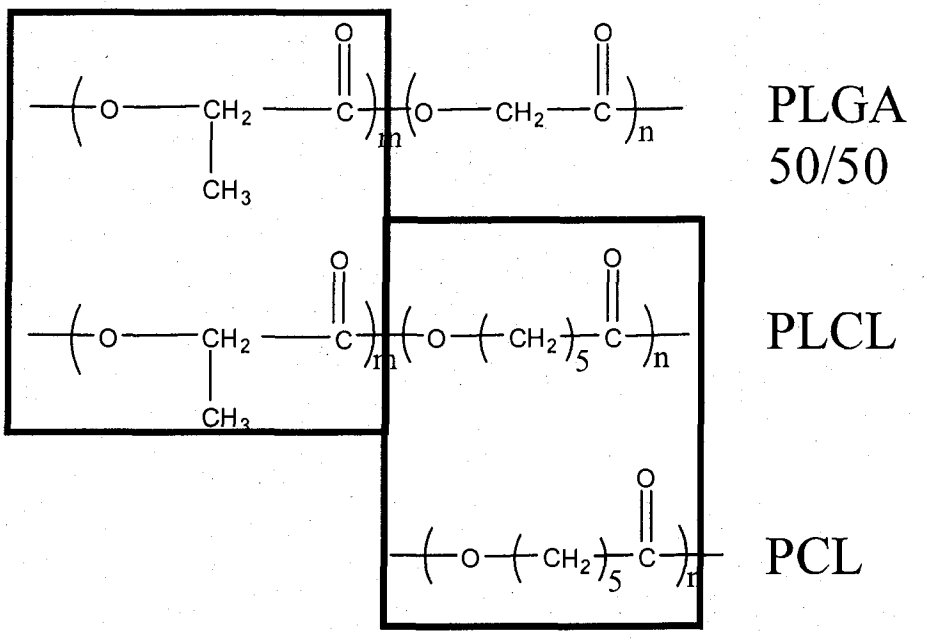

Figure 5.1.3 The function of PLCL molecule as a molecular linker

The two component blends, such as (PLGA 50/50)/PLCL and PLCL/PCL, are miscible at any ratio as a result of the homogeneous solutions and non-separated foams. Once another component is added into the polymer solution, the layered solution or the foam separation is always found to some extent. For example, the solution will separate into 2 layers in (PLGA 50/50)/PLCL/PCL blend with weight ratio of 1/1/1, with one layer of brown color and another layer with transparent color. The detail study has not been done yet, but we suggest that it may be miscible if PCL is less than 1/6 in (PLGA 50/50)/PLCL solution.

5.2 The Mechanism of open structures

5.2.1 Differential scanning calorimetry (DSC) analysis

The differential scanning calorimetry (DSC) of the (PLGA 50/50/PEG) polymer blends, as represented in Figure 5.2.1, indicates that the melting peaks become bigger with the increase of PEG concentrations in the polymer blends. The melting peaks in the blends are located at the same position of the pure PEG, which demonstrates that the PEG aggregation

results in forming crystals.

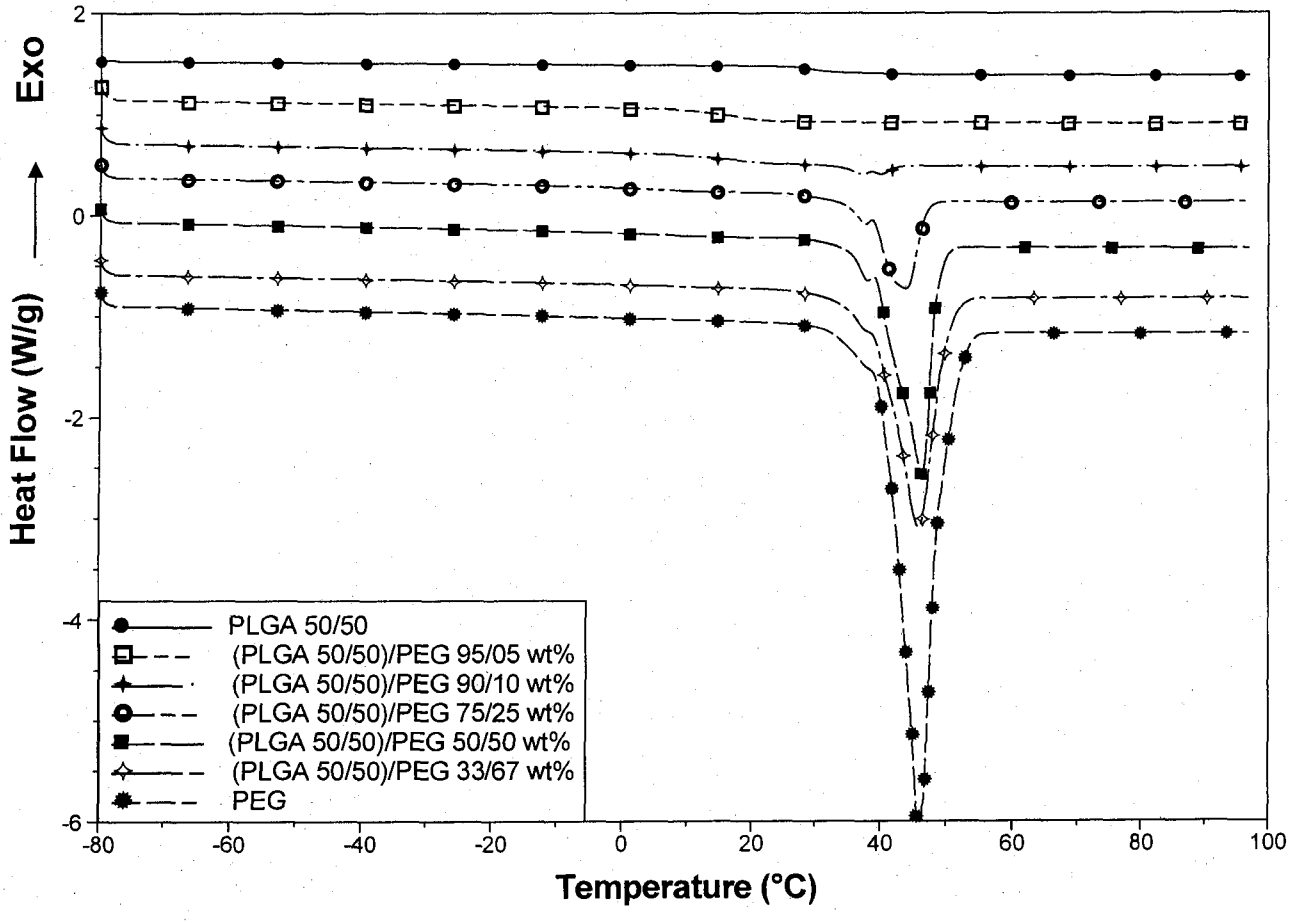

Figure 5.2.1 A thermal analysis of the (PLGA 50/50)/PEG blend system.

For the amorphous PLGA 50/50 film, the glass transition temperature (Tg) is about 30°C, which is lower than the pure PLGA 50/50 (Tg ~45-50°C), likely due to the chloroform residue. PEG is a highly crystallized polymer with a melting temperature (Tm) of 45°C and a Tg around -55°C [52], but we can not observe the Tg due to its high crystallinity [134]. The PEG plasticization effect can be observed by the fact that the Tgs of (PLGA

50/50)/PEG_95/5_wt% and (PLGA 50/50)/PEG_90/10_wt% films go down to 16°C-18°C which is much lower than the PLGA 50/50 film. The melting peak cannot be found in the (PLGA 50/50)/PEG_95/05_wt% film, which means that PEG molecules disperse evenly in the PLGA 50/50 film without crystal aggregations or maybe the amount of PEG is too low to measure. The tiny melting peak appears in the (PLGA 50/50)/PEG_90/10_wt% film and the melting peak becomes clearer and bigger when the PEG concentration go up to 25% or higher. Once the PEG concentration is higher than 25%, the Tg peaks can not be observed because they are overwhelmed by the strong Tm peaks. The appearance of melting peaks clearly shows that they form heterogeneous blend morphologies with PEG crystal clusters in PLGA 50/50 films.

In order to compare the composition difference between the films and the foams, the (PLGA 50/50)/PEG films with different ratios are soaked in a CO_2 vessel with the ethanol solution at the sub-critical condition (5.86 MPa and room temperature). The series of (PLGA 50/50)/PEG blend films are soaked in the ethanol/CO_2 solution for 24 h and foamed at by using a pressure quench method. Subsequently these scaffolds are dried in a vacuum oven (room temperature) for 7 days to get rid of the ethanol residue from the scaffolds. The thermal analysis of the (PLGA 50/50)/PEG polymer foams is also tested by DSC.

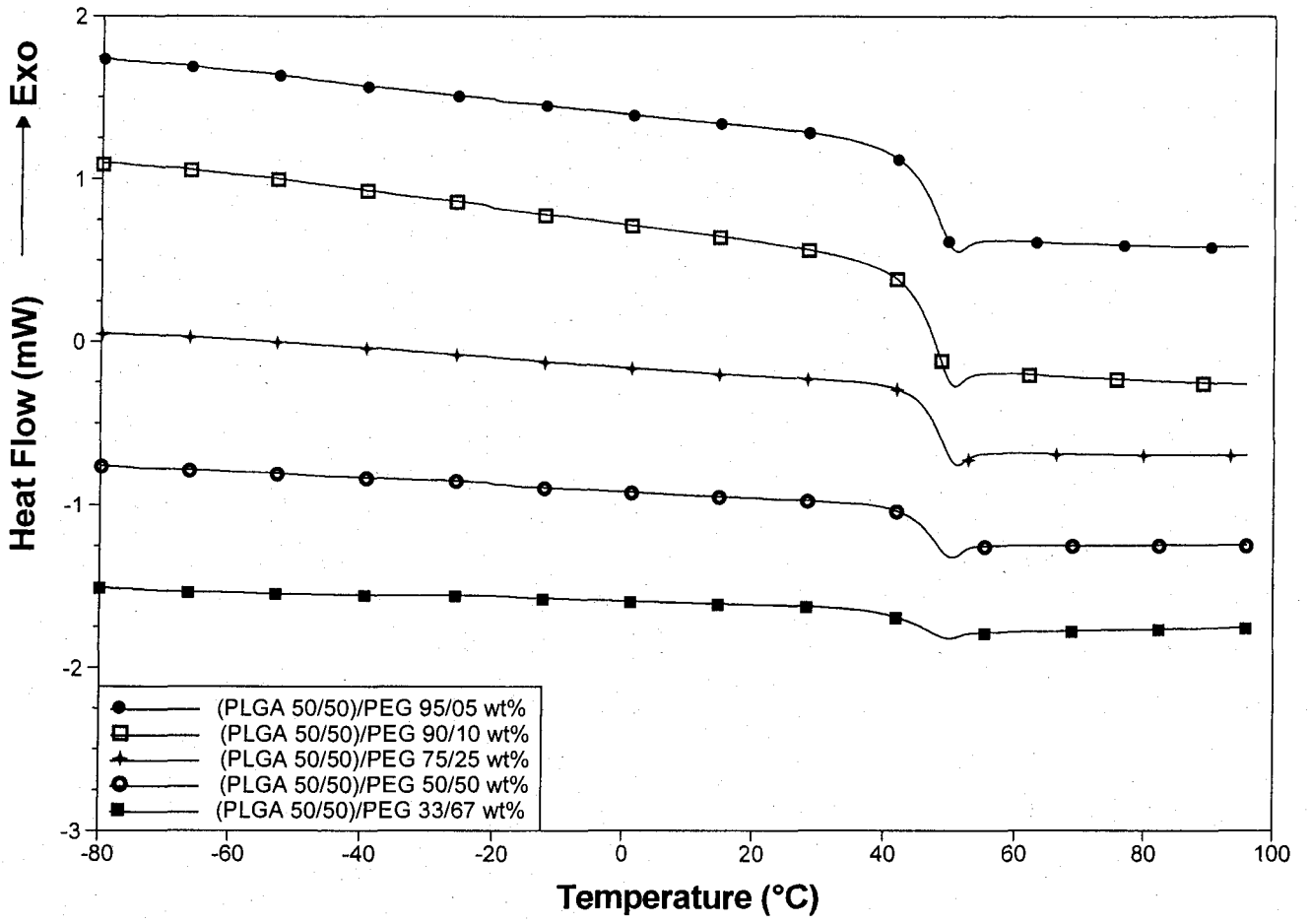

Figure 5.2.2 A thermal analysis of the (PLGA 50/50)/PEG/Ethanol/CO_2 system saturated in 5.86 MPa and room temperature for 24 h, and subsequently foamed by the pressure quench method.

From Figure 5.2.2, we observed that not only the melting peaks disappeared, but also all the glass transition peaks went back to the original position of pure PLGA 50/50 (~45°C). Because PEG is an ethanol-soluble polymer, and with the help of high pressure CO_2, ethanol molecules easily diffuse into the polymer matrix to dissolve the PEG molecules and diminish the hydrogen bonds between PEG molecules [149] [150]. At the same time, PEG molecules will also diffuse out from the PLGA matrix. Ethanol is a good solvent for PEG and an anti-solvent for PLGA 50/50, thus we can conclude that there is a much higher ethanol

concentration surrounding PEG molecules, rather than surrounding PLGA 50/50 molecules. Under high pressure conditions, hydrogen bonds will be generated between CO_2 and ethanol molecules [151]. This will significantly increase the CO_2 concentration in PEG/ethanol region. The PEG/ethanol/CO_2 concentration gradient, created between the (PLGA 50/50)/PEG polymer matrix and the solvent ethanol/CO_2 environment, will drive PEG molecules out from the polymer matrix. Once the foaming process happens, CO_2 molecules will nucleate and form bubbles. Because of the heterogeneous structures of the (PLGA 50/50)/PEG matrix, CO_2-rich domains (ethanol/PEG/CO_2 region) will nucleate and foam first due to the higher diffusivity and the higher uptake of CO_2 molecules in these domains. These CO_2 molecules will easily swell the polymer matrix since there are still ethanol/CO_2 molecules in the PLGA 50/50 region, and these ethanol/CO_2 molecules will significantly plasticize PLGA 50/50. By taking advantage of the plasticized polymer matrix, the CO_2 molecules can swell the pore walls and burst them more easily, even the skin layer. Figure 5.2.3 schematically describes the process.

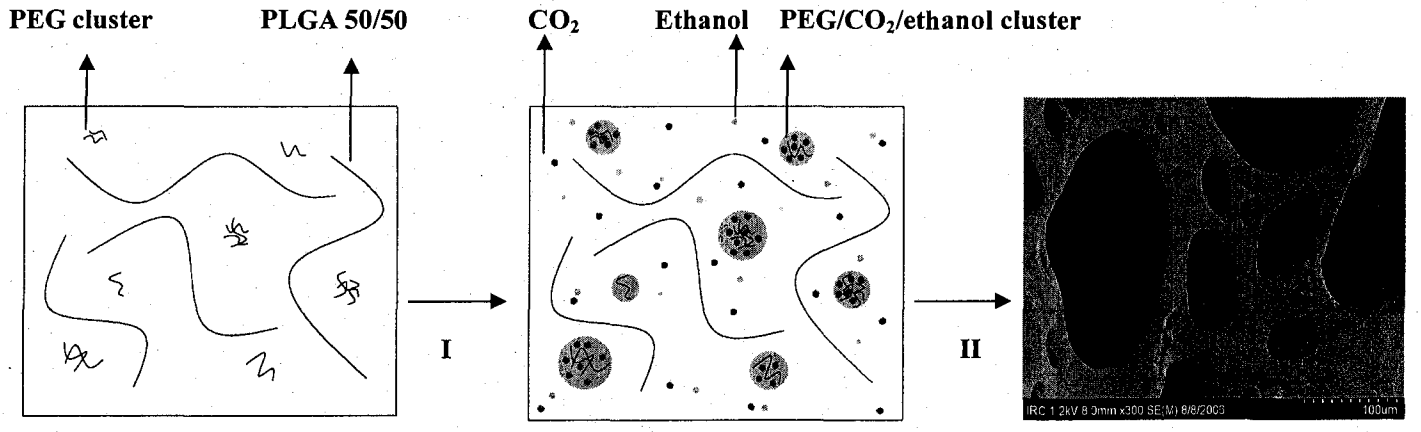

Figure 5.2.3 Schematics of the soaking and foaming process of the (PLGA 50/50)/PEG/ Ethanol/CO_2 system, **I**: CO_2/ethanol saturated at 5.86 MPa and room temperature; **II**: foamed by a pressure quench method.

The phase separation will happen between PLGA 50/50 and PEG domains once the

foaming process starts because the PEG molecules are dissolved and surrounded by ethanol/CO_2. After the cell growths finished, the PEG molecules will be totally separated from the PLGA 50/50 matrix. The PEG molecules will be either left in pores or be blown out of the scaffold. PEG molecules will be first dissolved, then partly extracted, and finally blown away, thus there is no any melting peak shown in the DSC diagram in these scaffolds.

Although there maybe still a little amount of PEG molecules in the polymer matrix after foaming, since PEG molecules located on the surface of scaffolds rather than in polymer matrixes, they will not affect their foams Tgs. Another result shown in the DSC diagram was that due to the extraction function of CO_2 and ethanol, the chloroform residue was also extracted away from the polymer matrix so that the glass transition peaks went back to the position of the pure PLGA 50/50 polymer (Figure 5.2.2).

5.2.2 Scaffold weight loss analysis

These foams were also checked by weight losses compared with the weights of the original films (Figure 5.2.4).

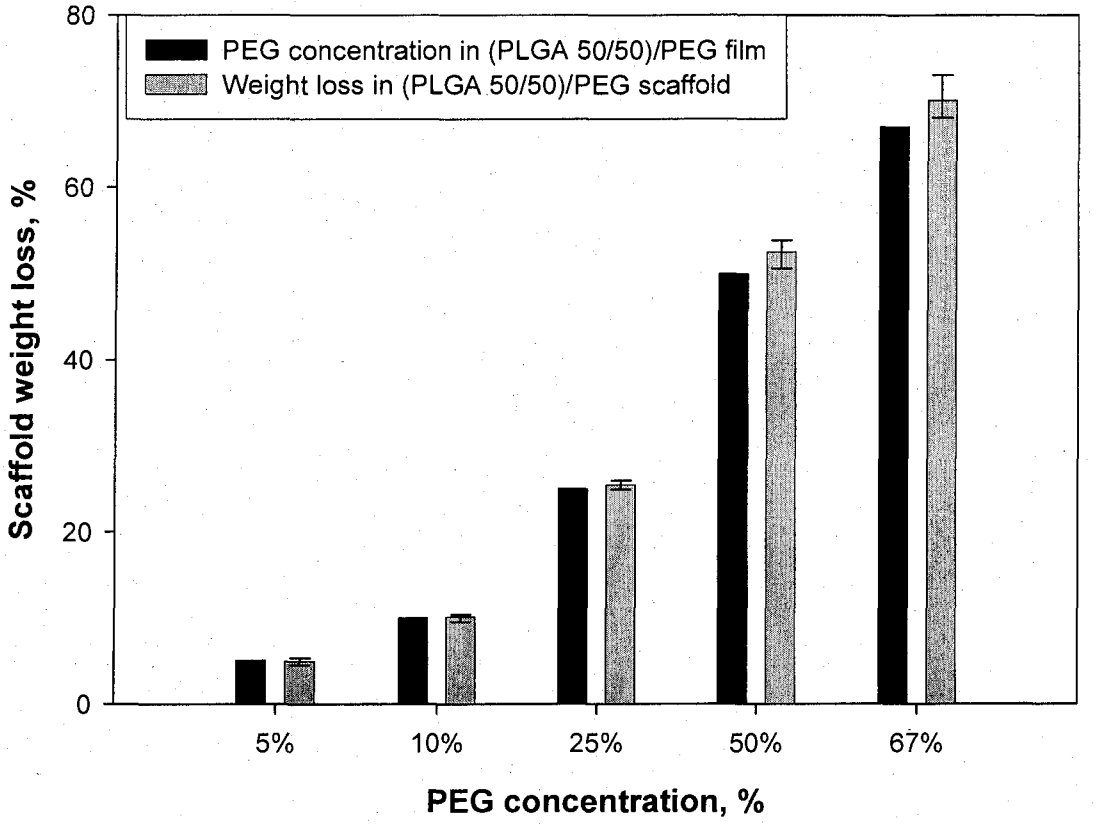

Figure 5.2.4 Scaffold weight losses as a function of PEG concentration in the (PLGA 50/50)/PEG/ethanol/CO_2 system (saturated in 5.86 MPa and room temperature for 24 h and subsequently foamed by a pressure quench method).

The weight losses almost equal the PEG weights in the polymer films. This also demonstrates that PEG molecules disappear in the process. For the foam with high PEG ratios, the weight loss is even larger than the total PEG amount, which means there is PLGA 50/50 mass loss to some extent in the whole process. Maybe the CO_2 gas can blow some of PLGA 50/50 off from the polymer matrix, especially when the CO_2 concentration is higher (Which is related with the high PEG concentration).

5.2.3 Scaffold sectioning micrography

The open porous structure can be sectioned into broken pieces, like Figure 5.2.5 described as follows. On the contrary, the closed structure can only be sectioned into integrated round structure. So from the sectioning results in Figure 5.2.6, we can clearly detect if the scaffolds are open or closed structures. We can see from the pictures that (PLGA 50/50)/PEG 950/05 wt% and (PLGA 50/50)/PEG 90/10 wt% are mostly composed of closed pores, but others showed many broken pieces in the pictures to identify that they are open structures.

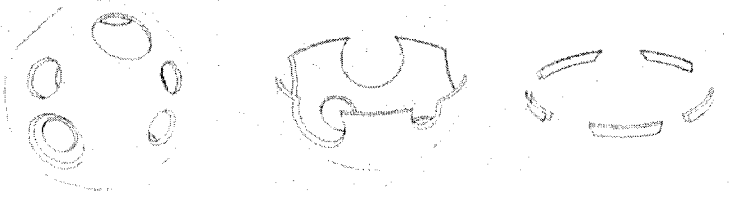

Figure 5.2.5. The schematics of scaffolds sectioning result for the open porous structure.

(PLGA 50/50)/PEG 95/5 wt%	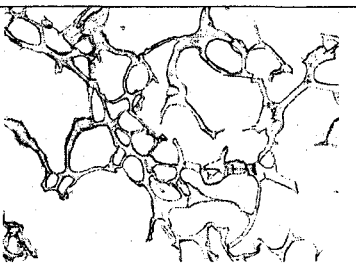
(PLGA 50/50)/PEG 90/10 wt%	
(PLGA 50/50)/PEG 75/25 wt%	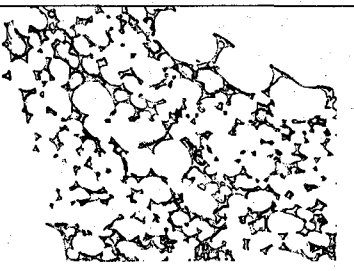
(PLGA 50/50)/PEG 50/50 wt%	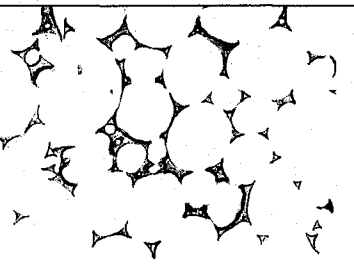
(PLGA 50/50)/PEG 33/67 wt%	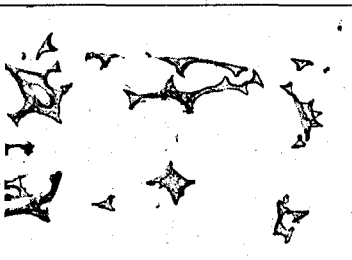

Figure 5.2.6 (PLGA 50/50)/PEG scaffolds sectioned at -25°C and 5μm. Pictures were taken by Olympus Microscope (IX81). The magnification is 100X.

5.2.4 Elemental analysis

The elemental analysis is carried out in films and scaffolds composed of PLGA 50/50, PEG and their blends. The results in Table 5.1 show that it is not accurate if we compare the compositions of theoretical value of C/O in pure PLGA 50/50 or PEG and experimental results. The possible reason may be that the moisture (water) is not totally dried out or the degradation has already happened because the elemental analysis experiment was done one year after we bought the materials. But if we compare the C/O ratio between these films and scaffolds, we can find the C/O ratio in scaffolds is lower than those in films, which demonstrate that part of PEG molecules left the scaffolds after the foaming process.

Table 5.1 The elemental analysis results in films and foams composed of PLGA 50/50, PEG and their blends.

Sample		C%	O%	C/O	Theoretical value C/O
Film	01# PLGA 50/50	46.59	50.98	0.91	0.94
	02# (PLGA 50/50)/PEG (95/05)	44.39	50.23	0.88	0.97
	03# (PLGA 50/50)/PEG (90/10)	45.31	48.70	0.93	0.99
	04# (PLGA 50/50)/PEG (75/25)	46.66	48.16	0.97	1.08
	05# (PLGA 50/50)/PEG (50/50)	48.23	44.71	1.08	1.22
	06# (PLGA 50/50)/PEG (33/67)	47.23	46.90	1.01	1.31
	07# PEG	51.91	38.56	1.35	1.50
Foam	08# PLGA 50/50	46.00	48.11	0.96	0.94
	09# (PLGA 50/50)/PEG (95/05)	45.83	49.73	0.92	0.97
	10# (PLGA 50/50)/PEG (90/10)	45.96	50.24	0.91	0.99
	11# (PLGA 50/50)/PEG (75/25)	44.35	48.78	0.91	1.08
	12# (PLGA 50/50)/PEG(50/50)	46.64	45.30	1.03	1.22
	13# (PLGA 50/50)/PEG (33/67)	44.13	48.11	0.92	1.31
	14# PEG	52.33	38.62	1.35	1.50

5.3 The effect of soaking time

Besides the (PLGA 50/50)/PEG series films soaked in ethanol for 24 h and foamed by a pressure quench method (see section 4.4.3), other soaking times (12 h, 24 h, 36 h, and 60 h) were also selected in order to study the effect of soaking time on the scaffold morphologies. The morphologies and pore size distributions of these scaffolds are shown in Figure 5.3.1, Figure 5.3.2, and Figure 5.3.3. The average pore size and opening size

are illustrated in Figures 5.3.4 and 5.3.5. All results show that the pore size and opening size increase with increasing of the PEG concentration in films, which indicate that the PEG has a critical effect on the morphology. The morphologies of (PLGA 50/50)/PEG series with a soaking time of 12 h are much similar with the series with a soaking time of 24 h, but they are different from the series with a soaking time of 36 h and 60 h, which indicate that the 12 h and 24 h soaking times are not in an equilibrium status and the PEG molecules can still diffuse out from the polymer matrix and go into ethanol solution. The morphologies with soaking times of 36 h and 60 h have bigger pore and opening sizes, which indicate that the films will not be easily foamed into open structures with the decrease of the PEG concentration in films.

(PLGA 50/50)/PEG
95/05 wt%

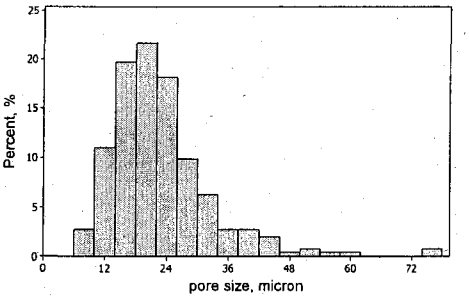

(PLGA 50/50)/PEG
90/10 wt%

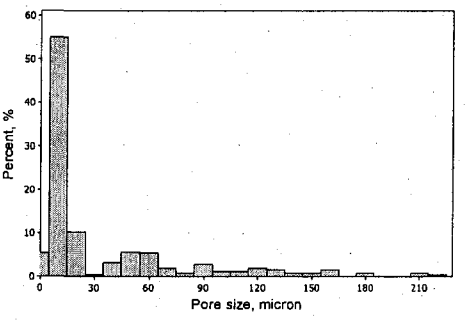

(PLGA 50/50)/PEG
75/25 wt%

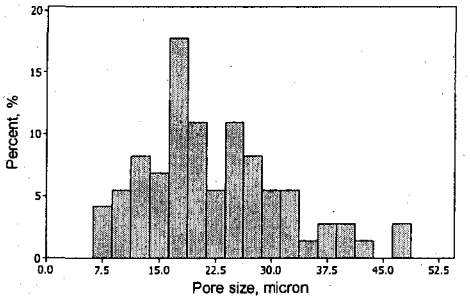

(PLGA 50/50)/PEG
50/50 wt%

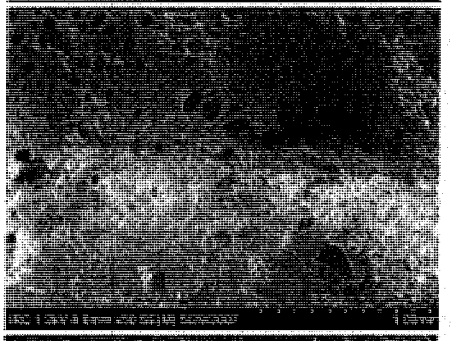

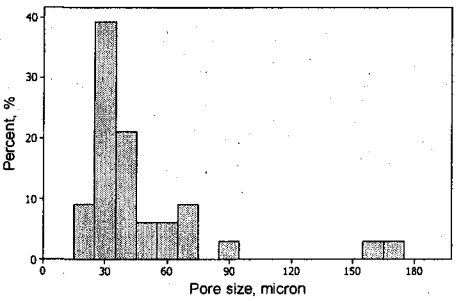

(PLGA 50/50)/PEG
33/67 wt%

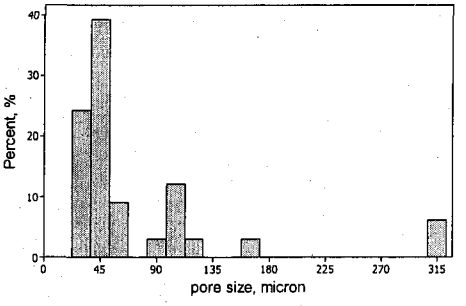

Figure 5.3.1 Morphologies of (PLGA 50/50)/PEG blends soaked at 5.86 MPa and room temperature with ethanol for 12 h and foamed by pressure quench method

(PLGA 50/50)/PEG
95/05 wt%

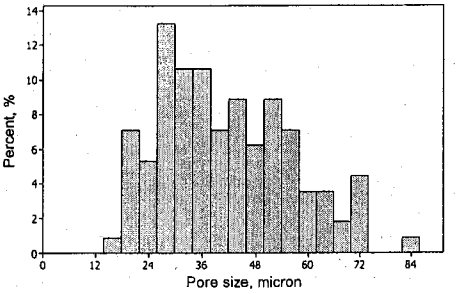

(PLGA 50/50)/PEG
90/10 wt%

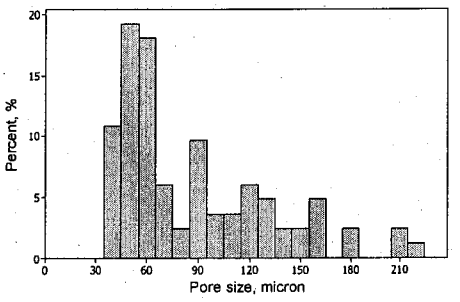

(PLGA 50/50)/PEG
75/25 wt%

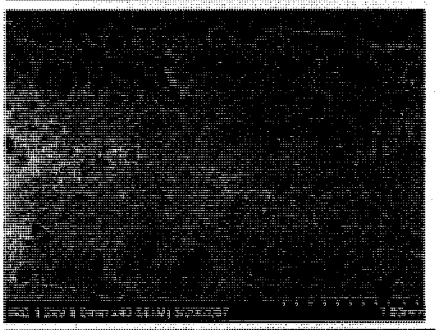

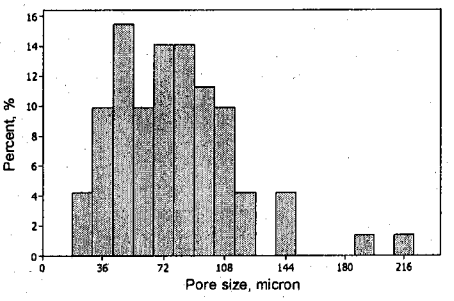

(PLGA 50/50)/PEG
50/50 wt%

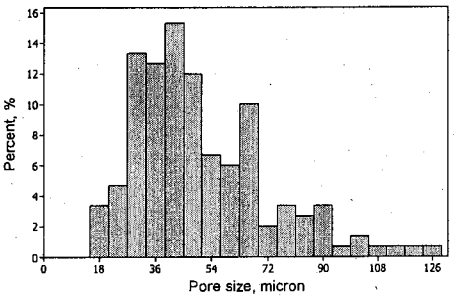

(PLGA 50/50)/PEG
33/67 wt%

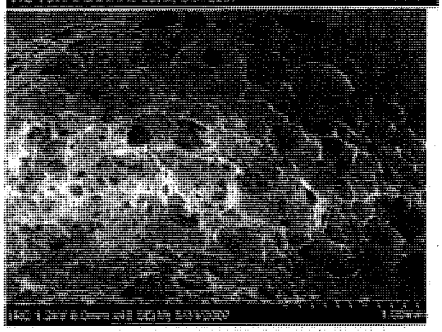

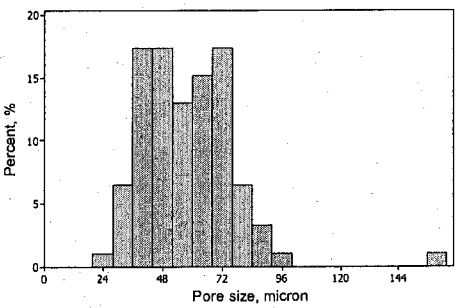

Figure 5.3.2 Morphologies of (PLGA 50/50)/PEG blends soaked at 5.86 MPa and room temperature with ethanol for 36 h and foamed by pressure quench method

(PLGA 50/50)/PEG 95/05 wt%

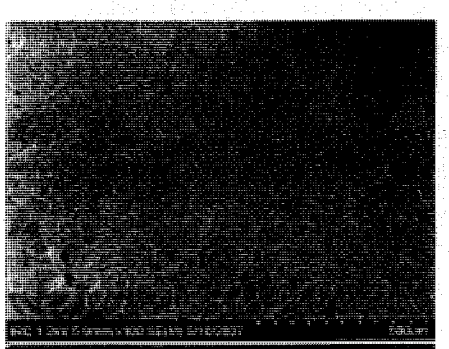

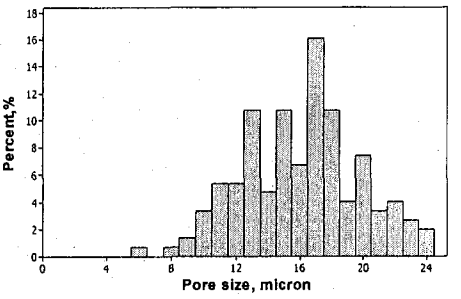

(PLGA 50/50)/PEG 90/10 wt%

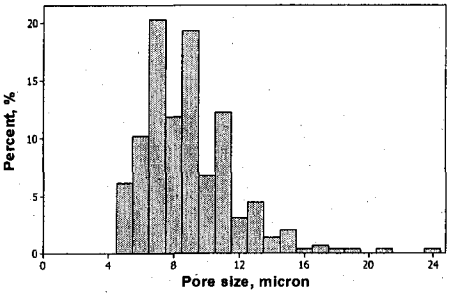

(PLGA 50/50)/PEG 75/25 wt%

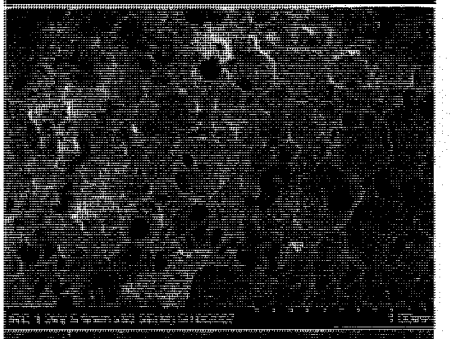

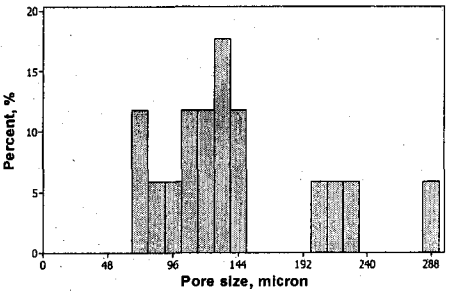

(PLGA 50/50)/PEG 50/50 wt%

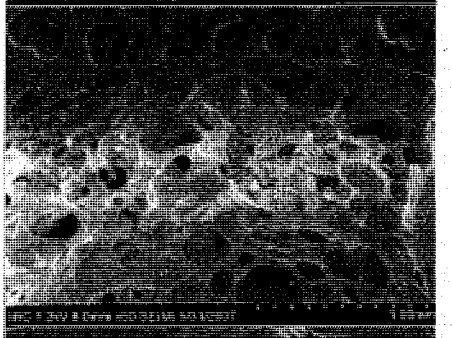

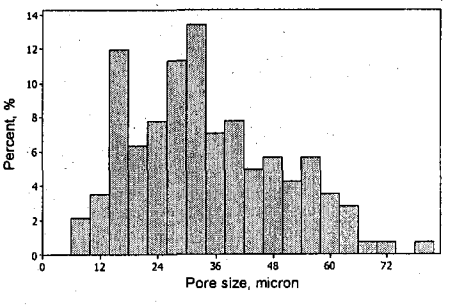

(PLGA 50/50)/PEG 33/67 wt%

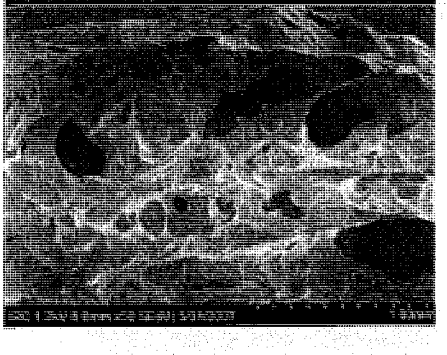

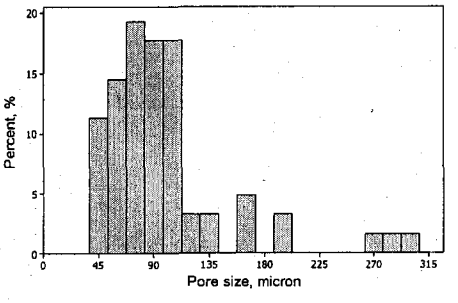

Figure 5.3.3 Morphologies of (PLGA 50/50)/PEG blends soaked at 5.86 MPa and room temperature with ethanol for 60 h and foamed by pressure quench method

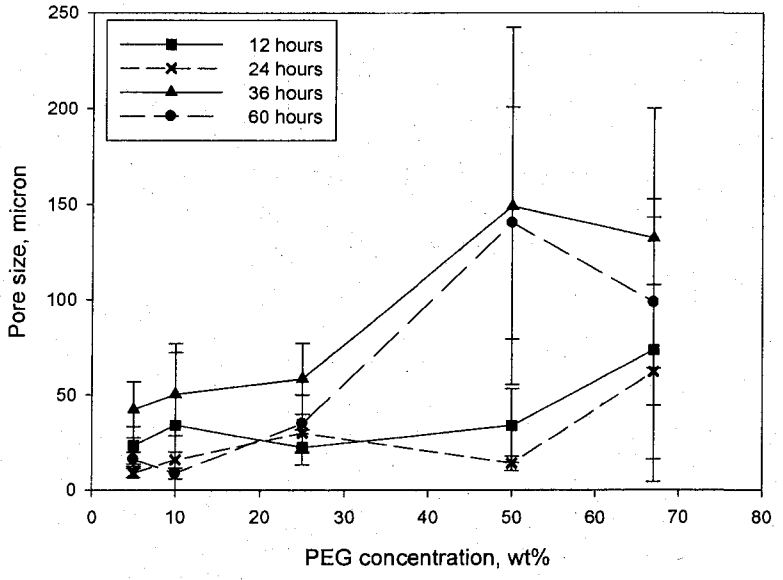

Figure 5.3.4 The pore size distributions of (PLGA 50/50)/PEG scaffolds soaked at different time and foamed by a pressure quench method at room temperature. The standard deviation of the experimental data was calculated with three repetitions of the experiment.

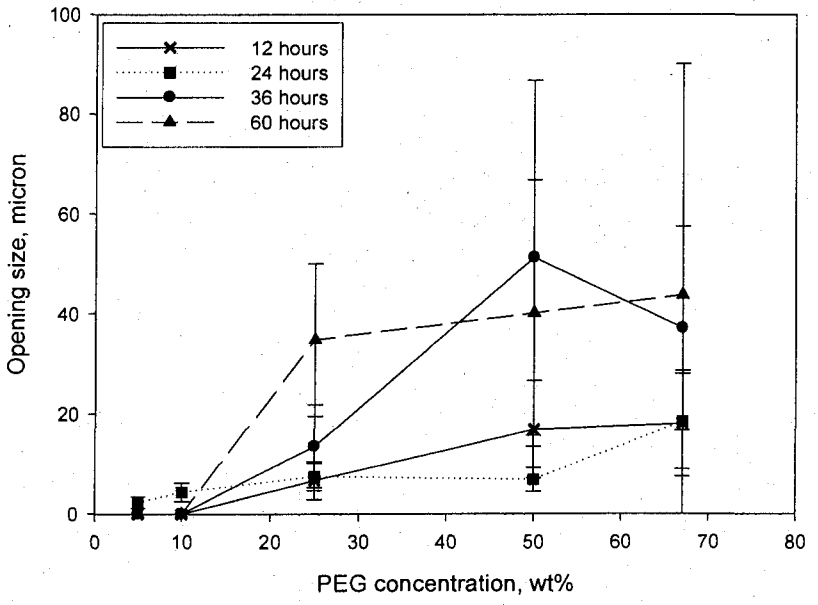

Figure 5.3.5 The opening size distributions of (PLGA 50/50)/PEG scaffolds soaked at different time and foamed by a pressure quench method at room temperature. The standard deviation of the experimental data was calculated with three repetitions of the experiment.

5.4 The effect of other processing conditions

Which element is the most important factor to affect the open structures? PEG's major function is as a plasticizer and forming heterogeneous structures in the (PLGA 50/50)/PEG films when the high PEG concentration is used in the system. The dissociated PEG (<5%) can plasticize PLGA 50/50 and enhance CO_2 solubility, but that is not enough to get open structures. When the PEG concentration increases, the crystals of PEG will form. The aggregation of PEG can not absorb a lot of CO_2 because its crystallinity prevents the CO_2 molecules diffuse in the PEG crystal regions, thus the open structures still can not be obtained. The ethanol vapour was introduced into the system to try to enhance the plasticization effect. The result shows that a partly open structure can be formed (Figure 5.4.1-a). Under this condition, there is no any PEG diffusing out from the polymer matrix before the foaming process. This is an evidence to show that the single component PEG can not be used to get open structures. Also it is shown that the low concentration of ethanol will not contribute significantly to form open structures. We also tried to use a low pressure to foam the polymer matrix at 2.76 MPa. A non-open structure is observed simply because the CO_2 solubility is low (Figure 5.4.1-b). The (PLGA 50/50)/PEG_33/67_wt% is soaked with 1 h and foamed by a pressure quench method to check their morphologies (Figure 5.4.1-c). When the soaking time is short (1 h), it evidently shows in the SEM picture that the polymer matrix is not saturated by CO_2 because there is still some non-porous regions in the scaffold. We also tried to decrease the CO_2 release rate from 2 s to 15 s to control the CO_2 nucleation and the cell growth. The result (Figure 5.4.1-d) shows that a big-pore scaffold without open structures is obtained. We also tried to leach PEG molecules from (PLGA 50/50)/PEG_33/67_wt% in an ethanol solution for 24 h; a non porous structure polymer film was obtained (Figure 5.4.1-e). This suggests that the PEG leaching technique itself will not

be able to get open structures in the PLGA/PEG system.

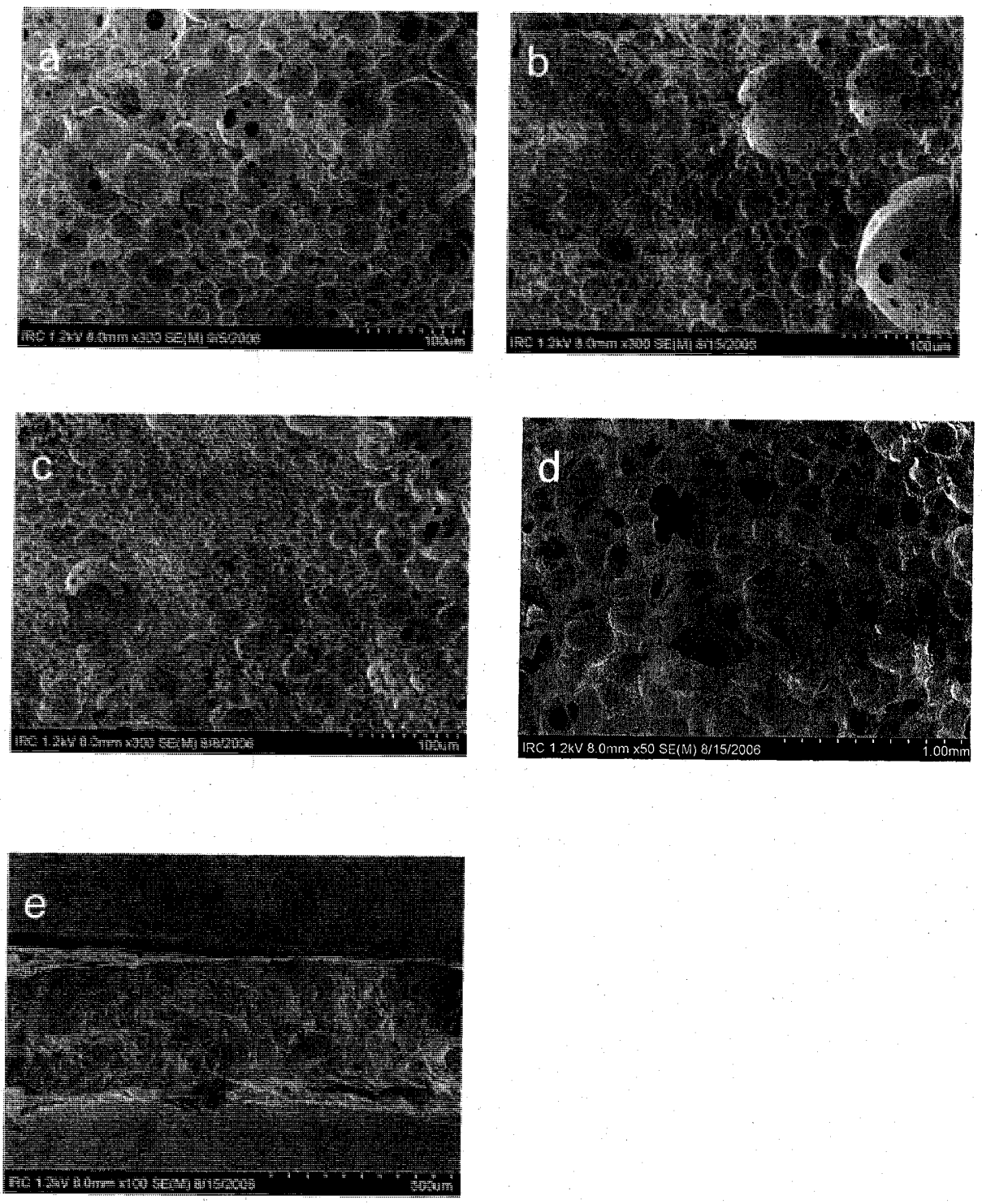

Figure 5.4.1 (PLGA 50/50)/PEG 33/67 wt% scaffolds fabricated by different processing conditions: (a) Soaked in the ethanol vapour/CO_2; (b) Soaked at 2.76 MPa; (c) soaked for 1 h;(d) Pressure release rate slow down to 15 s; (e) ethanol leaching for 24 h without CO_2 treatment.

From the above experiment results, it is concluded that the processing parameters are critical to control the final scaffold morphologies, including the ethanol concentration, the release rate, and the pressure.

6. Conclusions

Using the sub-critical CO_2 gas foaming technique, biodegradable polymeric scaffolds were fabricated. The scaffold morphologies of PLGA 50/50, PCL, PLCL and their blends were characterized and discussed. The PLGA 50/50 foamed at 5.86 MPa yields a porosity of over 90%. The porosity goes down drastically when the PCL concentration increase in PLCL/PCL blend from 76% (PLCL) to 0% (PCL). For (PLGA 50/50)/PLCL blend, the porosity changes from the range of 78% to 82% among the porosity of PLGA 50/50 (92%) and PLCL (76%). Through the DSC results and experimental observations, PLGA 50/50 is miscible with PLCL and PLCL is miscible with PCL, but PLGA 50/50 is immiscible with PCL.

Scaffolds with porosity gradients were fabricated with biodegradable polymers and their blends, i.e., PLGA 50/50, PLCL, PCL and their blends. Due to the immiscibility between PLGA 50/50 and PCL, the polymer layers can not be made from (PLGA 50/50)/PCL blend. In order to enhance the molecular interactions in the interfaces of the polymer films, PLCL is chosen as a molecular linker because of its miscibility with other two polymers. The usage of PLCL succeeded in the fabrication of gradient scaffolds without layer separation. The gradient morphologies are apparent in these layered scaffolds. For example, (PLGA 50/50)/ (PLCL/PCP_9/1)/ (PLCL/PCL_1/1) three-layered scaffold shows that the pore sizes in three layers can be from 38.0 μm, 12.7 μm, to 6.0μm. The six-layered PLCL/PCL blends scaffold becomes a gradient structure with gradually changes from one side composed of PCL (no any pore) to another side composed of PLCL (highly porous structure).

In the present study, the interconnected PLGA 50/50 scaffolds with micro pores sizes

are fabricated by using the (PLGA 50/50)/PEG/ethanol/CO_2 system. The pore sizes and interconnectivities can be controlled by adjusting polymer blend ratios. The (PLGA 50/50)/PEG blend in ratios of 95/5, 90/10, 75/25 , 50/50 and 33/67 wt% can be foamed into a wide range of pore sizes from 10 to 500 μm and opening sizes from 5 to 250 μm. It is demonstrated that most of PEG molecules existing in PLGA 50/50 matrix will be disappeared after the CO_2/ethanol soaking and foaming process. The (PLGA 50/50)/PEG/ethanol/CO_2 foaming results show that the skin layer of scaffolds is diminished once the PEG concentration is higher than 10%, and also the interconnectivity can be greatly improved with the increase of the PEG concentration. The CO_2 soaking and foaming conditions are also critical in obtaining the interconnected scaffolds with high porosities. The morphologies of (PLGA 50/50)/PEG series with a soaking time of 12 h are much similar with the series with a soaking time of 24 h, but they are different from the series with a soaking time of 36 h and 60 h, which indicate that the 12 h and 24 h soaking times are not in an equilibrium status and the PEG molecules can still diffuse out from the polymer matrix and go into ethanol solution. The morphologies with soaking times of 36 h and 60 h have bigger pore and opening sizes, which indicates that the films will not be easily foamed into open structures with the decrease of the PEG concentration in films. Without using ethanol or using other weaker soaking /foaming conditions (i.e., lower pressure, slower pressure release time), the experimental results show that the scaffolds will not express open structures due to the low CO_2 concentration and low nucleation effect.

The scaffold fabrication method is relatively simple and can be implemented without the use of costly equipments. The open porous scaffolds without skin may find applications in tissue engineering.

7. Future works

In this work, it was shown that the gradient structures can be fabricated by different layered polymers. By tailoring the blend ratios to control the morphology, the one directional drug delivery scaffolds can be realized. In order to better understand the roles of these scaffolds on the drug delivery, it would be interesting to conduct the following experiments:

1. To investigate the mechanical properties of the scaffolds. Find a solution to control the mechanical properties and the morphologies in the gradient structures. The rigid scaffold will stimulate the surrounding tissue to form a tissue scar at the edge of the scaffold and that will prevent the tissue regrowth; meanwhile, the scaffold without enough mechanical properties will collapse in vivo due to the surrounding tissue compression. The fabrication of gradient structure creats the possibility to generate proper scaffolds which satisfied these properties. For example, the rigid PCL or PCL/PLCL can be used as the outer layer of the scaffold to provide enough mechanical strength and prevent the drug escape. (PLGA 50/50)/PLCL blend can be made into highly porous structure as the inner layer of the tubular scaffold to load drugs.
2. To study the drug loading and diffusion behaviors, especially the one directional diffusion behaviors. The successful one-directional scaffolds should have more significant drug/release efficiency than those homogeneous scaffolds. The drug-loaded tubular scaffolds can be put into designed vials in vitro to measure the drug concentration inside and outside of the tubes periodically.
3. To study the scaffolds degradation behaviors. The degradation property is another important factor in the design of scaffolds because the scaffold

degradation must match the tissue re-growth. The simple experiment is to measure the weight loss of scaffolds with time in vitro.

8. Supplement

8.1 The effect of chloroform

Chloroform is a good solvent and also can be used as a plasticizer. PLGA 50/50 with different chloroform concentrations were foamed at 5.86 MPa and room temperature by a pressure quench method. Morphologies of these scaffolds are shown in Figure 8.1. When chloroform concentration is higher, the highly porous structure with higher expansion volume is obtained. Once the chloroform concentration goes down, the denser scaffold is made. Although the highly porous structure can be obtained by adding high concentration chloroform in PLGA 50/50, the chloroform residue is still a concern in tissue engineering. According to the United States Pharmacopeia (USP), the chloroform concentration limit in polymers used in tissue engineering field (i.e., suture) is 50 ppm [156]. But till now there is no detail definition of chloroform limit in scaffolds for the nerve regeneration.

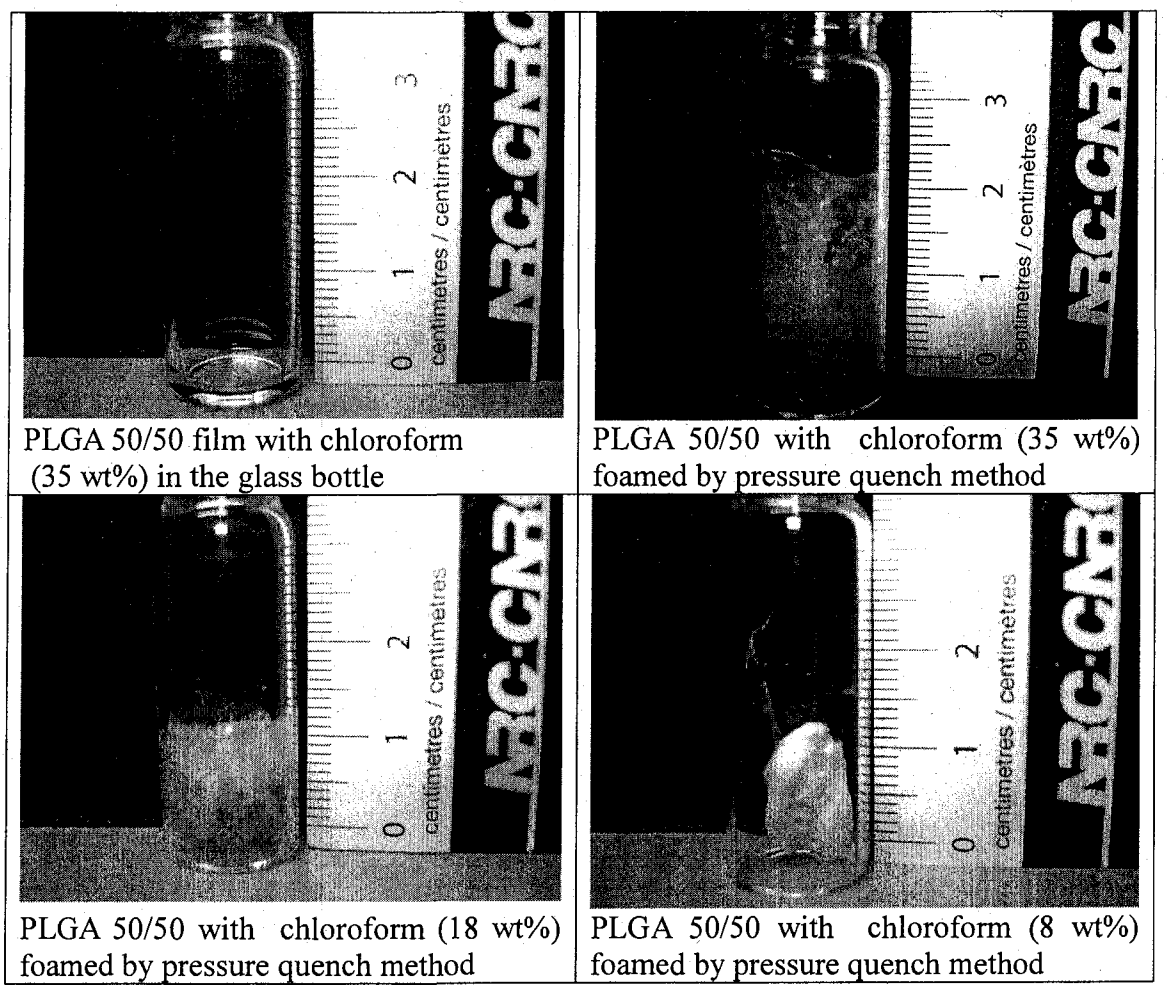

PLGA 50/50 film with chloroform (35 wt%) in the glass bottle

PLGA 50/50 with chloroform (35 wt%) foamed by pressure quench method

PLGA 50/50 with chloroform (18 wt%) foamed by pressure quench method

PLGA 50/50 with chloroform (8 wt%) foamed by pressure quench method

Figure 8.1 Morphologies of PLGA 50/50 foamed with different concentration of chloroform by pressure quench method

8.2 The effect of molecular weight

PLGA 50/50 with different molecular weight were purchased from Durect Inc. and the molecular weights were measured by GPC (TDA-302, Viscoteck).

Table 8.1 GPC result of PLGA 50/50 with different molecular weights

	Viscosity* dL/g	Mw	Mn	Mp	Mw/Mn
PLGA 50/50-1	0.55-0.75	44911	23121	47302	1.942
PLGA 50/50-2	0.76-0.94	76545	40655	75921	1.883
PLGA 50/50-3	0.95-1.25	125132	62710	151778	1.995

* means that the viscosity is provided by the company, measured in HFIP. Other properties were characterized by GPC.

PLGA 50/50 films with different molecular weight were soaked at 400, 600, 5.86 MPa by pressure quench method. Figure 8.2.1 shows the morphologies of these foams. At 2.76 MPa, all foams show big pore sizes indicating the difficult nucleating and foaming condition. The highly porous structures can be obtained at higher pressure conditions. The high magnification SEM pictures of these foams obtained at 5.86 MPa (in Figure 8.2.2) indicate that PLGA 50/50-3 with the highest molecular weight has the smallest average pore size (20.4 μm). PLGA 50/50-1 and PLGA 50/50-2 have average pore sizes of 40.8 μm and 56.1 μm, respectively. Their foam densities are 0.081, 0.085 and 0.126 g/cm^3 from PLGA 50/50-1, PLGA 50/50-2 to PLGA 50/50-3 (Figure 8.2.3).

These films also foamed by a temperature method (soaked at 5.86 MPa and foamed at

different temperatures, i.e. at 35°C and 30 s, and at 60°C and 15 s). The morphologies are shown in Figure 8.2.4. The interesting phenomenon is that the big bubbles formed in the foams indicating the bubble coalescence in the temperature-quenching process. The PLGA 50/50-3 has the less bubble-coalescence. At 60°C foaming condition, the collapsed foam structures tell that the temperature is so high that the polymer cannot maintain its highly porous structure.

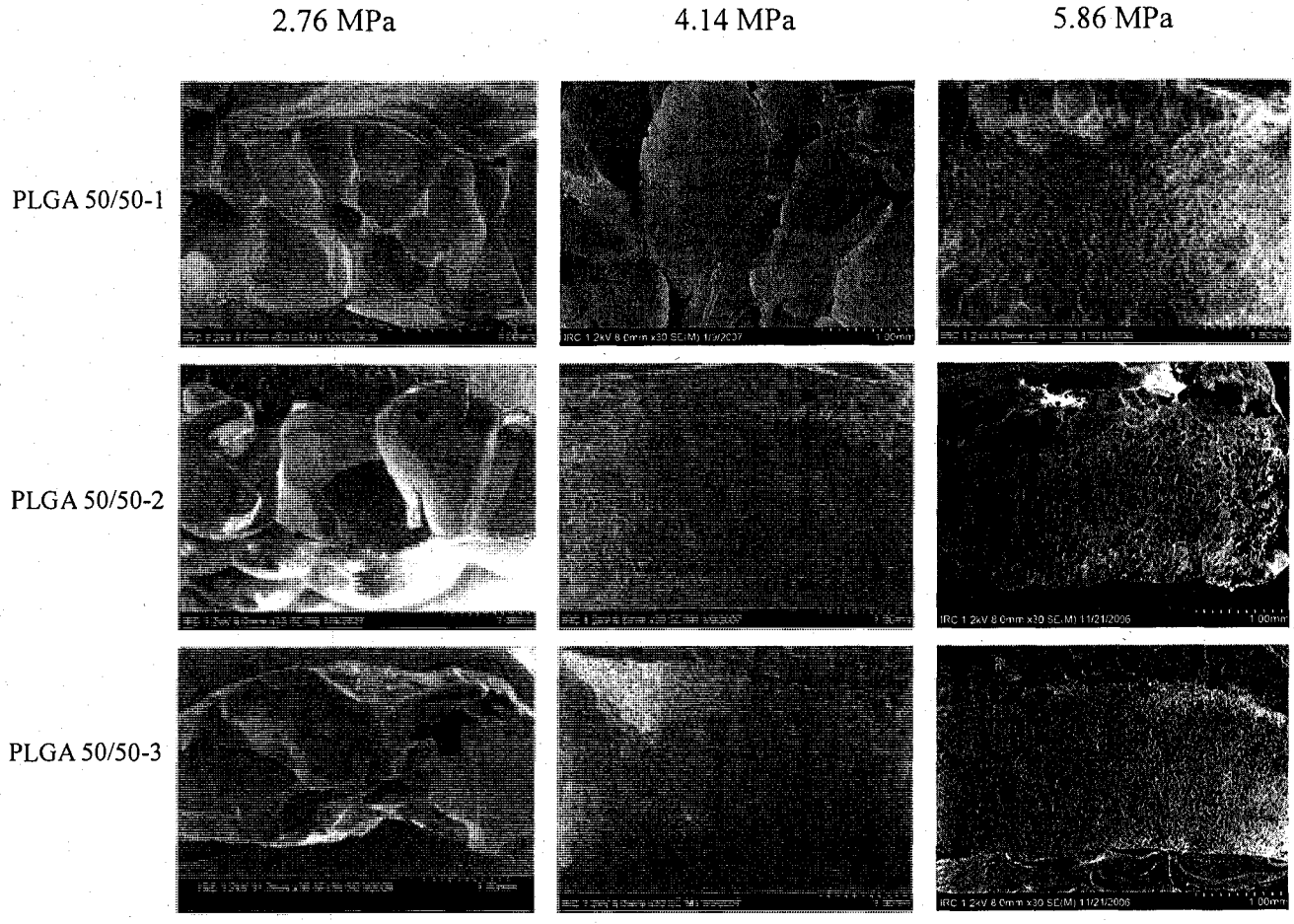

Figure 8.2.1 Morphologies of PLGA 50/50 with different molecular weight soaked at 2.76 MPa, 4.14 MPa, and 5.86 MPa and room temperature and foamed by a pressure quench method

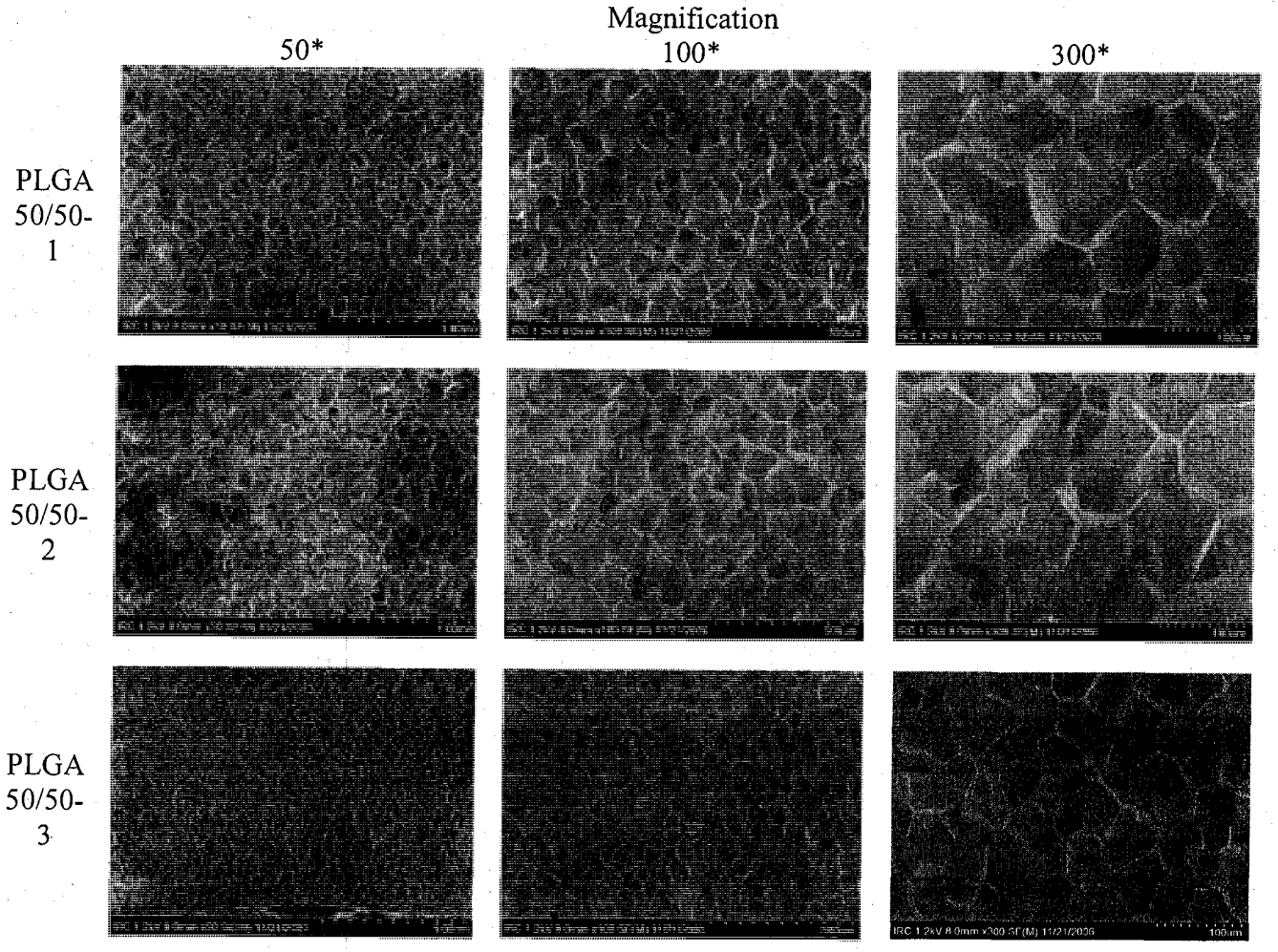

Figure 8.2.2 Morphologies of PLGA 50/50 films with different molecular weight foamed at 5.86 MPa by a pressure quench method at room temperature.

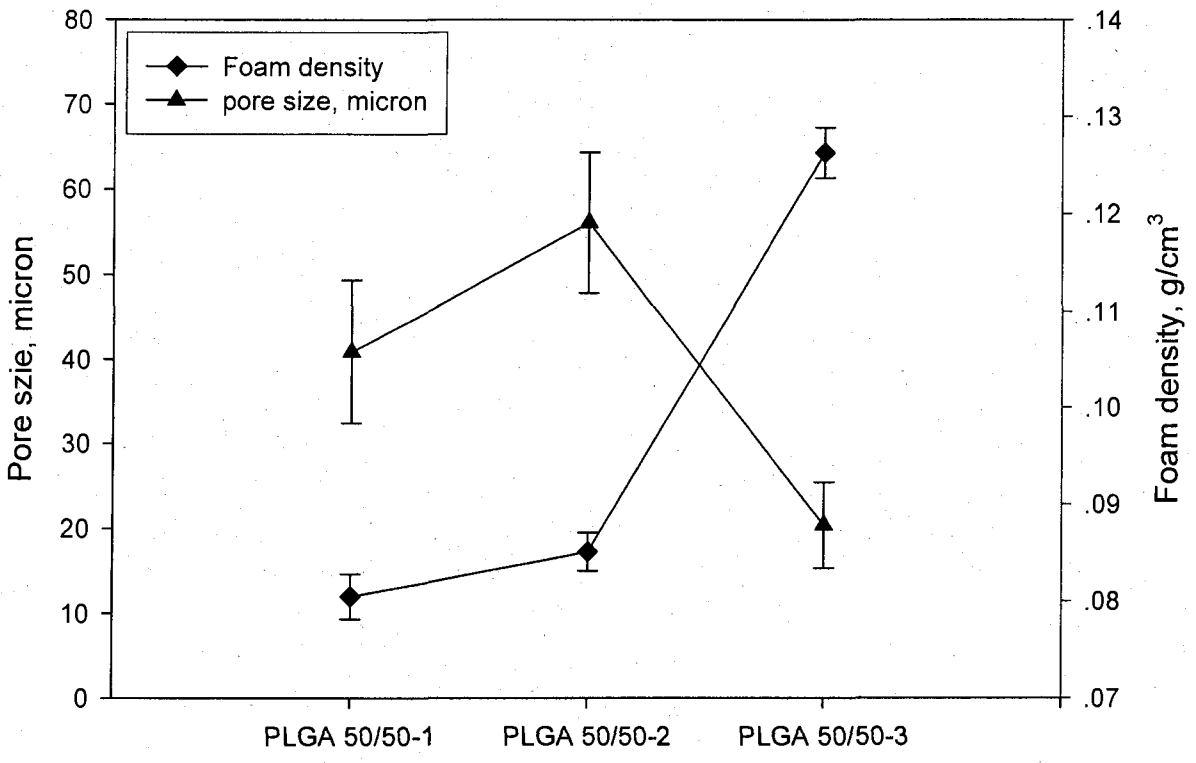

Figure 8.2.3 Foam density and pore size distribution of PLGA 50/50 films with different molecular weight foamed at 5.86 MPa by a pressure quench method

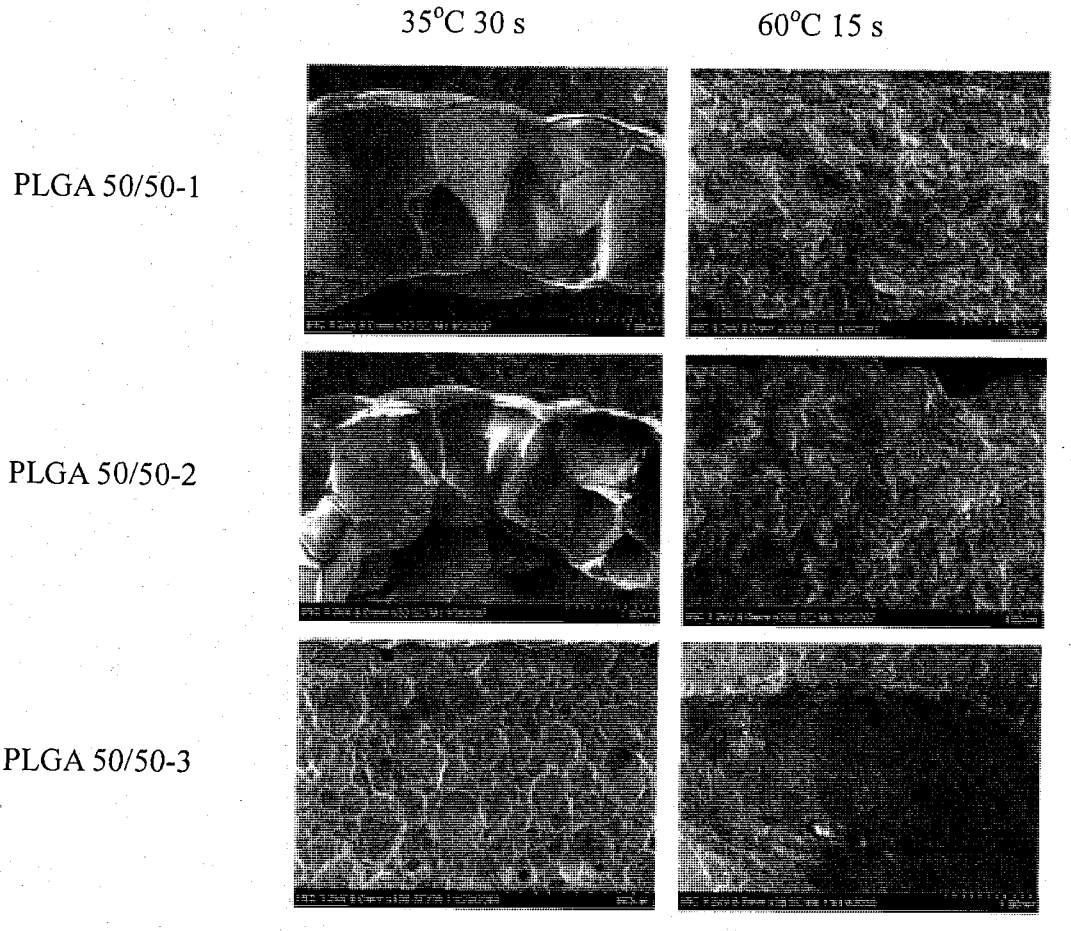

Figure 8.2.4 Morphologies of PLGA 50/50 with different molecular weight soaked at 5.86 MPa and room temperature and foamed by a temperature quench method at 35°C and 60°C.

References

1. Langer R, Vacanti JP. Tissue engineering. Science 1993 May;260(5110):920-926.
2. Agrawal CM, Athanasiou KA, Heckman JD. Biodegradable pla-pga polymers for tissue engineering in orthopaedics. Porous materials for tissue engineering, 1997. p. 115-128.
3. Mooney DJ, Kaufmann PM, Sano K, McNamara KM, Vacanti JP, Langer R. Transplantation of hepatocytes using porous, biodegradable sponges. Transplantation Proceedings 1994 Dec;26(6):3425-3426.
4. Freed LE, Vunjaknovakovic G, Biron RJ, Eagles DB, Lesnoy DC, Barlow SK, et al. Biodegradable polymer scaffolds for tissue engineering. Bio-Technology 1994 Jul;12(7):689-693.
5. Mikos AG, Thorsen AJ, Czerwonka LA, Bao Y, Langer R, Winslow DN, et al. Preparation and characterization of poly(l-lactic acid) foams. Polymer 1994;35(5):1068-1077.
6. Raghunath J, Rollo J, Sales KM, Butler PE, Seifalian AM. Biomaterials and scaffold design: Key to tissue-engineering cartilage. Biotechnology and Applied Biochemistry 2007 Feb;46:73-84.
7. Martina M, Hutmacher DW. Biodegradable polymers applied in tissue engineering research: A review. Polymer International 2007 Feb;56(2):145-157.
8. Nomura H, Tator CH, Shoichet MS. Bioengineered strategies for spinal cord repair. Journal of Neurotrauma 2006 Mar-Apr;23(3-4):496-507.
9. Nazhat SN, Abou Neel EA, Kidane A, Ahmed I, Hope C, Kershaw M, et al. Controlled microchannelling in dense collagen scaffolds by soluble phosphate glass fibers. Biomacromolecules 2007 Feb;8(2):543-551.
10. Holland TA, Bodde EWH, Cuijpers V, Baggett LS, Tabata Y, Mikos AG, et al. Degradable hydrogel scaffolds for in vivo delivery of single and dual growth factors in cartilage repair. Osteoarthritis and Cartilage 2007 Feb;15(2):187-197.
11. Neuenschwander S, Hoerstrup SP. Heart valve tissue engineering. Transplant Immunology 2004 Apr;12(3-4):359-365.
12. Ohkawa K, Yamada M, Nishida A, Nishi N, Yamamoto H. Biodegradation of chitosan-gellan and poly(l-lysine)-gellan polyion complex fibers by pure cultures of soil filamentous fungi. Journal of Polymers and the Environment 2000 Apr;8(2):59-66.
13. Sung HJ, Meredith C, Johnson C, Galis ZS. The effect of scaffold degradation rate on three-dimensional cell growth and angiogenesis. Biomaterials 2004 Nov;25(26):5735-5742.
14. 3DM-Inc. Puramatrix™. 2001 [cited; Available from: http://www.puramatrix.com/products.html#att
15. Cohn D, Salomon AF. Designing biodegradable multiblock pcl/pla thermoplastic elastomers. Biomaterials 2005 May;26(15):2297-2305.
16. Casper CL, Yamaguchi N, Kiick KL, Rabolt JF. Functionalizing electrospun fibers with biologically relevant macromolecules. Biomacromolecules 2005 Jul-Aug;6(4):1998-2007.
17. Li M, Mondrinos MJ, Chen X, Gandhi MR, Ko FK, Lelkes PI. Co-electrospun poly(lactide-co-glycolide), gelatin, and elastin blends for tissue engineering scaffolds. Journal of Biomedical Materials Research Part A 2006 Dec;79A(4):963-973.
18. Gomes ME, Reis RL. Biodegradable polymers and composites in biomedical applications: From catgut to tissue engineering - part 1 - available systems and their properties. International Materials Reviews 2004 Oct;49(5):261-273.
19. Hardin-Young J TJ, Ross R, Parenteau N Principles of tissue engineering. 2nd ed. NewYork: Academic Press, 2000.
20. Kohn P. In: Robert Lanza RL, Joseph P. Vacanti, editor. Principles of tissue engineering. 2nd ed. New York: Academic Press, 1997. p. 273-285.
21. Vunjak-Novakovic G, Kaplan DL. Tissue engineering: The next generation. Tissue Engineering 2006 Dec;12(12):3261-3263.
22. Goraltchouk A, Scanga V, Morshead CM, Shoichet MS. Incorporation of protein-eluting microspheres into biodegradable nerve guidance channels for controlled release. Journal of Controlled Release 2006 Jan;110(2):400-407.
23. Holland SJ, Tighe BJ. Advances in pharmaceutical sciences. San Diego: Academic, 1992. p. 101-103.
24. Richardson TP, Peters MC, Ennett AB, Mooney DJ. Polymeric system for dual growth factor delivery. Nature Biotechnology 2001 Nov;19(11):1029-1034.
25. Heyde M, Partridge KA, Oreffo ROC, Howdle SM, Shakesheff KM, Garnett MC. Gene therapy used for tissue engineering applications. Journal of Pharmacy and Pharmacology 2007 Mar;59(3):329-350.

26. Ikada Y. Challenges in tissue engineering. Journal of the Royal Society Interface 2006 Oct;3(10):589-601.
27. Nie HM, Wang CH. Fabrication and characterization of plga/hap scaffolds for delivery of bmp-2 plasmid composite DNA. Journal of Controlled Release 2007 Jul;120(1-2):111-121.
28. Langer RS, Vacanti JP. Tissue engineering: The challenges ahead. Scientific American 1999 Apr;280(4):86-89.
29. Costa FF, Le Blanc K, Brodin B. Concise review: Cancer/testis antigens, stem cells, and cancer. Stem Cells 2007 Mar;25(3):707-711.
30. Anversa P, Leri A, Rota M, Hosoda T, Bearzi C, Urbanek K, et al. Concise review: Stem cells, myocardial regeneration, and methodological artifacts. Stem Cells 2007 Mar;25(3):589-601.
31. Duplomb L, Dagouassat M, Jourdon P, Heymann D. Concise review: Embryonic stem cells: A new tool to study osteoblast and osteoclast differentiation. Stem Cells 2007 Mar;25(3):544-552.
32. Levenberg S, Burdick JA, Kraehenbuehl T, Langer R. Neurotrophin-induced differentiation of human embryonic stem cells on three-dimensional polymeric scaffolds. Tissue Engineering 2005 Mar;11(3-4):506-512.
33. Furnish EJ, Schmidt C. Tissue engineering of the peripheral nervous system. In: Patrick CW MA, McIntire LV, editor. Frontiers in tissue engineering Elsevier, 1998. p. 514-535.
34. Fenrich K, Gordon T. Canadian association of neuroscience review: Axonal regeneration in the peripheral and central nervous systems - current issues and advances. Canadian Journal of Neurological Sciences 2004 May;31(2):142-156.
35. Priestley JV, Ramer MS, King VR, McMahon SB, Brown RA. Stimulating regeneration in the damaged spinal cord. Journal of Physiology-Paris 2002 Jan-Mar;96(1-2):123-133.
36. Goldberg JL, Barres BA. The relationship between neuronal survival and regeneration. Annual Review of Neuroscience 2000;23:579-612.
37. Evans GRD. Challenges to nerve regeneration. Seminars in Surgical Oncology 2000 Oct-Nov;19(3):312-318.
38. Lundborg G. Nerve injury and repair. NewYork: CHURCHILL LIVINGSTONE, 2005.
39. Chamberlain LJ, Yannas IV, Arrizabalaga A, Hsu HP, Norregaard TV, Spector M. Early peripheral nerve healing in collagen and silicone tube implants: Myofibroblasts and the cellular response. Biomaterials 1998 Aug;19(15):1393-1403.
40. Geuna S, Nicolino S, Raimondo S, Gambarotta G, Battiston B, Tos P, et al. Nerve regeneration along bioengineered scaffolds. Microsurgery 2007;27(5):429-438.
41. Toba T, Nakamura T, Lynn AK, Matsumoto K, Fukuda S, Yoshitani M, et al. Evaluation of peripheral nerve regeneration across an 80-mm gap using a polyglycolic acid (pga) - collagen nerve conduit filled with laminin-soaked collagen sponge in dogs. International Journal of Artificial Organs 2002 Mar;25(3):230-237.
42. Cao X, Schoichet M. Issue engineering strategies for axonal regeneration on following spinal cord injury. In: Dillow AK LA, editor. Biomimetic materials and design 2002. p. 417-442.
43. Gage FH. Mammalian neural stem cells. Science 2000 Feb;287(5457):1433-1438.
44. Oudega M, Hagg T. Nerve growth factor promotes regeneration of sensory axons into adult rat spinal cord. Experimental Neurology 1996 Aug;140(2):218-229.
45. Houweling DA, Lankhorst AJ, Gispen WH, Bar PR, Joosten EAJ. Collagen containing neurotrophin-3 (nt-3) attracts regrowing injured corticospinal axons in the adult rat spinal cord and promotes partial functional recovery. Experimental Neurology 1998 Sep;153(1):49-59.
46. Schnell L, Schneider R, Kolbeck R, Barde YA, Schwab ME. Neurotrophin-3 enhances sprouting of corticospinal tract during development and after adult spinal-cord lesion. Nature 1994 Jan;367(6459):170-173.
47. Grill R, Murai K, Blesch A, Gage FH, Tuszynski MH. Cellular delivery of neurotrophin-3 promotes corticospinal axonal growth and partial functional recovery after spinal cord injury. Journal of Neuroscience 1997 Jul;17(14):5560-5572.
48. Xu XM, Guenard V, Kleitman N, Aebischer P, Bunge MB. Combination of bdnf and nt-3 promotes supraspinal axonal regeneration into schwann-cell grafts in adult-rat thoracic spinal-cord. Experimental Neurology 1995 Aug;134(2):261-272.
49. Wang AJ, Ao Q, Cao WL, Yu MZ, He Q, Kong LJ, et al. Porous chitosan tubular scaffolds with knitted outer wall and controllable inner structure for nerve tissue engineering. Journal of Biomedical Materials Research Part A 2006 Oct;79A(1):36-46.
50. Zhang N, Zhang CH, Wen XJ. Fabrication of semipermeable hollow fiber membranes with highly aligned texture for nerve guidance. Journal of Biomedical Materials Research Part A 2005 Dec;75A(4):941-949.
51. Moore MJ, Friedman JA, Lewellyn EB, Mantila SM, Krych AJ, Ameenuddin S, et al. Multiple-

channel scaffolds to promote spinal cord axon regeneration. Biomaterials 2006 Jan;27(3):419-429.
52. Mark J. Polymer data handbook: Oxford Universiy Press, 1999.
53. Durect-Co. Lactel® website. 2007 [cited; Available from: http://www.absorbables.com/tech/biodegradation.asp
54. Ruhe PQ, Hedberg EL, Padron NT, Spauwen PHM, Jansen JA, Mikos AG. Biocompatibility and degradation of poly(dl-lactic-co-glycolic acid)/calcium phosphate cement composites. Journal of Biomedical Materials Research Part A 2005 Sep;74A(4):533-544.
55. Agrawal AK, Bhalla R. Advances in the production of poly(lactic acid) fibers. A review. Journal of Macromolecular Science-Polymer Reviews 2003;C43(4):479-503.
56. Grayson ACR, Voskerician G, Lynn A, Anderson JM, Cima MJ, Langer R. Differential degradation rates in vivo and in vitro of biocompatible poly(lactic acid) and poly(glycolic acid) homo- and co-polymers for a polymeric drug-delivery microchip. Journal of Biomaterials Science-Polymer Edition 2004;15(10):1281-1304.
57. Bini TB, Gao SJ, Xu XY, Wang S, Ramakrishna S, Leong KW. Peripheral nerve regeneration by microbraided poly(l-lactide-co-glycolide) biodegradable polymer fibers. Journal of Biomedical Materials Research Part A 2004 Feb;68A(2):286-295.
58. Bakar M, Djaider F. Effect of plasticizers content on the mechanical properties of unsaturated polyester resin. Journal of Thermoplastic Composite Materials 2007 Jan;20(1):53-64.
59. Karageorgiou V, Kaplan D. Porosity of 3d biornaterial scaffolds and osteogenesis. Biomaterials 2005 Sep;26(27):5474-5491.
60. Hutmacher DW. Scaffold design and fabrication technologies for engineering tissues - state of the art and future perspectives. Journal of Biomaterials Science-Polymer Edition 2001;12(1):107-124.
61. Liu XH, Ma PX. Polymeric scaffolds for bone tissue engineering. Annals of Biomedical Engineering 2004 Mar;32(3):477-486.
62. Teo WE, Ramakrishna S. A review on electrospinning design and nanofibre assemblies. Nanotechnology 2006 Jul;17(14):R89-R106.
63. Murugan R, Ramakrishna S. Nano-featured scaffolds for tissue engineering: A review of spinning methodologies. Tissue Engineering 2006 Mar;12(3):435-447.
64. Zhong SP, Teo WE, Zhu X, Beuertnan R, Ramakrishna S, Yung LYL. Development of a novel collagen-gag nanofibrous scaffold via electrospinning. Materials Science & Engineering C-Biomimetic and Supramolecular Systems 2007 Mar;27(2):262-266.
65. Sander EA, Alb AM, Nauman EA, Reed WF, Dee KC. Solvent effects on the microstructure and properties of 75/25 poly(d,l-lactide-co-glycolide) tissue scaffolds. Journal of Biomedical Materials Research Part A 2004 Sep;70A(3):506-513.
66. Yang Q, Chen L, Shen XY, Tan ZQ. Preparation of polycaprolactone tissue engineering scaffolds by improved solvent casting/particulate leaching method. Journal of Macromolecular Science Part B-Physics 2006 Nov;45(6):1171-1181.
67. Chen GP, Ushida T, Tateishi T. Development of biodegradable porous scaffolds for tissue engineering. Materials Science & Engineering C-Biomimetic and Supramolecular Systems 2001 Nov;17(1-2):63-69.
68. Lv QA, Feng QL, Hu K, Cui FZ. Three-dimensional fibroin/collagen scaffolds derived from aqueous solution and the use for hepg2 culture. Polymer 2005 Dec;46(26):12662-12669.
69. Lee SB, Kim YH, Chong MS, Hong SH, Lee YM. Study of gelatin-containing artificial skin v: Fabrication of gelatin scaffolds using a salt-leaching method. Biomaterials 2005 May;26(14):1961-1968.
70. Cho SH, Oh SH, Lee JH. Fabrication and characterization of porous alginate/polyvinyl alcohol hybrid scaffolds for 3d cell culture. Journal of Biomaterials Science-Polymer Edition 2005;16(8):933-947.
71. Whang K, Thomas CH, Healy KE, Nuber G. A novel method to fabricate bioabsorbable scaffolds. Polymer 1995 Feb;36(4):837-842.
72. Wan Y, Wu H, Wen DJ. Porous-conductive chitosan scaffolds for tissue engineering, 1 - preparation and characterization. Macromolecular Bioscience 2004 Sep;4(9):882-890.
73. Shin KC, Kim BS, Kim JH, Park TG, Do Nam J, Lee DS. A facile preparation of highly interconnected macroporous plga scaffolds by liquid-liquid phase separation ii. Polymer 2005 May;46(11):3801-3808.
74. Hua FJ, Park TG, Lee DS. A facile preparation of highly interconnected macroporous poly(d,l-lactic acid-co-glycolic acid) (plga) scaffolds by liquid-liquid phase separation of a plga-dioxane-water ternary system. Polymer 2003 Mar;44(6):1911-1920.
75. Yeong WY, Chua CK, Leong KF, Chandrasekaran M. Rapid prototyping in tissue engineering: Challenges and potential. Trends in Biotechnology 2004 Dec;22(12):643-652.
76. Tsang VL, Bhatia SN. Three-dimensional tissue fabrication. Advanced Drug Delivery Reviews 2004

Sep;56(11):1635-1647.
77. Zein I, Hutmacher DW, Tan KC, Teoh SH. Fused deposition modeling of novel scaffold architectures for tissue engineering applications. Biomaterials 2002 Feb;23(4):1169-1185.
78. Sun W, Starly B, Nam J, Darling A. Bio-cad modeling and its applications in computer-aided tissue engineering. Computer-Aided Design 2005 Sep;37(11):1097-1114.
79. Ma P. Tissue fabrication. Materials Today 2004;5 30-40.
80. Kim TK, Yoon JJ, Lee DS, Park TG. Gas foamed open porous biodegradable polymeric microspheres. Biomaterials 2006 Jan;27(2):152-159.
81. Gendron R, Champagne MF, Delaviz Y, Polasky ME. Foaming polystyrene with a mixture of co2 and ethanol. Journal of Cellular Plastics 2006 Mar;42(2):127-138.
82. Singh L, Kumar V, Ratner BD. Generation of porous microcellular 85/15 poly ((dl)-lactide-co-glycolide) foams for biomedical applications. Biomaterials 2004 Jun;25(13):2611-2617.
83. Rodeheaver BA, Colton JS. Open-celled microcellular thermoplastic foam. Polymer Engineering and Science 2001;41(3):380-400.
84. Kemmere M, Meyer T. Supercritical carbon dioxide in polymer reaction engineering: Wiley-VCH, 2005.
85. de Sousa FCG, Evans JRG. Tubular hydroxyapatite scaffolds. Advances in Applied Ceramics 2005 Feb;104(1):30-34.
86. Freier T, Montenegro R, Koh HS, Shoichet MS. Chitin-based tubes for tissue engineering in the nervous system. Biomaterials 2005 Aug;26(22):4624-4632.
87. Buttafoco L, Boks NP, Engbers-Buijtenhuijs P, Grijpma DW, Poot AA, Dijkstra PJ, et al. Porous hybrid structures based on p(dlla-co-tmc) and collagen for tissue engineering of small-diameter blood vessels. Journal of Biomedical Materials Research Part B-Applied Biomaterials 2006 Nov;79B(2):425-434.
88. Motlagh D, Yang J, Lui KY, Webb AR, Ameer GA. Hemocompatibility evaluation of poly(glycerol-sebacate) in vitro for vascular tissue engineering. Biomaterials 2006 Aug;27(24):4315-4324.
89. Pham QP, Sharma U, Mikos AG. Electrospun poly(epsilon-caprolactone) microfiber and multilayer nanofiber/microfiber scaffolds: Characterization of scaffolds and measurement of cellular infiltration. Biomacromolecules 2006 Oct;7(10):2796-2805.
90. Harley BA, Hastings AZ, Yannas IV, Sannino A. Fabricating tubular scaffolds with a radial pore size gradient by a spinning technique. Biomaterials 2006 Feb;27(6):866-874.
91. Nalawade SP, Picchioni F, Janssen L. Supercritical carbon dioxide as a green solvent for processing polymer melts: Processing aspects and applications. Progress in Polymer Science 2006 Jan;31(1):19-43.
92. Tomasko DL, Li HB, Liu DH, Han XM, Wingert MJ, Lee LJ, et al. A review of co2 applications in the processing of polymers. Industrial & Engineering Chemistry Research 2003 Dec;42(25):6431-6456.
93. Leitner W, Jessop P. Chemical synthesis using supercritical fluids. Weinheim: Wiley-VCH, 1999.
94. Sun XH, Liu HJ, Li G, Liao X, He JS. Investigation on the cell nucleation and cell growth in microcellular foaming by means of temperature quenching. Journal of Applied Polymer Science 2004 Jul;93(1):163-171.
95. Goel SK, Beckman EJ. Generation of microcellular polymeric foams using supercritical carbon-dioxide .1. Effect of pressure and temperature on nucleation. Polymer Engineering and Science 1994 Jul;34(14):1137-1147.
96. Verreck G, Decorte A, Li HB, Tomasko D, Arien A, Peeters J, et al. The effect of pressurized carbon dioxide as a plasticizer and foaming agent on the hot melt extrusion process and extrudate properties of pharmaceutical polymers. Journal of Supercritical Fluids 2006 Oct;38(3):383-391.
97. Pantoula M, Panayiotou C. Sorption and swelling in glassy polymer/carbon dioxide systems - part i. Sorption. Journal of Supercritical Fluids 2006 Apr;37(2):254-262.
98. Tang M, Du TB, Chen YP. Sorption and diffusion of supercritical carbon dioxide in polycarbonate. Journal of Supercritical Fluids 2004 Mar;28(2-3):207-218.
99. Arai Y, Sako T, Takebayashi Y. Supercritical fluids: Molecular interactions, physical properties, and new applications: Viley, 2005.
100. Berens AR, Huvard GS. Interaction of polymers with near-critical carbon-dioxide. Acs Symposium Series 1989;406:207-223.
101. Shieh YT, Lin YG. Equilibrium solubility of co2 in rubbery eva over a wide pressure range: Effects of carbonyl group content and crystallinity. Polymer 2002 Mar;43(6):1849-1856.
102. Kazarian SG, Chan KLA. Ftir imaging of polymeric materials under high-pressure carbon dioxide. Macromolecules 2004 Jan;37(2):579-584.

103. Fleming OS, Chan KLA, Kazarian SG. High-pressure co2-enhanced polymer interdiffusion and dissolution studied with in situ atr-ftir spectroscopic imaging. Polymer 2006 Jun;47(13):4649-4658.
104. Nalawade SP, Picchioni F, Janssen L, Patil VE, Keurentjes JTF, Staudt R. Solubilities of sub- and supercritical carbon dioxide in polyester resins. Polymer Engineering and Science 2006 May;46(5):643-649.
105. Elvassore N, Vezzu K, Bertucco A. Measurement and modeling of co2 absorption in poly (lactic-co-glycolic acid). Journal of Supercritical Fluids 2005 Jan;33(1):1-5.
106. Liu DH, Tomasko DL. Carbon dioxide sorption and dilation of poly(lactide-co-glycolide). Journal of Supercritical Fluids 2007 Jan;39(3):416-425.
107. Mawson S, Johnston KP, Combes JR, Desimone JM. Formation of poly(1,1,2,2-tetrahydroperfluorodecyl acrylate) submicron fibers and particles from supercritical carbon-dioxide solutions. Macromolecules 1995 Apr;28(9):3182-3191.
108. Oliveira NS, Dorgan J, Coutinho JAP, Ferreira A, Daridon JL, Marrucho IM. Gas solubility of carbon dioxide in poly(lactic acid) at high pressures. Journal of Polymer Science Part B-Polymer Physics 2006 Mar;44(6):1010-1019.
109. Bonavoglia B, Storti G, Morbidelli M. Modeling of the sorption and swelling behavior of semicrystalline polymers in supercritical co2. Industrial & Engineering Chemistry Research 2006 Feb;45(3):1183-1200.
110. Pesci AI, Freed KF. Lattice theory of polymer blends and liquid-mixtures - beyond the flory-huggins approximation. Journal of Chemical Physics 1989 Feb;90(3):2017-2026.
111. Sato Y, Takikawa T, Sorakubo A, Takishima S, Masuoka H, Imaizumi M. Solubility and diffusion coefficient of carbon dioxide in biodegradable polymers. Industrial & Engineering Chemistry Research 2000 Dec;39(12):4813-4819.
112. De Angelis MG, Merkel TC, Bondar VI, Freeman BD, Doghieri F, Sarti GC. Hydrocarbon and fluorocarbon solubility and dilation in poly(dimethylsiloxane): Comparison of experimental data with predictions of the sanchez-lacombe equation of state. Journal of Polymer Science Part B-Polymer Physics 1999 Nov;37(21):3011-3026.
113. Kirby CF, McHugh MA. Phase behavior of polymers in supercritical fluid solvents. Chemical Reviews 1999 Feb;99(2):565-602.
114. Goel SK, Beckman EJ. Generation of microcellular polymeric foams using supercritical carbon-dioxide .2. Cell-growth and skin formation. Polymer Engineering and Science 1994 Jul;34(14):1148-1156.
115. Xu Q, Ren XW, Chang YN, Wang JW, Yu L, Dean K. Generation of microcellular biodegradable polycaprolactone foams in supercritical carbon dioxide. Journal of Applied Polymer Science 2004 Oct;94(2):593-597.
116. Harris LD, Kim BS, Mooney DJ. Open pore biodegradable matrices formed with gas foaming. Journal of Biomedical Materials Research 1998 Dec;42(3):396-402.
117. Nawaby AV, Farah AA, Liao X, Pietro WJ, Day M. Biodegradable open cell foams of telechelic poly(epsilon-caprolactone) macroligand with ruthenium(ii) chromophoric subunits via sub-critical co2 processing. Biomacromolecules 2005 Sep-Oct;6(5):2458-2461.
118. Liao X, Nawaby AV, Day M. Layered open cell poly ((l)-lactic acid) nanomorphology. Abstracts of Papers of the American Chemical Society 2005 Aug;230:U3690-U3690.
119. Itagaki H, Ochiai A, Nakamori T. The microenvironment in polymer solids with added plasticizers. An attempt to measure the size and distribution of free volume in poly(methyl methacrylate) solids. European Polymer Journal 2006 Aug;42(8):1939-1952.
120. Kazarian SG, Vincent MF, Bright FV, Liotta CL, Eckert CA. Specific intermolecular interaction of carbon dioxide with polymers. Journal of the American Chemical Society 1996 Feb;118(7):1729-1736.
121. Taki K, Nitta K, Kihara S, Ohshima M. Co2 foaming of poly(ethylene glycol)/polystyrene blends: Relationship of the blend morphology, co2 mass transfer, and cellular structure. Journal of Applied Polymer Science 2005 Sep;97(5):1899-1906.
122. Wargo SL, Kumar TR, Russell AJ. Gradient scaffold in tissue engineering. Cell Transplantation 2006;15:S127-S127.
123. Sato Y, Takikawa T, Takishima S, Masuoka H. Solubilities and diffusion coefficients of carbon dioxide in poly(vinyl acetate) and polystyrene. Journal of Supercritical Fluids 2001 Feb;19(2):187-198.
124. Zhang Y, Gangwani KK, Lemert RM. Sorption and swelling of block copolymers in the presence of supercritical fluid carbon dioxide. Journal of Supercritical Fluids 1997 Oct;11(1-2):115-134.
125. Wu YT, Akoto-Ampaw PJ, Elbaccouch M, Hurrey ML, Wallen SL, Grant CS. Quartz crystal microbalance (qcm) in high-pressure carbon dioxide (co2): Experimental aspects of qcm theory and co2

adsorption. Langmuir 2004 Apr;20(9):3665-3673.
126. Durect. Chemical physical properties. 2007 [cited; Available from: http://www.absorbables.com/properties.htm
127. Guan R, Xiang BL, Xiao ZX, Li YL, Lu DP, Song GW. The processing-structure relationships in thin microcellular pet sheet prepared by compression molding. European Polymer Journal 2006 May;42(5):1022-1032.
128. Kumar V, Weller J. Production of microcellular polycarbonate using carbon-dioxide for bubble nucleation. Journal of Engineering for Industry-Transactions of the Asme 1994 Nov;116(4):413-420.
129. Dubin C. The archimedean principle. 1 ed: Houille Blanche-Revue Internationale De Leau, 2005.
130. Mettler me-163 balance operation manual.
131. Muth O, Hirth T, Vogel H. Investigation of sorption and diffusion of supercritical carbon dioxide into poly(vinyl chloride). Journal of Supercritical Fluids 2001 Apr;19(3):299-306.
132. Pascault JP, Williams R. Formulation and characterization of thermoset-thermoplastic blends. 1 ed. New York: Wiley-interscience, 1999.
133. Couchman PR. Compositional variation of glass-transition temperatures .2. Application of thermodynamic theory to compatible polymer blends. Macromolecules 1978;11(6):1156-1161.
134. De Kesel C, Lefevre C, Nagy JB, David C. Blends of polycaprolactone with polyvinylalcohol: A dsc, optical microscopy and solid state nmr study. Polymer 1999 Apr;40(8):1969-1978.
135. Siripurapu S, Coughlan JA, Spontak RJ, Khan SA. Surface-constrained foaming of polymer thin films with supercritical carbon dioxide. Macromolecules 2004 Dec;37(26):9872-9879.
136. St Lawrence S, Willett JL, Carriere CJ. Effect of moisture on the tensile properties of poly(hydroxy ester ether). Polymer 2001 Jun;42(13):5643-5650.
137. Matsuyama K, Mishima K. Phase behavior of co2 plus polyethylene glycol plus ethanol at pressures up to 20 mpa. Fluid Phase Equilibria 2006 Nov;249(1-2):173-178.
138. Cleek RL, Ting KC, Eskin SG, Mikos AG. Microparticles of poly(dl-lactic-co-glycolic acid)/poly(ethylene glycol) blends for controlled drug delivery. Journal of Controlled Release 1997 Oct;48(2-3):259-268.
139. Handa YP, Zhang ZY, Nawaby V, Tan J. Gas solubility and foamability of various forms of syndiotactic polystyrene. Cellular Polymers 2001;20(4):241-253.
140. Zhai WT, Yu J, Ma WM, He JS. Cosolvent effect of water in supercritical carbon dioxide facilitating induced crystallization of polycarbonate. Polymer Engineering and Science 2007 Sep;47(9):1338-1343.
141. Blasi P, D'Souza SS, Selmin F, DeLuca PP. Plasticizing effect of water on poly(lactide-co-glycolide). Journal of Controlled Release 2005 Nov;108(1):1-9.
142. Dalmolin I, Skovroinski E, Biasi A, Corazza ML, Dariva C, Oliveira JV. Solubility of carbon dioxide in binary and ternary mixtures with ethanol and water. Fluid Phase Equilibria 2006 Aug;245(2):193-200.
143. Mark JE. Polymer data handbook. New York: Oxford university press, 1999.
144. Adamson AW, Gast A. Physical chemistry of surfaces. 6 ed: Wiley, 1997.
145. Zhai WT, Yu J, Wu LC, Ma WM, He JS. Heterogeneous nucleation uniformizing cell size distribution in microcellular nanocomposites foams. Polymer 2006 Oct;47(21):7580-7589.
146. Colton JS, Suh NP. The nucleation of microcellular thermoplastic foam with additives .1. Theoretical considerations. Polymer Engineering and Science 1987 Apr;27(7):485-492.
147. Wiesmet V, Weidner E, Behme S, Sadowski G, Arlt W. Measurement and modelling of high-pressure phase equilibria in the systems polyethyleneglycol (peg)-propane, peg-nitrogen and peg-carbon dioxide. Journal of Supercritical Fluids 2000 Feb;17(1):1-12.
148. Wang XT, Venkatraman SS, Boey FYC, Loo JSC, Tan LP. Controlled release of sirolimus from a multilayered plga stent matrix. Biomaterials 2006 Nov;27(32):5588-5595.
149. Mishima K, Tokuyasu T, Matsuyama K, Komorita N, Enjoji T, Nagatani M. Solubility of polymer in the mixtures containing supercritical carbon dioxide and antisolvent. Fluid Phase Equilibria 1998 Feb;144(1-2):299-305.
150. Mishima K, Matsuyama K, Nagatani H. Solubilities of poly(ethylene glycol)s in the mixtures of supercritical carbon dioxide and cosolvent. Fluid Phase Equilibria 1999 Jul;161(2):315-324.
151. Gupta SK, Lesslie RD, King AD. Solubility of alcohols in compressed gases - comparison of vapor-phase interactions of alcohols and homomorphic compounds with various gases .1. Ethanol in compressed helium, hydrogen, argon, methane, ethylene, ethane, carbon-dioxide, and nitrous-oxide. Journal of Physical Chemistry 1973;77(16):2011-2015.
152. ChemicaLogic-Co. Carbon dioxide phase diagram. 1999 [cited; Available from:

www.chemicalogic.com/download/phase_diagram.html
153. Handbook of chemistry and physics. 87 ed, 2006-2007.
154. Duarte ARC, Martins C, Coimbra P, Gil MHM, de Sousa HC, Duarte CMM. Sorption and diffusion of dense carbon dioxide in a biocompatible polymer. Journal of Supercritical Fluids 2006 Oct;38(3):392-398.
155. Cravo C, Duarte ARC, Duarte CMM. Solubility of carbon dioxide in a natural biodegradable polymer: Determination of diffusion coefficients. Journal of Supercritical Fluids 2007 Mar;40(2):194-199.
156. Guidance on croparticles with varying concentrations of residual impurities: Residual solvents,. International Conference on Harmonization, 1997. p. 67377-67388.
157. Mizoguchi K, Hirose T, Naito Y, Kamiya Y. Co2-induced crystallization of poly(ethylene-terephthalate). Polymer 1987 Jul;28(8):1298-1302.
158. Naffakh M, Gomez MA, Ellis G, Marco C. Isothermal crystallization kinetics of peek/vectra (r) blends by dsc and time-resolved synchrotron x-ray diffraction. Polymer Engineering and Science 2006 Oct;46(10):1411-1418.
159. Takada M, Tanigaki M, Ohshima M. Effects of co2 on crystallization kinetics of polypropylene. Polymer Engineering and Science 2001 Nov;41(11):1938-1946.

Appendices

A1: CO_2 phase diagram (P vs. T)[152]

(According to www.chemicalogic.com/download/**phase_diagram**.html)

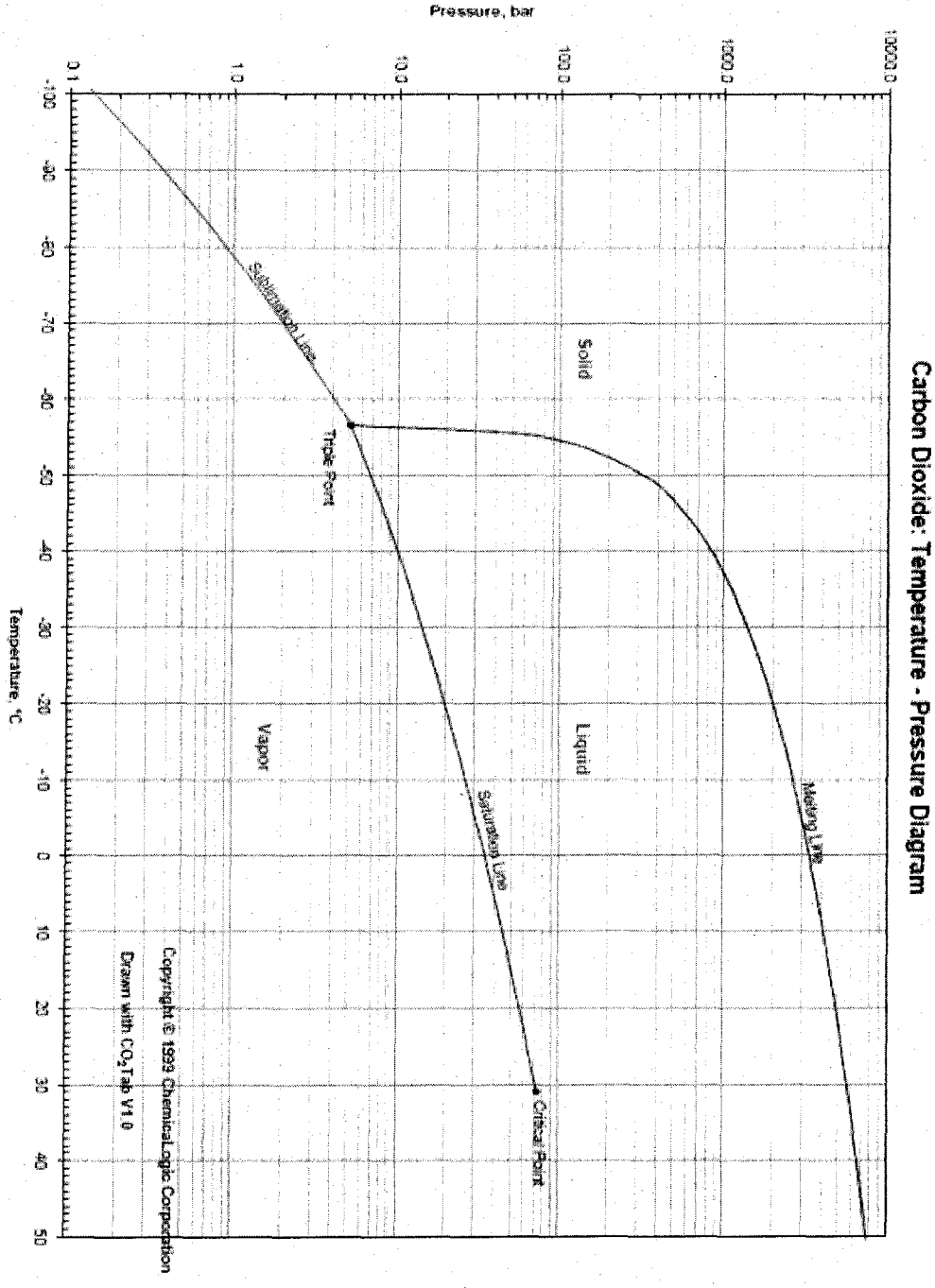

A2: Distilled water density under different temperatures [153]

Density table for distilled water:
(Cited from http://www.hbcpnetbase.com/)

Temperature(°C)	Density(g/ml)
15.0	0.9991
15.5	0.9990
16.0	0.9990
16.5	0.9989
17.0	0.9988
17.5	0.9987
18.0	0.9986
18.5	0.9985
19.0	0.9984
19.5	0.9983
20.0	0.9982
20.5	0.9981
21.0	0.9980
21.5	0.9979
22.0	0.9978
22.5	0.9977
23.0	0.9975
23.5	0.9974
24.0	0.9973
24.5	0.9972
25.0	0.9970
25.5	0.9969
26.0	0.9968
26.5	0.9966
27.0	0.9965
27.5	0.9964
28.0	0.9962
28.5	0.9961
29.0	0.9959
29.5	0.9958
30.0	0.9956
30.5	0.9955
31.0	0.9953
31.5	0.9952
32.0	0.9950

A3: Mophologies of polymer films

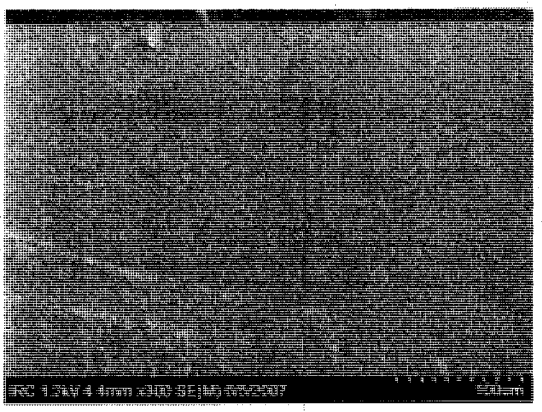

PLGA 50/50 film

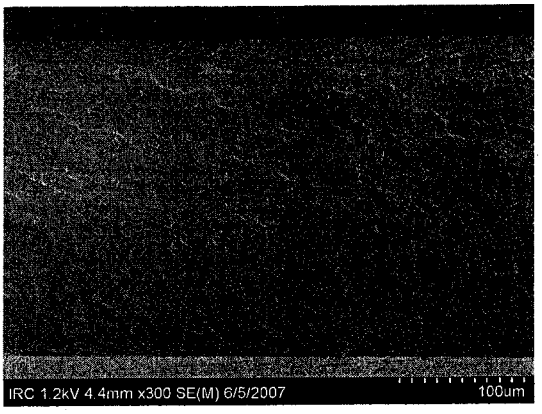

(PLGA 50/50)/PEG 95/05 wt% film

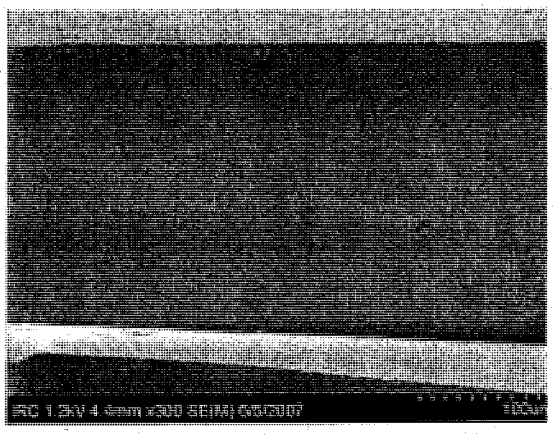

(PLGA 50/50)/PEG 90/10 wt% film

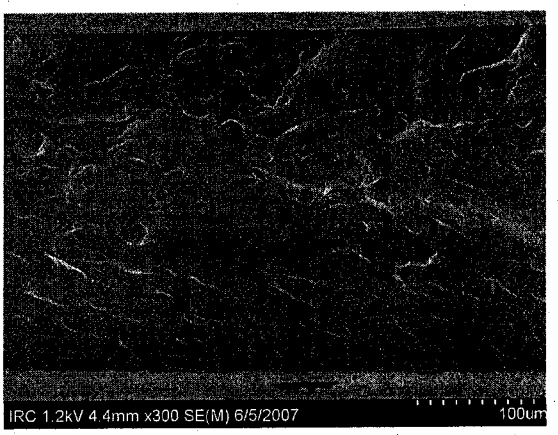

(PLGA 50/50)/PEG 75/25 wt% film

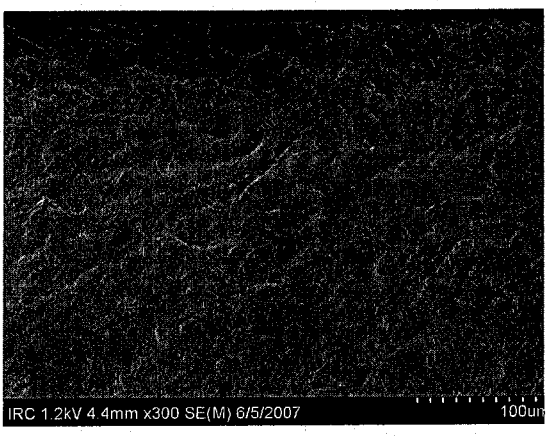

(PLGA 50/50)/PEG 50/50 wt% film

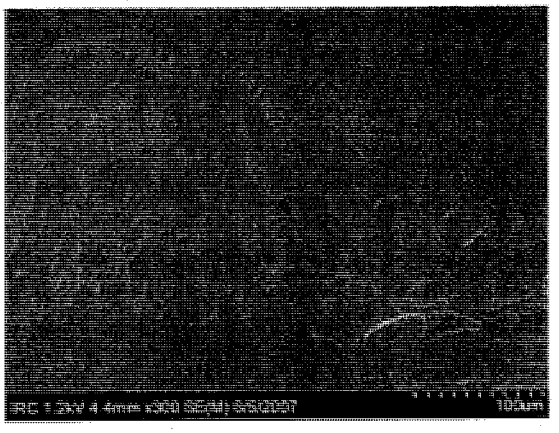

(PLGA 50/50)/PEG 33/67 wt% film

A4: Fick's laws of diffusion [154, 155]

Fick's laws of diffusion describe diffusion and can be used to solve for the diffusion coefficient D. They were derived by Adolf Fick in the year 1855.

Fick's first law is used in steady-state diffusion, i.e., when the concentration within the diffusion volume does not change with respect to time ($J_{in} = J_{out}$).This theory is based on the hypothesis that the rate transfer of a diffusing substance through unit area of a section is proportional to the concentration gradient measured normal to the section. In one (spatial) dimension, this is $J = -D\frac{\partial C}{\partial x}$,

where D is the diffusion coefficient, C the concentration of the diffusion substance, x the coordinate perpendicular to the section and J is the flux per unit of area.

Fick's second law is used in non-steady or continually changing state diffusion, i.e., when the concentration within the diffusion volume changes with respect to time. The differential equation of diffusion, known as Fick's second law derives from the first one and, if the diffusion is one dimensional, i.e., if there is a gradient concentration in only one direction (along the x-axis), the amount of diffusing substance in the element is given by the expression $\frac{\partial C}{\partial t} = D\frac{\partial^2 C}{\partial x^2}$.

A particular solution of the differential equation (Fick's second law of diffusion) describing the time dependence of the diffusing material out of the sample can be derived, considering that there is a uniform initial distribution and that the surface concentrations are equal, the boundary conditions are: C= 0 for x = 0 and for x=1, at t = 0, where l is the thickness of the film and $C=C_0$,

for $0 < x < l$, at t=0,

$$M(t) = \frac{8M_0}{\pi^2} \sum_{n=o}^{\infty} \frac{1}{(2n+1)^2} e^{\left(((-(2n+1)/l)\pi)^2 Dt\right)}$$

where M(t) is the mass of diffusing substance at time t and M_0 is the equilibrium sorption attained theoretically after infinite time. The analytical solution of Fick's second law of diffusion, that describes the sorption process, results from the application of the Laplace transform:

$$\frac{M(t)}{M_0} = 1 - \frac{8}{\pi^2} \sum_{n=o}^{\infty} \frac{1}{(2n+1)^2} \exp\left(\frac{-D(2n+1)^2 \pi^2 t}{l^2}\right)$$

The solution for Fick's law short times then reduces to the following equation:

$$\frac{M(t)}{M_0} = 1 - \frac{8}{\pi^2} \exp\left(\frac{-D\pi^2 t}{l^2}\right)$$

For the initial stage of diffusion:

$$\frac{M(t)}{M_0} = 2\left(\frac{D*t}{\pi*l^2}\right)^{\frac{1}{2}}$$

For a constant diffusion coefficient, the desorption vs. $t^{1/2}$ curve is a straight line.